StratoBlimp

The future of high altitude atmospheric measurements

DSE fall 2012

TU Delft Delft University of Technology

Challenge the future

This page intentionally left blank

Team:

S.K. Brunner, 1331604
P.J.S. Danneels, 1397230
N.G.C. Janssen, 4008138
T.P. Langejan, 4030508
P.C. Luteijn 1534256
T.L. Mohren, 4010280
G. Moors, 4047311
P. van Oorschot, 1378945
J.A. Siebers, 1507729
J.D. Tossyn, 1546651

Tutor:

Ir. B.D.W. Remes (Micro Aerial Vehicle Laboratory)

Coaches:

Dr. Ir. C.J.M. Verhoeven (Electronics Research Laboratory)
Ir. S. Engelen (Space Systems Engineering)
Ir. S. Bouarfa (Air Transport and Operations)
Ir. M.C. Holtslag (Wind Energy Research Group)

Change record

version	date	chapter(s) effected	editor	brief description of change
1.00	12-12-2012	all	N. Jansen & P.C. Luteijn	New document created
2.00	18-01-2013	all	N. Jansen & P.C. Luteijn	First draft compiled
3.00	23-01-2013	all	N. Jansen & P.C. Luteijn	Final draft compiled
4.00	29-01-2013	all	P.C. Luteijn	Revised final draft compiled

Contents

List of Figures

List of Tables

Nomenclature

Abbreviations

AC	Aerodynamic center
ADC	Analog-to-digital converter
AES	Advanced Encryption Standard
API	Application Programming Interface
BPSK	Binary Phase Shift Keying
CAN	Controller area network
CG	Center of gravity
CNC	Computer Numerical Control
CP	Center of pressure
CSV	Comma Separated Values
DSE	Design Synthesis Exercise
EIRP	Equivalent Isotropically Radiated Power
EOM	Equations of motion
ERP	Effective Radiated Power
FBD	Functional Breakdown Diagram
FCS	Flight Control System
FDM	Flight Dynamic Model
FFD	Functional Flow Diagram
FSPL	Free Space Path Loss
GPS	Global Positioning System
GUI	Graphical user interface
I^2C	Inter-Integrated Circuit
IMU	Inertial measurement unit
ISA	International Standard Atmosphere
ISARRA	International Society for Atmospheric Research using Remotely piloted Aircraft
KISS	Keep it simple stupid
KNMI	Koninklijk Nederlands Meteorologisch Instituut
LiPo	Lithium Polymer
LSB	Least significant bit
MAC	Mean aerodynamic chord
MAV	Micro Aerial Vehicle
NOAA	National Oceanic and Atmospheric Administration
PL	Payload
PLR	Payload Recovery
Prod	Production
Prof	Profitability
RC	Remote Control
Rec %	Recovery percentage
RTM	Resin Transfer Moulding
SPI	Serial Peripheral Interface Bus
UART	Universal asynchronous receiver/transmitter
UAV	Unmanned Aerial Vehicle
UHMWPE	Ultra high molecular weight polyethylene
VLM	Vortex Lattice Method

VLM	Vortex lattice method	
Wi-Fi	Wireless Fidelity	
XML	Extensible Markup Language	

Symbols

α	Angle of attack	$^\circ$
α_{app}	Apparent angle of attack	$^\circ$
ΔL	Difference in lift between the two wings	N
δ_{cs}	Control surface deflection	$^\circ$
δ_s	Servo deflection	$^\circ$
$\dot{\theta}$	Rotational velocity	rps
ϵ	Camber ratio	–
γ	Flight path angle	Rad
γ_d	Downward flight path angle	Rad
λ	Taper ratio	–
Λ_{LE}	Leading edge sweep	–
ρ	Density	kg/m^3
σ	Static margin	m
σ_z	Bending stress	MPa
σ_{tail}	Stress on tail	MPa
τ	Thickness ratio	–
A	Aspect ratio	–
a	Lift curve slope	–
b	Span	m
c	Chord length	mm
C_D	3D drag coefficient	–
C_d	Airfoil drag coefficient	–
C_L	3D lift coefficient	–
C_l	Airfoil lift coefficient	–
C_p	Pressure coefficient	–
c_r	Root chord	m
c_t	Tip chord	m
c_{avg}	Average chord length	cm
$C_{D_{0_{tail}}}$	Zero lift drag tail	–
$C_{D_{0_{wing}}}$	Zero lift drag wing	–
C_{D_0}	Zero lift drag	–
$C_{D_{d*}}$	Fuselage diameter ratio	–
$C_{D_{fuselage}}$	Fuselage drag	–
$C_{D_{i_{wing}}}$	Induced drag wing	–
$C_{D_{interference}}$	Interference drag	–
C_{D_i}	Induced drag	–
$C_{D_{l*}}$	fuselage length	–
$C_{D_{parasitic}}$	Parasitic drag	–
$C_{D_{trim}}$	Trim drag	–
$C_{f_{fus}}$	Friction coefficient fuselage	–
$C_{f_{lam}}$	Laminar friction coefficient	–
$C_{f_{turb}}$	Turbulent friction coefficient	–
C_{L_α}	Change in lift coefficent per α	–
C_{l_β}	Moment around X axis due to β	–

$C_{l_{\delta a}}$	Moment around X axis due to aileron deflection	–
$C_{l_{\delta r}}$	Moment around X axis due to rudder deflection	–
$C_{L_{max}}$	Maximum lift coefficient	–
C_{l_p}	Moment around X axis due to p	–
C_{l_r}	Moment around X axis due to r	–
C_{m_α}	Moment around Y axis due to α	–
$C_{m_{\delta e}}$	Moment around Y axis due to elevator deflection	–
$C_{m_{\dot{\alpha}}}$	Moment around Y axis due to $\dot{\alpha}$	–
$C_{m_{cg}}$	Moment coefficient around the CG	–
C_{m_q}	Moment around Y axis due to q	–
C_{m_U}	Moment around Y axis due to U	–
C_{mac}	Moment coefficient around the AC	–
C_{n_β}	Moment around Z axis due to β	–
$C_{n_{\delta a}}$	Moment around Z axis due to aileron deflection	–
$C_{n_{\delta r}}$	Moment around Z axis due to rudder deflection	–
$C_{n_{\dot{\beta}}}$	Moment around Z axis due to β	–
C_{N_h}	Normal force coefficient of the horizontal tailplane	–
C_{n_p}	Moment around Z axis due to p	–
C_{n_r}	Moment around Z axis due to re	–
C_{N_w}	Normal force coefficient of the wing	–
C_{X_α}	Force along X axis due to α	–
$C_{X_{\delta e}}$	Force along X due to elevator deflection	–
C_{X_q}	Force along X axis due to q	–
C_{X_U}	Force along X axis due to U	–
C_{Y_β}	Force along Y axis due to β	–
$C_{Y_{\delta a}}$	Force along Y axis due to aileron deflection	–
$C_{Y_{\delta r}}$	Force along Y axis due to rudder deflection	–
$C_{Y_{\dot{\beta}}}$	Force along Y axis due to a change β	–
C_{Y_p}	Force along Y axis due to p	–
C_{Y_r}	Force along Y axis due to r	–
C_{Z_α}	Force along Z axis due to α	–
$C_{Z_{\delta e}}$	Force along Z axis due to elevator deflection	–
$C_{Z_{\dot{\alpha}}}$	Force along Z axis due to $\dot{\alpha}$	–
C_{Z_q}	Force along Z axis due to q	–
C_{Z_U}	Force along Z axis due to U	–
D	Drag force	N
dBi	Antenna forward gain compared to hypothetical isotropic antenna	dB
dBm	Ratio of measured power referenced to one mW	dB
E	Routh Hurwitz spiral stability criterium	–
F_B	Body reference frame	–
F_h	Load force by horizontal tail	N
F_v	Load force by vertical tail	N
$f_{broadcast}$	Broadcast frequency	Hz
$F_{h_{max}}$	Maximum load force by horizontal tail	N
$F_{v_{max}}$	Maximum load force by vertical tail	N
G_{RR}	Proportional roll-rate gain for roll control	–
h	Airfoil camber	mm
I_{tube}	Moment of inertia of thin walled tube	mm^4
I_{xx}	Moment of inertia about the x-axis	$mm4$

k	Boltzman's constant	
K_g	Gust alleviation factor	–
K_I	Constant	–
$K_{D,Course}$	Differentiator gain for course control	–
$K_{I,Pitch}$	Integrator gain for pitch control	–
$K_{P,Course}$	Proportional gain for course control	–
$K_{P,Pitch}$	Proportional gain for pitch control	–
$K_{P,Pitch}$	Proportional gain for roll control	–
L	Avogadro's number	
L	Lift force	N
l	Average control surface length	cm
l_t	Tail length	mm
$l_{fuselage}$	Length of the fuselage	m
M	Mach number	–
m	Mass	kg
M_a	Molecular mass of air	g/mol
M_x	Bending moment about the x-axis	$N \cdot mm$
M_{crit}	Critical mach number	–
M_{tail}	Bending moment on tail	$N \cdot mm$
n_gust	Gust load factor	g
$n_{maxload}$	Maximum load factor	–
P	Air pressure	Pa
$P_{transmit}$	Transmission power	dB
R	Routh Hurwitz Dutch roll stability criterium	–
R_g	Ideal gas constant	$Pa \cdot cm^3/mol \cdot K$
r_i	Inner tube radius	mm
r_o	Outer tube radius	mm
$range_{max}$	Maximum range	km
Re	Reynolds number	–
RoD	Rate of Descent	$\frac{m}{s}$
S	Wing surface area	m^2
SF	Safety factor	–
T	Air temperature	K
t	Airfoil thickness	mm
T_{servo}	Servo torque	$kg \cdot cm$
U_{de}	Gust velocity	m/s
V	Velocity	m/s
V_A	Manoeuvring speed	m/s
V_D	Dive speed	m/s
V_{fall}	Free fall velocity	m/s
W	Weight	N
$w_{fuselage}$	Width of the fuselage	m
x_{AC}	Position on x axis of the AC of the wing	m
x_a	Aerodynamic x-axis	–
x_b	Body x-axis	–
x_{cg}	Position on x axis of the CG	m
x_h	Position on x axis of the AC of the horizontal tailplane	m
x_{tr}	Flow transition point	–
y_a	Aerodynamic y-axis	–

y_b	Body y-axis	–
z	Distance from neutral line along z_b-axis	mm
z_a	Aerodynamic z-axis	–
z_b	Body z-axis	–

Preface

This is the final report of the Design Synthesis Exercise StratoBlimp assignment. Group 07, a team of 10 students at the TU Delft, has worked on this assignment for 10 weeks. The final results of the design process are presented in this report. The final report is the fourth in a series of reports produced. The results of the preceding reports are presented in this the final report and can be read as a stand-alone report that covers the entire StratoBlimp design process.

The aim of the StratoBlimp assignment is to design a vehicle which will ascend using a weather balloon with as a main goal to capture the blackness of space and is capable of carrying a payload that performs high-altitude atmospheric measurements. A mission allowing the system to descend back to earth is also part of the mission requirements. Different methods and design strategies to complete this mission have been considered and the team has come up with a well designed prototype that meets the mission requirements. Effort will also be put into continuing this project beyond the scope of the DSE.

We want to acknowledge Bart Remes, Chris Verhoeven, Soufiane Bouarfa, Maarten Holtslag and Steven Engelen for their continuous support troughout the project. Edith Janssen for the production of the parachute. Lambach Aircraft, Forze, DUT Racing and the D:Dream Hall management team for the production of prototypes and providing required tools and materials. MAVlab for tools, insights and paparazzi help. Team ATMOS for help on the Datalogger and continuous support. Paparazzi community and KNMI for their helpful additions. Ander Gidenstam for his support on JSBSim related issues. SSE Department for the use of the cleanroom which could be used for a vacuum test. Otto Bergsma for his help with the Kolibri software. Finally we want to thank the Delft Robitics Institute for their financial support.

Summary

Weather institutes worldwide launch weather balloons multiple times a day. A relatively small percentage of the measurement equipment is retrieved, since the retrieving cost is often a lot larger than the value of the sensor units. Having the disability of not reusing the measurement systems is by far a sustainable way of performing atmospheric measurements and impacts the environment negatively. The Stratoblimp system is designed to have a lower impact on the environment and to reduce cost with respect to the current system.

The objective for the StratoBlimp DSE group, under guidance of Ir. Bart Remes, was to design a innovative system which can guide the payload of a weather balloon back to the launch location. The system should be able to glide, i.e. without propulsion, back autonomously. A two-way communication link provides the ground station with the necessary velocity and position data, from the ground the autopilot settings can be altered and a new landing location can be selected. A HD video camera is incorporated in the prototype vehicle to film the entire mission and special attention is given to filming the blackness of space. The content of this report documents the design process of the StratoBlimp system.

An analysis of the mission requirements showed the numerous challenges. A large range has to be covered in extreme atmospheric conditions, while low Reynolds numbers complicate the glide performance at high altitudes. To reach an altitude of 35 km the mass of the return vehicle has to be lower than 1 kg, therefore the lightest materials were selected for the structural design of the return vehicle. To allow for the two way communication a directional helical disk antennae is used for the ground station. A market analysis shows the StratoBlimp project is indeed economically feasible if the vehicle can prove it can perform enough cycles.

The final design choices are summarized below.

- A blended wing body with conventional fuselage mounted tail surfaces is selected. It is optimized for internal volume, high glide ratio and high wing loading.
- For the main wing of the return vehicle and the horizontal tail surface a S3016 airfoil is selected. The use of this airfoil maximizes the glide performance for different altitudes, which maximizes the operation range of the return vehicle. This airfoil is also selected for its efficiency at lower lift coefficients, therefore if the wind speeds get too high the return vehicle will glide at higher speeds. Especially in the jet-stream this will be beneficial.
- To cope with the high loads and harsh conditions during the mission a core of Rohacell 31 foam and a skin of kevlar 49 fibre sheet is selected for the return vehicle.
- Autonomous flight is accomplished by a Paparazzi based autopilot. It is an open-source program developed by the ENAC university in Toulouse in corporation with the MAVlab of Delft University of Technology. The advantage of open-source software is that anything can be restructured to the requirements of the vehicle, which is especially useful for out of the ordinary projects like StratoBlimp.

- An auto-tracking helical dish antenna is selected for the ground station. On the return vehicle a dipole antenna is used. Both antennas are connected with a 868 MHz Xbee transceiver and can be used license-free within current regulations. The data sent back to the ground station contains GPS position data, airspeed, barometric altitude, battery status and attitude. Also the mission parameters such as landing location can be changed in-flight.
- For expensive payload the system needs to be able to perform more than 20 flights to compete economically with the currently available systems.

The StratoBlimp system has the potential to replace the current weather balloon system, where the system has three advantages over the currently available systems on the market. It is safer, because the system is able to avoid restricted airspaces. Cheaper, because no units have to be retrieved, i.e. all units glide back to the ground station. Reuse, making it more sustainable. Because of these advantages the Stratoblimp can make a significant contribution to high altitude atmospheric observations.

Introduction

Since the end of the 19th century weather balloons have provided a significant contribution in atmospheric sciences. For high-altitude atmospheric observations, meteorological institutes such as the Dutch KNMI still rely on daily measurements taken by weather balloons. These balloons ascend to altitudes up to 35 kilometers and may drift as far as 150 kilometers from its launch site before bursting. The sensor unit hanging under the balloon then descends with the help of a parachute. Because the effort and cost involved in finding these units is considerable, only the expensive units are retrieved. The cheaper models are not actively collected and only a fraction is returned by honest finders. Although the institutes are aware of the environmental impact the heavy metals in the sensor units present, there is no sustainable alternative available. The StratoBlimp project is initialised to tackle this problem, where the main goal is described in the project objective:

> Design a next generation high altitude weather balloon system that is capable of autonomous soft precision landings, within a budget of 10000 euro, by 10 students in 10 weeks time.

This report documents the detailed design of an autonomous UAV that can replace the current weather balloon system. The system consists of a balloon, return vehicle and ground station. The bottom up design philosophy was used. This means that unlike the top down design the first step is to take a look at what functions must be performed, what the optimal existing components are to perform these functions and lastly how they can be integrated. For StratoBlimp this means small, low mass and low power consumption components are required to create a feasible and cheap solution. This method is useful when off-the-shelf technology needs to be used and there is not much choice in components.

The report will start off with a brief summary of the concept selection and early design choices which can be found in the top level design chapter, the this part of the report focusses mainly on development of the ground station and return vehicle concept. In the operations chapter the entire mission is sketched and the effect of local regulations on the design are discussed. Sustainability covers the impact of the system on the environment. This is extremely important for the market perspective of the StratoBlimp. Even if the system is more expensive than what is used at the moment, it can still prove to be useful when environmental impact is substantially less than current solutions. The aerodynamic and stability properties are discussed next. From the dimensions and loads calculated in these chapters the structural properties of the vehicle are calculated and material for the vehicle is selected. A production plan for the development of the prototype is also included in the structures chapter. The performance of the balloon is analysed. And the maximum range of operation, respective to the glide efficiency at different altitudes is computed for the return vehicle. The component selection and layout of the vehicle are discussed preceding the aircraft systems chapter that covers the avionics, autopilot and communications. The Release and safety chapter discusses the different options concerning the return vehicle release from the balloon and the parachute deployment. The market analysis looks into the business perspective of StratoBlimp system and investigates the production costs and profit margins. Furthermore the review covers whether requirements are met and the feasibility of the design is checked. Finally the post DSE chapter covers the planning for 2013 up to the demonstration flight in September.

Chapter 1 Project organisation

This chapter describes the team organisation. Sections 1.1 and 1.2 deal with the description of the organizational tasks. Team roles are explained in this chapter, they are switched amongst the group members every week. Sections 1.3 to 1.5 deal with the engineering task allocation.

1.1 Team functions

For the team organization of the StratoBlimp project four team functions are divided, besides their full-time engineering functions, the following managing and presenting functions are defined:

1. *Project manager* - The project manager is the main manager of the entire project, responsible for several tasks. First he leads the meetings with the project team and the supervisors and makes sure they happen in an efficient and structural manner. Second he defines the goals that need to be achieved that week and makes the task division. Third he makes sure that all the tasks are performed within the pre-set planning and leads the team to achieve specific goals. Fourth he keeps an eye on the project goals and objectives, so they are achieved while honouring the preconceived constraints.

2. *Secretary* - The secretary is responsible for minuting all the meetings and keeping track of the logbook which needs to be filled in by every team member at the end of the day. He performs the financial analysis and monitors the budget. Finally he keeps track of and archives all the paperwork in the corresponding folders.

3. *Quality assurer* - The quality assurer has two main tasks, keeping track of the work that has been performed and checking that this work is of acceptable quality. Furthermore he makes sure that all the documents are checked by multiple team members and takes decisions on whether a section needs rework before it can be integrated into the final report.

4. *Presenters* - The presenters create a presentation where the supervisors are informed about the progress made during each week. After every report deadline, an extra presentation is created to inform the supervisors about the contents of the report.

The organogram in figure 1.1 shows how the hierarchical organization is implemented in the project. The main responsible person of the project is the project manager who is assisted by the secretary and the quality assurer. The presenters are not in this diagram. The project manager is backed by the other team members which are required to achieve the desired result.

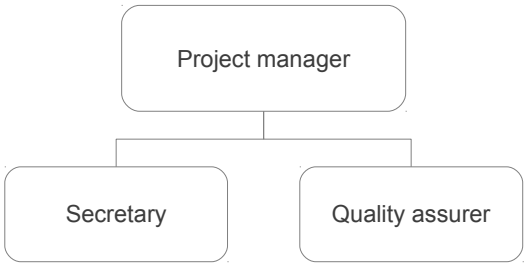

Figure 1.1: Organogram of the managing functions

1.2 Organisational planning

To distribute the previously defined functions over the team members, a rotating system is created. This way everyone performs each function at least once during the DSE. The project manager and secretary change positions every week. The quality assurer is responsible for a report during the total duration till one of the four main deadlines. The task allocation can be seen in table 1.1, the numbers in the first column correspond to the numbers in the enumeration in section 1.1.

Table 1.1: Task allocation, numbers correspond to enumeration in section 1.1: 1. Project manager 2. Secretary 3. Quality assurer 4. Presenter

Week	46	47	48	49	50	51	2	3	4	5
Thom Langejan		4					2/4	1		
Peter van Oorschot	4		3	3	3	4		2	1	
Nick Janssens	3	4				3	3	3/4	2/3	1/3
Thomas Mohren	1	3	4				4			2
Jeroen Siebers	2	1		4		4				
Jeroen Tossyn		2	1		4				4	
Peter Luteijn			2	1	4	3	3	3	3	3/4
Pieter Danneels			4	2	1			4		
Gunther Moors				4	2	1			4	
Stefan Brunner	4					2	1			4

1.3 Interest survey

To organise the team for this project several steps have been undertaken. First an interest survey has been undertaken amongst the team members. The reason for this survey is to get to know each others strengths, weaknesses, experience and interests. Table 1.2 shows the results of the interest survey. In this table an 'E' means the corresponding person has experience in this field and an 'I' means the person has an interest in the particular field.

The different fields are shown in the first row and are respectively structures, aerodynamics, control and simulation, performance and power, operations, communication, sustainable engineering and systems engineering. These fields are taken from the project guide [1].

Table 1.2: Interest survey results

	STRUC	AERO	C&S	P&P	OPS	COMMS	SUST	SE
Thom Langejan	I		I		I			
Peter van Oorschot			I	I	E	I		
Jeroen Siebers		I	I	I	I			
Thomas Mohren	I	I					I	
Nick Janssen	I	I	I				E	
Jeroen Tossyn	E				I			E
Peter Luteijn			E	I		I		
Pieter Danneels			I		I	E	E	E
Gunther Moors	E		I		I	E		E
Stefan Brunner	I		E	I		I		

1.4 Department hierarchy

Knowing all the different fields that are present during this project a department division is made and shown in a department hierarchy. The department hierarchy in figure 1.2 is a graphical overview that visualizes how the various departments are related to each other. The systems engineering (SE) and design integration (DI) are positioned at the heart of the project and are central during the entire design. They are enclosed by the aerodynamics, structures and control departments. Each of these departments has subdivisions present in the outer shell.

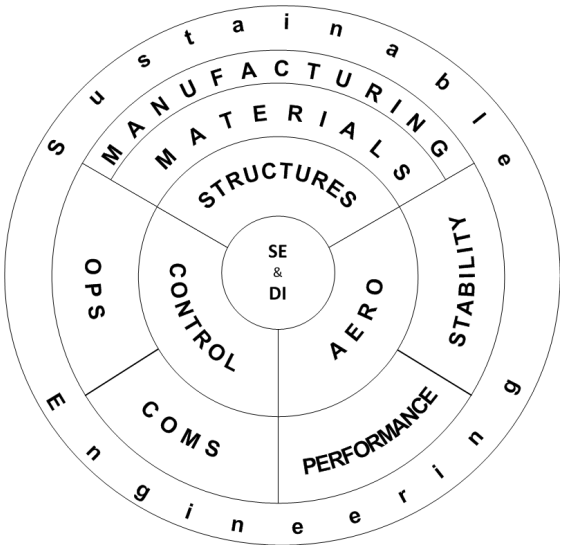

Figure 1.2: Graphical overview of the departments and their relations. Layers stacked on top of each other indicates departments are dependent on the lower layer

Aerodynamics governs performance and stability, where stability shares a relationship with its neighbouring structures department. Everything performance related governed by the aerodynamic department share a relationship with the stability shell of this department. Hence, performance touches the control department and the communications outer shell, stating the performance aspect is related to the way it is controlled.

The control department governs operations and communications. As described in the aerodynamic department, communications shares a relationship with this, but also shares its outer shell with operations. The relationship between operations and communications is an obvious marriage. Hence, operations is controlling the communications.

The structures department is the link between control and aerodynamic departments. Hence aerodynamics & control share a relationship with this department. The structure is defined by these two departments, which include the middle materials shell and outer manufacturing shell. Hence, the structure defines the material and the material defines the manufacturing. Throughout the course of this project, this department hierarchy is respected in every step of the design process. It is important to define the departments for this project, because it gives structure and helps to clearly define responsibilities.

Sustainable engineering finalizes the department hierarchy and is the most outer shell. During the entire design, the aerodynamic, control and structures department have a sustainable design mindset and incorporate the sustainable design philosophy in their own department.

1.5 Human resource allocation

From the interest survey, people have been assigned to one of the departments defined in section 1.4. This will become important when the design phase is reached. For each of the departments listed in figure 1.2 responsible persons have been assigned. The responsibilities of each department and the responsible persons for the departments are listed in table 1.3.

Table 1.3: Responsibilities of each department

Department	Description	Responsible
Materials & structures	Structural integrity of the return vehicle and the balloon, as well as for the chosen materials and manufacturing process.	Nick Janssen, Jeroen Tossyn & Jeroen Siebers
Flight systems	Aerodynamics, stability and performance of the return vehicle as well as the balloon.	Thomas Mohren & Stefan Brunner
Mission control	Operations of the entire mission, flight control systems and the communication between the ground station and the return vehicle.	Pieter Danneels, Peter Luteijn, Peter van Oorschot & Thom Langejan
Design Integration	Integrating all the above departments, as well as integrating sustainability in the design of the StratoBlimp system.	Gunther Moors

Chapter 2 Top level concept design

This section describes in which manner the final concept was chosen and which design choices resulted from this. These design choices are leading and form a basis throughout the whole final design. The concept generation is explained in section 2.1.

2.1 Concept generation

The concept generation started with exploring all the functions and requirements which the return vehicle and weather balloon must be able to fulfill during its mission. These functions and requirements resulted in some initial concepts for the return vehicle, ground station and the release mechanism.

Having gathered all these initial concepts, a weighed trade-off method was performed. This method took different selection criteria into account, i.e. range of the return vehicles, payload/mass, stability, turnaround time, reliability, manufacturability and control. Other selection criteria were used for the ground station and release mechanism. Three return vehicle concepts were selected to be most suitable for the mission: A fixed wing drop shape glider, a flying wing and a paraglider.

The latter was later discarded because of its low glide ratio. This means only the flying wing and fixed wing drop shape gliders were further considered as possible designs. Artist impressions of the designs can be found in figure 2.1.

The weighed trade-off method resulted in a direct link communication method, since the satellite communication is less reliable and is more expensive. As a release mechanism, a hot wire will burn through a rope that releases the return vehicle from the balloon. It was chosen because of its low mass.

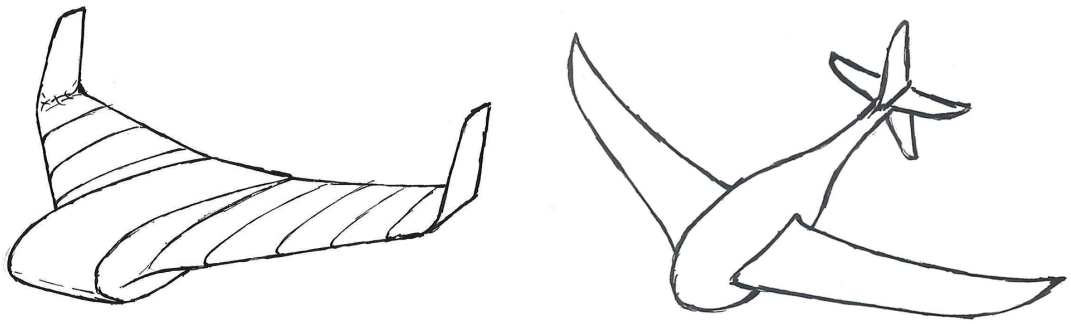

Figure 2.1: Top level flying wing and drop shape glider concept designs

The two return vehicle options were further looked into and their performance compared in the following areas: high altitude stability, control, aerodynamics, layout configuration, airfoil selection, flight systems, flight loads, materials, structural characteristics and manufacturing methods. The selection took place considering the following criteria: stability, control, performance and structural mass. In the end due to the difference in stability the fixed wing drop shape glider came out as the best concept, but only by a small margin. The team approved of this choice under the condition that the cross tail was replaced by a conventional tail. The cross

tail was considered too fragile to be able to perform a belly landing, which was and still is the prefered landing of choice. It was noted that both concept could be developed into a succesful design.

An indication of the list with all the components that need to be present in the return vehicle was made:

- Parachute
- Autopilot control board
- Autopilot sensor board
- GPS module
- Servos
- Safe mode control board
- Sensor package
- Camera
- Extra battery for camera
- GPS antenna

A broad range of structure types and materials were considered to build the return vehicle. A foam core with composite skin is common a common construction technique for UAVs because of its low mass and impact resistance. A list of many types of foam was made, summing up important propterties such as density and E-modulus. In section 7.1.2 the final choice for core material is discussed. A composite skin has excellent load carrying capabilities for its mass compared to metals and materials such as wood. Glass fibre, carbon and aramide are the three options to consider, the advantages and disadvantages for each fibre are discussed in section 7.1.

For the communication a direct link was considered the cheapest and most reliable option. The 868 MHz frequency band allows a transmittion power of 500 mW, more transmitting power is allowed if a licence is obtained. This would give room for a larger bandwith, and could be interesting for potential clients. Biodegradable latex was selected for weather balloon material and hydrogen was selected over helium as the prefered gas to fill the balloon.

Chapter 3 Operations

This chapter contains the mission profile in section 3.1. A functional overview is given in section 3.2 in the form of a functional flow diagram and a functional breakdown diagram. Section 3.3 gives the regulations applicable to the system. Finally the landing feasibility is discussed in section 3.4.

3.1 Mission profile

The mission profile describes a typical mission. The mission starts with the pre-launch procedure, followed by the ascent, flight and the post flight procedure. The total mission takes up to 4 hours. The different phases are discussed in detail in this section, followed by an operations diagram in figure 3.3.

3.1.1 Pre-launch

At the start of the mission the system undergoes a visual inspection to check for damaged or missing parts and the weather is checked. In case of strong winds, gusts, heavy rain and/or lightning near the launch and landing location the mission is cancelled. A flight plan is loaded to the autopilot control board. The ground station is turned on, followed by the return vehicle and the camera in the payload compartment. Communication and GPS are initiated, the sensors are calibrated, the servos are moved over their full deflection range and the datalogger starts logging. The return vehicle sends its status to the ground station and continues doing this periodically for the duration of the mission. The autopilot goes into ascent mode which prevents it from trying to control its attitude while the vehicle is suspended under the balloon. If the pre-flight checks show no problems, the balloon is filled and connected to the return vehicle.

The flight plan can include data on restricted air space and alternative landing locations, if applicable for the mission. Mandatory is to have one landing location at the launch location.

3.1.2 Ascent by balloon

The balloon is released in a field clear of trees, buildings and other obstacles and ascends to an altitude between 30 and 35 km. Assuming an average ascent rate of 5 m/s (see section 8.1) this will take 2 hours. In this phase the balloon drifts with the wind. To get the expected drift, one year of KNMI weather balloon GPS data is used which includes a total of 664 cases. At the end of each flight burst altitude is reached. In figure 3.1 the ground position for these bursts can be found.

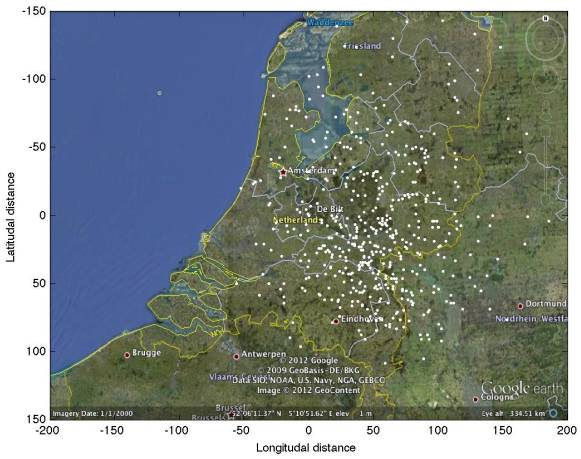

Figure 3.1: Burst positions for 664 cases with initial position the KNMI in De Bilt, Netherlands

By grouping this data the drift distance distribution over all cases was found and plotted in figure 3.2. From this figure it can be concluded that only a small percentage of the cases, about 5%, drift more than 150 km and all cases stay within 250 km. It should be noted that due to the use of another type of balloon with a different payload, the burst altitude for most balloons within the KNMI data is approximately 25 km, with only some balloons going over 30 km altitude. Because of a stable wind regime above 25 km, the drift will be continuous for the last 10 km.

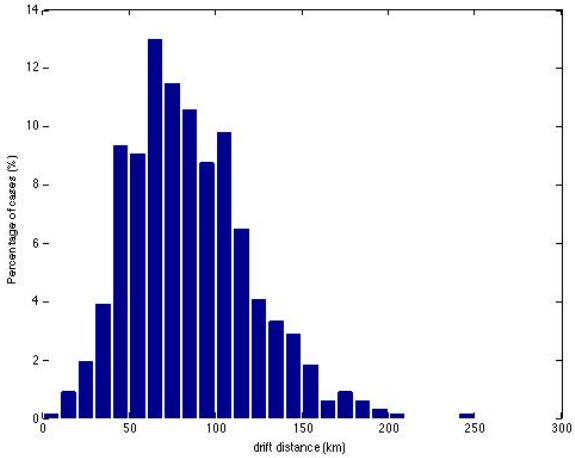

Figure 3.2: Drift distance for 664 cases with launch location the KNMI in De Bilt, Netherlands

The atmospheric properties for altitudes between sea level and 40 km are given in table 3.1. More data can be found in the graphs in appendix A. Table 3.1 shows the vehicle will operate in a temperature range of 217 to 288 K (-56 to +15 °C). At 35 km the density is 0.7% of the density at sea level. As these are the constant values according the ISA the values experienced

may vary. Therefore the temperature range is increased to cover temperatures from -70 to +40 °C.

Table 3.1: Atmospheric properties for altitudes between sea level and 40 km with 5 km increments, according to ISA

Altitude $[km]$	Temperature $[K]$	Pressure $[Pa]$	Density $[kg/m^3]$
0	288	101325	1.225
5	256	54020	0.736
10	223	26436	0.413
15	217	12045	0.194
20	217	5475	0.088
25	222	2511	0.040
30	227	1172	0.018
35	237	559	0.008
40	251	278	0.004

During ascent the autopilot routinely determines the distance to the landing location. Combining this with the range at that time allows an estimate to be made of how long and how far the balloon can drift before the return vehicle is unable to glide to the landing location. In case the drift gets too close to the maximum range, the vehicle is released prematurely from the balloon. There is a time margin between the start of the release and the start of this check, to prevent a release at low altitudes. When using multiple landing locations this check is performed for multiple cases to keep the vehicle in range of at least one of these locations.

The range, expressed in ground distance from the current altitude, is based on the performance characteristics of the vehicle and the wind speed. Although the ascent is different from the descent, the measured wind speed during ascent is accurate enough for an estimate on the wind speed during the glide.

3.1.3 Release from balloon

The vehicle can be released from the balloon both before and after burst. The release after burst requires the wire that connected the balloon and the vehicle to be cut, including the part of the balloon that is still attached to this wire. In case the balloon bursts the vehicle will go into a free fall which results in a change in the output of the sensors. The control board will in turn send the command to release the wire.

The decision to release before burst can be made autonomously or via the ground station. This can be due to different reasons:

- The balloon drifts out of glide range
- The balloon drifts out of communication range
- The required altitude is reached
- The mission time is limited
- The balloon drifts towards an area it should not enter

The vehicle gains speed during the free fall. The autopilot gently corrects for spin and keeps the vehicle in a dive. When the desired airspeed is reached the nose is pulled up.

3.1.4 Descent by gliding

At this point the return vehicle is in stable flight and controlled by the autopilot. The speed is kept at a set value by controlling the pitch and the nose is pointed in the required heading. The glide to the landing location will take up to one and a half hour.

Due to the lower air density at higher altitudes, as shown in table 3.1, a higher airspeed is required at higher altitudes. This is required to have enough air moving around the wings to generate lift and around the control surfaces to change the attitude. This means the response of the autopilot is also different for different altitudes.

The main parameters for the flight are the speed, both airspeed and ground speed, and track, the direction in which the glider flies. For the airspeed it is decided upon to glide at the optimal L/D to maximise the range. In case of headwind however this strategy doesn't give the maximum range. Therefore flying at a smaller angle of attack, depending on the magnitude of the headwind, is a better option. For the direction it is easiest to fly in a straight line to the landing location. Possible reasons not to do this could be the difference in wind direction at different altitudes or restricted airspace. Waypoints are used to set or change the flight path.

Between 16 and 7 km the vehicle might enter a jetstream where the wind speed can exceed 50 $knots$ (26 m/s) [5] [6]. The strategy here is to fly at a higher speed, instead of the ideal L/D, with a lower angle of attack to keep positive ground speed. An important aspect of the jetstream is the turbulence at the edge due to the wind shear between the high jetstream speeds inside and the slower wind speeds outside it. The resulting load on the vehicle are included in the flight loads.

In case the range is more than sufficient, other options are possible. The flight time can be maximised to stay in the air for a maximal time or minimised to get to the landing location as fast as possible. This can be set before the mission or changed from the ground station.

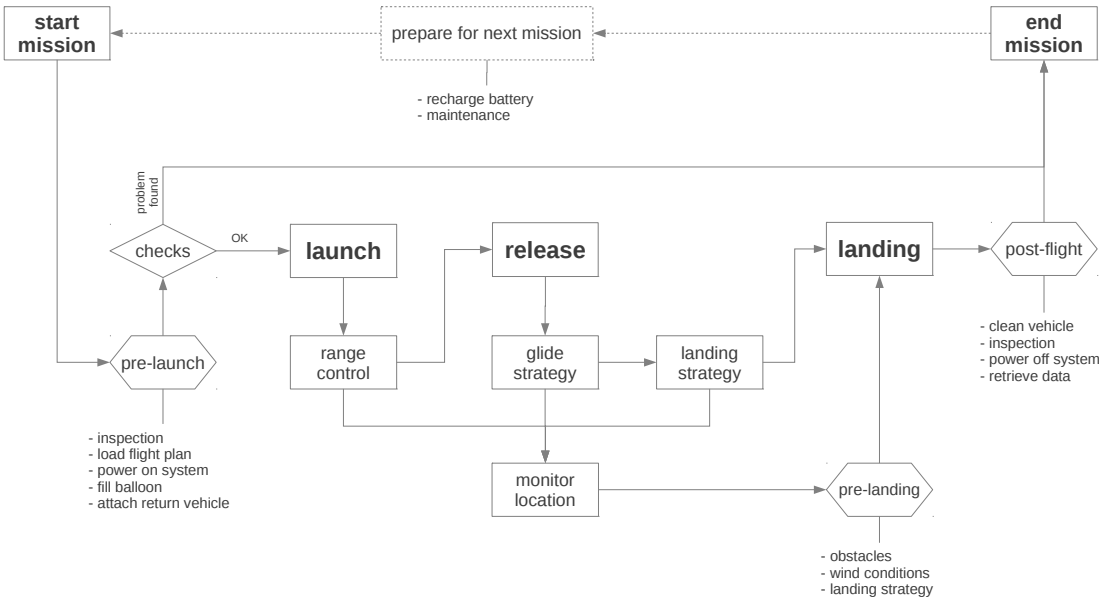

Figure 3.3: Operation diagram for a typical mission

3.1.5 Approach and landing

When the return vehicle reaches the landing location it will fly in circles. The radius of these circles is a function of the altitude, with decreasing radius as it gets closer to the ground. The flight path will be the shape of an upside down cone. The circling is done to lose altitude while the cone shape is needed to maintain a good angle between the vehicle and the landing location, which is where the ground station will be located. During circling a comparison can be set up between the ground speed and air speed to determine the wind direction and wind speed so the vehicle is able to land with headwind. Sending data or a landing direction from the ground station is also an option.

When these values are determined, a glide path needs to be determined. This glide path can be determined according to a 14 m/s cruise air speed and a glide ratio of 16:1 with respect to the air speed. When the right altitude is reached the vehicle goes to its glide path. By flying into the wind the ground speed is reduced to a minimum during landing. During the final approach the vehicle descends at constant speed until it hits the ground.

For the landing of the return vehicle, a belly landing on a grass field is chosen. At a speed of 14 m/s, with a descent speed of less than 1 m/s, the chance of damage to the return vehicle is small. Only solid obstacles increase the risk. A grass field is chosen, because this landing site can be found at lots of places. Landing procedures and feasibility will be explained in more detail in section 3.4.

3.1.6 Post flight

After landing, the camera and the ground station are shut down. The vehicle is cleaned and undergoes a visual check. The data recorded by the camera and datalogger are loaded to a computer, ready to be processed. This marks the end of the mission.

3.2 Functional overview

The Functional Flow Diagram (FFD), figure 3.4, and Functional Breakdown Diagram (FBD), figure 3.5, are both systems engineering tools which help identifying specific functions and interrelations in the system as a whole. The FFD shows the logical order in which functions in the system must be performed in the time domain, while the FBD shows the hierarchical relations between those functions, starting with overall groups and branching out in more detailed constituent parts. Both diagrams focus on the return vehicle specifically, including the release mechanism, but not the balloon or ground station.

3.3 Regulations

The regulations concerning weather balloons in the Netherlands are written down in "Regeling kabelvliegers en kleine ballons" [8], translated "Regulation line flyers and small balloons". The main points of interest for the project and their implications are summarised in table 3.2.

These regulations should be seen as strict requirements from which can not be deviated. Any deviation from these regulations will result in the system not being allowed to operate as intended. One might wonder why the return vehicle is designed to be only 1 kg, while according to category 3.1 the maximum mass is 3 kg. The maximum dimensions of the balloon in category 1.1 are the limiting factor in this case. Balloons of the size specified can reach 35 km altitude only with a payload mass less than 1 kg.

Contact has been made with regulations to ask whether the return vehicle could fly under the current regulations. Their reply was that at this point the return vehicle does not fall under "Regeling kleine ballons en kabelvliegers". This means there is no regulation that would allow flight for the StratoBlimp at this moment. The best chances of testing the prototype is to get

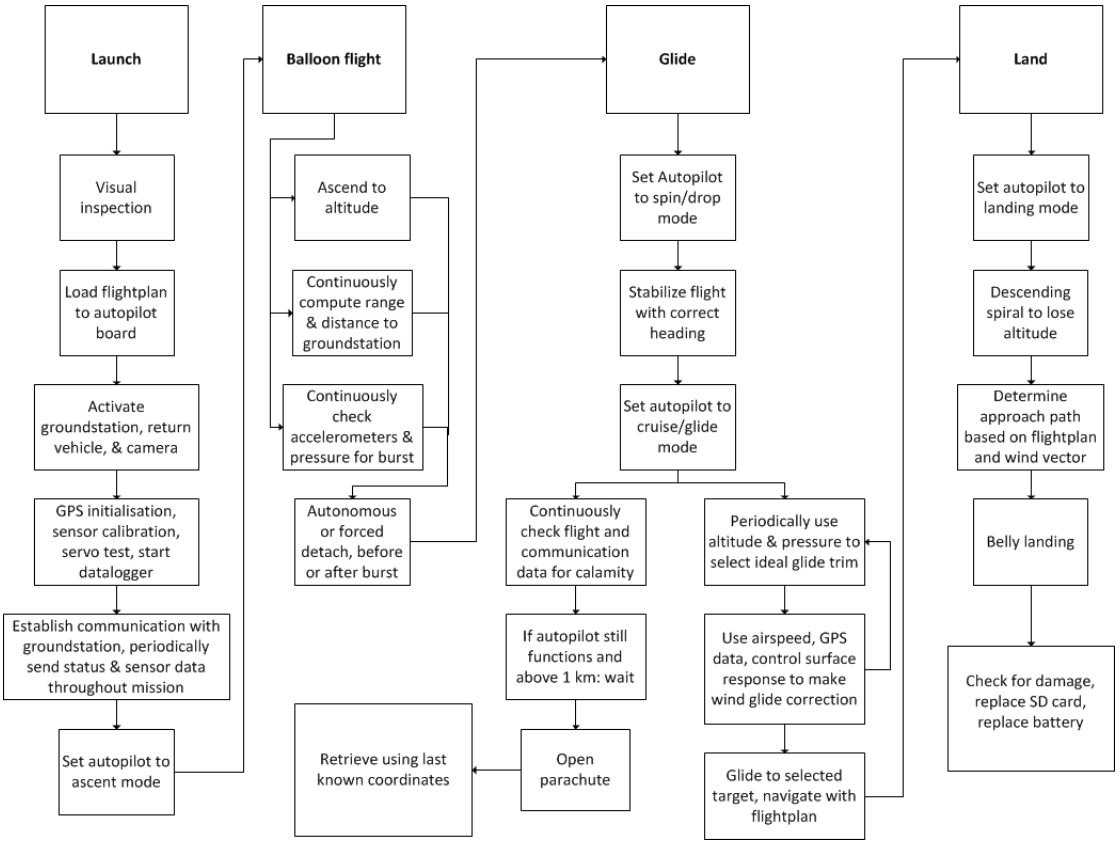

Figure 3.4: Functional Flow Diagram of the return vehicle

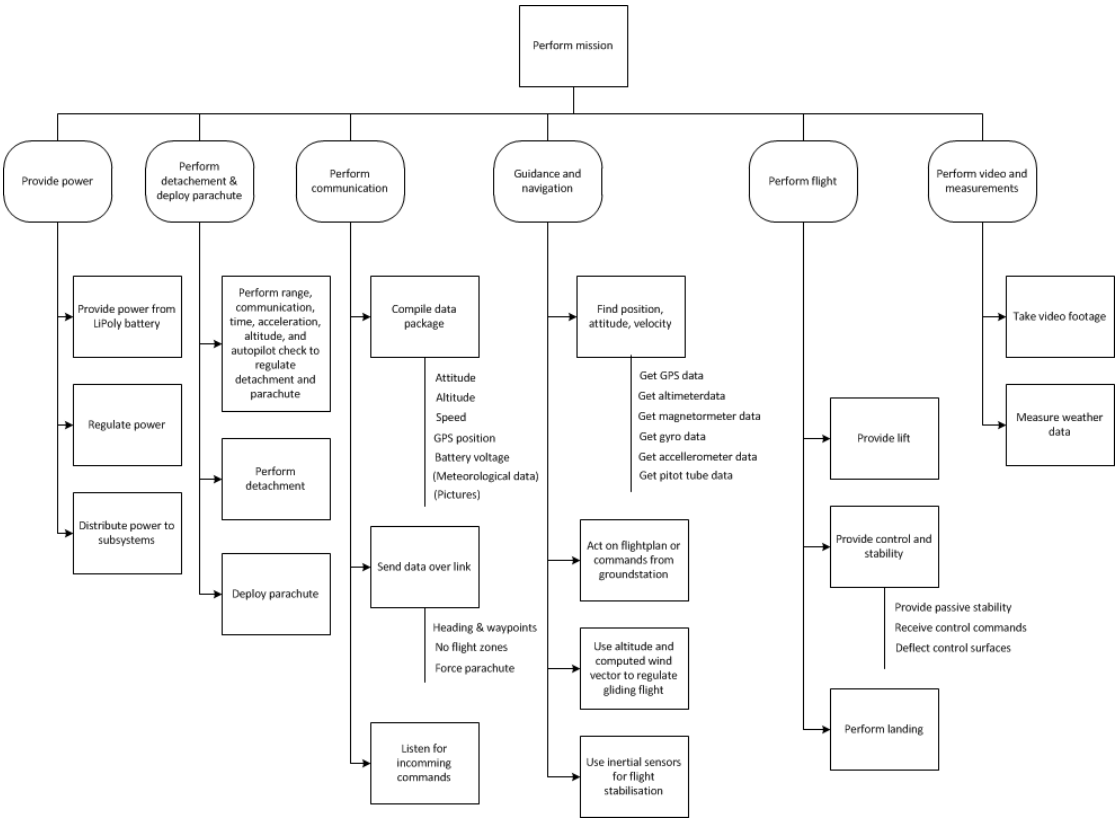

Figure 3.5: Functional Breakdown Diagram of the return vehicle

Table 3.2: Summary of weather balloon regulations

Category	Article	Implication
Applicability	1.1(d)	- The ascent falls under the category of the small free balloons. - The maximum diameter of the balloon at sea level in ISA conditions is 2 m or under the same conditions has a maximum volume of 4 m^3.
Operation	3.1(a)	The system can only be used for scientific purposes.
	3.1(b)	The system can not be flown outside of the Netherlands, unless permission is obtained from local government.
	3.1(c)	Maximum mass of 3 kg.
	3.1(d)	Maximum surface-density of 130 kg/m^2 if the mass is more than 2 kg.
	3.1(e)	An automatic release mechanism between the balloon and the return vehicle is required which breaks if a force of no more than 230 N is applied.
Parachute	3.2	For any object over 30 grams and a surface-density of 50 kg/m^2 a parachute is required which allows for a descent rate of 5 m/s or less.
Launch Conditions	3.3	When launching the balloon within an 8 km radius of a controlled airspace, permission from the air traffic controller is required.
	3.4	When launching the balloon within 3 km of an uncontrolled airport, this has to be notified to the airport at least 2 hours in advance. Permission can be denied.
	3.5	When launching the balloon within 3 km of a glider airport, the users of the glider airport have to be consulted in advance.

an exception for a single test flight. It is expected that if the team is able to show that the test is performed safely an exception will be granted.

Currently weather balloons are launched daily by the KNMI. The payload is dropped with a parachute and lands at a random spot. If the return vehicle is shown to be at least as safe, it is expected that permission for a single test will be granted. Since it takes a lot of time to acquire permission from the regulators, it will not be possible to arrange this during the running time of the DSE. Therefore this is scheduled as a post-DSE activity. The post-DSE schedule is further discussed in chapter 14.

3.4 Feasibility of landing requirements

Requirements on the return vehicle specify a descent rate of 1 m/s at landing and precision landing within 10 m of the chosen landing spot. First the descent rate will be discussed.

For a glide ratio of 16:1 and at a landing speed of 14 m/s the descent rate is less than 1 m/s. Because of the inaccuracy of the GPS module it is not possible to glide until stall speed is reached or descent rate can be determined. At stall speed, the return vehicle can easily stall because of a small gust. If the return vehicle stalls, the descent rate can easily be increased. This is the reason to fly at cruise speed for landing and to be at the edge of the requirement on descent speed.

The 10 m landing radius requirement is not as easy to reach because of the accuracy of the GPS module. Due to an inaccuracy in vertical direction of up to 2.5 m [54], the return vehicle can still be flying at 2.5 m height when the landing spot is reached. At this height, the vehicle will glide for 2.5 times the glide ratio which means that it will fly away for 40 m. It is possible to install a system to determine a more accurate height with respect to the ground. This system would make use of sonar, but since we are landing on grass, this sonar system is not quite accurate. This is because the tops op grass can be higher than the ground and the autopilot can react in an unwanted way. Testing this system will point out if this system will improve the landing accuracy and can be used by the autopilot.

Next to this inaccuracy in height, the GPS also has an inaccuracy in horizontal position. This accuracy is 2.5 m which also has to be taken into account. This inaccuracy only counts for the same airspeed as the ground speed. In case of constant wind the accuracy will be better.

Wind gusts can influence the accuracy, the severity of gusts influencing the accuracy depends on the reaction of the autopilot on these gusts. At this phase no simulations could be made so this needs to be tested post-DSE. For now an error at landing of 42.5 m was taken into account.

Due to this inaccuracy the landing site needs to be a grass field with a radius of 40 m. Within this 40 m radius any obstacles need to be removed. For such a landing site, one can think of a field owned by an agricultural professional. Because the return vehicle will be gliding to the landing site, special attention needs to be given to high obstacles that might obstruct a free glide path from all directions. The same applies for communications, unobstructed line of sight is equally important.

Chapter 4 Sustainability & awareness

The KNMI launches 700 weather balloons every year. Once burst, these land somewhere within a radius of 300 km from the launch site. Since the payload generally costs no more than 50 euros, it is not economic to recover this. This means in most cases the payload will land in the environment where it remains as litter. A typical radiosonde consists of a casing made of foam and plastic. The casing is filled with alkaline or lithium batteries, and a sensor pack which consists of a printed circuit board, a helix GPS antenna, a temperature sensor and a transmitting antenna. These parts are packed in an impact resistant casing and will land by parachute such that the case is still intact after landing. This means hazardous materials from the batteries will not pollute the environment immediately. However both the casing material and content remain, and on the long term hazardous chemicals may leak out. The only current measure against this problem is adding a note to the sondes stating that the finder can keep it, deliver it to the local chemical waste department, or send it back to the KNMI address included. For the more expensive ozone-sondes a reward is offered to anyone who sends it back to the KNMI.

The StratoBlimp project offers a sustainable solution for this problem. First of, the payload will be flown back to the launch site which reduces the litter in the environment to zero. With returning and reusable return vehicles, 700 sondes can be saved every year by the KNMI. Assuming the KNMI uses standard sondes powered by 6 AA alkaline batteries, and adding the fact that 20 % of the sondes is returned by finders [59], leads to the conclusion that a total of 3360 batteries are lost in the environment every year. A return vehicle can bring this amount back to zero. Moreover the system is designed to have as little impact as possible on the environment. The latex weather balloons used are biodegradable [2], opposed to plastic or toxic Chloroprene balloons. The weather balloon will be filled with hydrogen, as this gas is abundantly available within the earth's resources, unlike helium, which is gathered by filtering large amounts of air and is getting scarcer.

Furthermore, expensive measurement equipment as described in chapter 12, like ozone concentration and UV radiation sensors become more accessible when the StratoBlimp system is on the market, as the recovery becomes much easier. These measurements can be used to get a more accurate picture of the atmospheric composition. As such StratoBlimp might contribute to climate research.

Finally the event of a failure needs to be considered. The strength of the return vehicle lies in the re-usability of the concept. In case of a failure the parachute deploys and the return vehicle will descend and land much like an ordinary weather balloon unit, staying in one piece. After a crash the return vehicle will be recovered. The incentive to do this is greater than when using a regular radio sonde because of the higher cost of a vehicle.

To further decrease the impact on the environment, more research could be done on making the body out of bio-degradable fibers and resin. However, since the return vehicle is designed to always be found this would probably not be useful. The same reasoning applies to containing the electronics to prevent toxic materials from leaking in case of a crash. The most interesting option to decrease impact of the return vehicle is to in some way return the balloon pieces as well. Latex may be bio-degradable, but it can pose a threat to wildlife. To accomplish this, the mission objective and concept need to be changed drastically, but it is an option to look into for future prototypes of the StratoBlimp system.

Chapter 5 Aerodynamics

This chapter covers the aerodynamic design of the return vehicle. Section 5.2 covers the choice of airfoil and the three dimensional optimisation of the wing. Section 5.3 is about the design of the fuselage. Section 5.4 governs initial sizing of the tail. In section 5.5 a prediction of the drag of the components is made. Section 5.6 illustrates the glide performance and behaviour of the complete return vehicle. Section 5.7 describes the verification and validation steps taken. Finally section 5.8 deals with technical risks i.e. uncertainties in the design process. Evaluation of the stability of the vehicle is not part of this chapter but will be dealt with in chapter 6.

5.1 Aerodynamic design points

The main difference between the StratoBlimp return vehicle and other MAVs is the design for flight at both sea level and up to 35 km altitude, thus requiring performance in a broad range of Reynolds numbers (Re). The different altitudes will have an effect on the drag prediction, the stability derivatives and control surface efficiency. Therefore these parameters need to be computed for several different flight conditions, ranging from low Mach numbers (M) and relatively high Re to transsonic M and low Re. The reynolds number is a parameter describing what form an airflow around a given shape will take. It is calculated with equation 5.1, where V is the velocity, l is a reference length of the object in the airflow and ν is the kinematic viscosity.

$$Re = \frac{Vl}{\nu} \tag{5.1}$$

$$V = \sqrt{\frac{2W}{C_L \rho S}} \tag{5.2}$$

From equation 5.2 the required speed to generate enough lift (L) for flight can be computed. An initial wing surface S of 0.16 m^2 is assumed, see section 5.2. W is the weight of the return vehicle, and ρ is the air density. A lift coefficient C_L of 0.3 was assumed up to 20 km and 0.6 from 20 km upwards (since low density will probably force a higher angle of attack α). This is an abrupt change, but it is accurate enough to provide preliminary insight into the flight regime. Compressibility needs to be taken into account at M above 0.3. Therefore a Prantl Glauert correction [11] has been implemented at 30 and 35 km altitude. Table 5.1 shows the required V and corresponding Re and M for the given flight levels [21] [22].

Table 5.1: Altitudes with the corresponding Mach and Reynolds numbers

Altitude (km)	Velocity (m/s)	Re ($-$)	Mach number ($-$)
0	18.3	$184 \cdot 10^3$	0.054
5	23.6	$157 \cdot 10^3$	0.074
10	31.4	$130 \cdot 10^3$	0.105
15	45.8	$92 \cdot 10^3$	0.155
20	47.9	$44 \cdot 10^3$	0.162
25	72.0	$29 \cdot 10^3$	0.241
30	105.4	$19 \cdot 10^3$	0.349
35	158.6	$12 \cdot 10^3$	0.513

To maintain grip on the analysis and design process with respect to aerodynamics, and allow for comparison between different altitudes, four reference heights are established, representing the span of different flight regimes the return vehicle has to operate in. These will be 0, 10, 20, and 30 km. Sea level is an interesting altitude because it governs landing conditions and is therefore included. From the velocity requirement in table 5.1 the return vehicle needs the first few kilometers to build op speed through falling before flight can be achieved. Flight at 35 km is therefore not feasible, so the other design points are set using 10 km increments.

Aerodynamic design options and parameters (aspect ratio, taper, etc.) will be examined at these altitudes, and finally performance, mainly glide ratio $\frac{L}{D}$, will be analysed. $\frac{L}{D}$ governs gliding flight and thus the range of the vehicle. Note that if it turns out that the glide ratio is very low at high altitudes, one can conclude that optimising the design to increase the glide ratio by a certain percentage in that regime will not have as much beneficial effect on the range as when one were to increase the glide ratio by the same percentage at low altitudes. Another consideration is the wind, which is expected to have little effect at high altitudes, but more closer to the ground.

5.2 Wing design

This chapter is devoted to the wing design process and illustrates the final parameters. First the airfoil selection will be discussed, followed by the optimisation process of the three dimensional geometry. Finally the aileron design is outlined. The final wing design parameters are given in table 5.4.

5.2.1 Airfoil

The return vehicle must be able to fly as efficiently as possible in a wide array of conditions. For analysis purposes this manifests itself as a Reynolds number that varies between $12 \cdot 10^3$ and $184 \cdot 10^3$ for gliding, and up to $1.0 \cdot 10^6$ for dives. Airfoils that perform well at low Reynolds numbers have a shape such that the airflow stays attached for as long as possible. This results in a combination of the following features:

- Gradual curvature to keep the rate of change of momentum of the flow as constant as possible
- Small thickness to prevent large displacement of air
- Sharp nose to prevent the momentum of the flow from increasing rapidly at the nose
- Slight camber to increase lift without causing separation

A Selection of several airfoils specifically designed with this in mind has been studied [9] [17] [14], most of which were obtained from 'Airfoils at Low Speeds' [9]. A list of possible candidates is given in table 5.2

Table 5.2: Candidate airfoils

E 205	Gö 795
E 374	S 3014
HL 74 3512	S 3016
HK 8556	S 3021
NACA 4412	SD 8000

These airfoils have been compared to each other, with as main criterion the C_d and C_l combination, which should be promising over a reasonable angle of attack range and Reynolds number range. A criterion of secondary importance is the $C_{l_{max}}$: a higher $C_{l_{max}}$ decreases stall speed and results in a softer landing. From the initial selection two outliers were identified: the Selig S 3016, whose geometry is illustrated in figure 5.1, and the SD 8000, illustrated in figure 5.2. As can be seen they are very similar, having thicknesses of 9.52 and 8,86 % respectively, and camber of 2.09 and 1.71 % respectively. The leading edge of the S 3016 is a bit sharper, while the maximum thickness location of the SD 8000 is positioned slightly more forward. The SD 8000 has slightly better lift over drag ratios, but is not documented in great detail, and shows less predictable transition behaviour (laminar to turbulent). Therefore it was decided to use the Selig S 3016 airfoil.

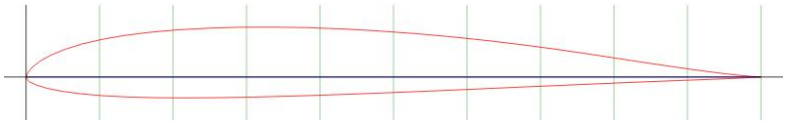

Figure 5.1: Selig S 3016 airfoil shape

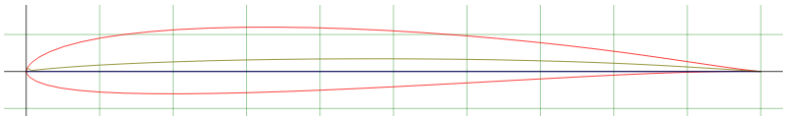

Figure 5.2: SD 8000 airfoil shape

S 3016 lift-drag curves

The experimental $C_l - C_d$ and $C_l - \alpha$ curves of the airfoil [9] are given in figure 5.3. Computational (Panel method) $C_l - C_d$ and $C_l - \alpha$ curves, computed with XFLR5 [10] are given in figure 5.4. These figures can be used to compare the experimental and computational data, for validation of the airfoil data, which in turn serves as part of the verification process for subsequent operations with XFLR5

Mach critical

The lowest pressure coefficient from XFLR5 is used to calculate the critical free stream Mach number (M_{crit}) a.k.a the mach number at which a shock wave forms over the airfoil [20]. The result is shown in figure 5.5. Note that the location of lowest pressure coefficient (C_p) and thus highest Mach number is the wing tip at both $\alpha = 0°$, and at $\alpha \geq 6°$. The lowest M_{crit} is 0.4 at an α of 9°. M_{crit} in nominal gliding flight (α between 2° and 6°) will be between 0.5 and 0.7.

Turbulators

A large proportion of total drag at low Reynolds numbers is caused by laminar separation bubbles. These are regions where flow cannot stay laminar, separates from the airfoil, makes the transition to turbulent in mid-air, and then reattaches. This results in a high energy loss and corresponding drag [9]. Ideally the flow over the airfoil is completely laminar, or otherwise with direct transition to turbulent or with laminar bubbles as small as possible. At lower Re the flow is more likely to remain laminar, but bubbles are also more common. A bubble occurs most frequently just aft of the minimum pressure point along the airfoil. The flow is accelerated over the airfoil, but as soon as it passes the minimum pressure point it slows down again and

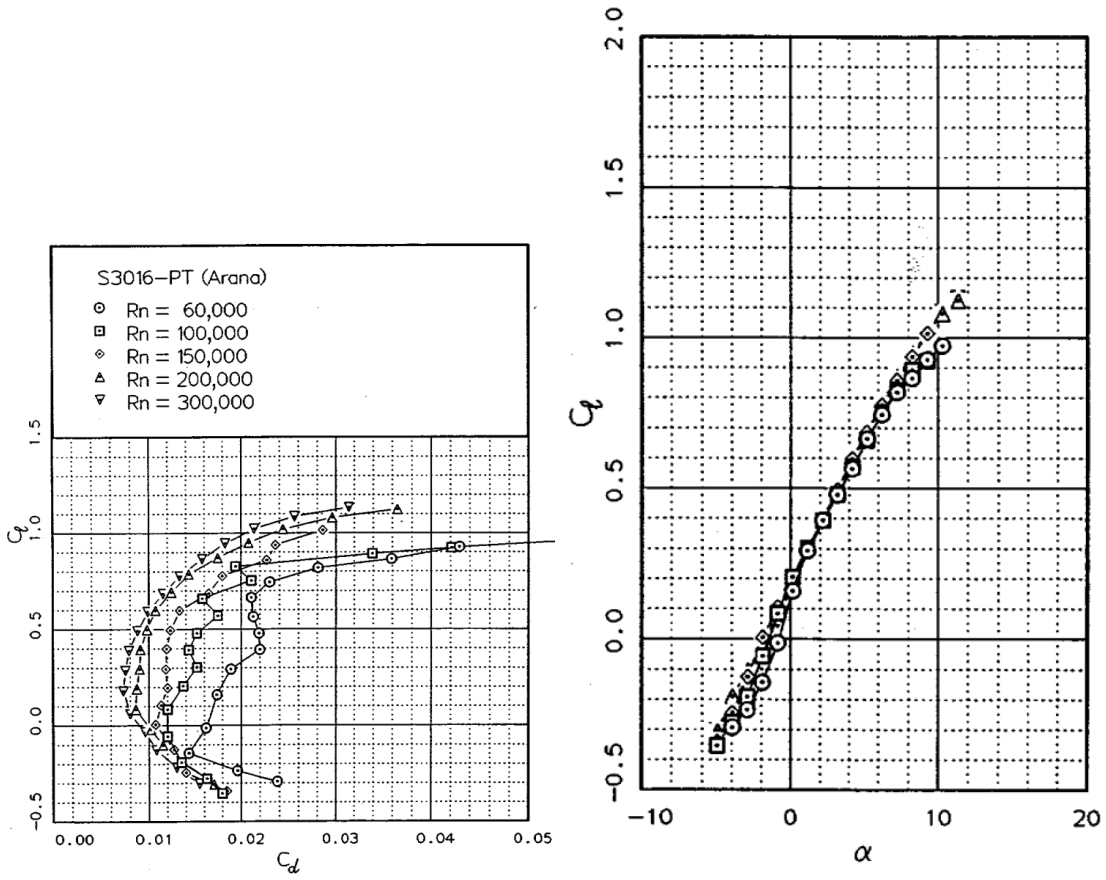

Figure 5.3: Experimental S3016 airfoil $C_l - C_d$ and $C_l - \alpha$ curves [9]

separation can occur. Since the pressure gradient is the largest on the top side of the airfoil, this is the part most sensitive to bubbles [14]. The airfoil selection is very important in dealing with the effects of separation.

A turbulent flow is less sensitive to separation and as it separates, it reattaches more easily. Hence, turbulent airfoils have a more predictable performance. However, in general a turbulent boundary layer produces more drag than a laminar one. Turbulator wire or strips can be placed near the leading edge to ensure turbulent flow over the entire airfoil, or if the separation bubble location is known, just before it. In general, turbulators are mostly used for airfoils operating in Re for which they were not designed [19]. The S3016 is specifically designed, using bubble ramps [9], for the conditions that it will operate in, and adding turbulators is likely to have a negative effect on performance, especially when considering flight at varying conditions, since the laminar - turbulent boundary will shift over the top of the airfoil.

Should turbulators be used, their dimensions need to be precisely determined for them to be effective. A too large turbulator will trigger the separation bubble instead of turning the flow turbulent. The turbulator needs to be positioned just in front of the separation point to minimize the drag until separation and to stabilize the separation at a defined point. To accurately determine the effect of turbulators, wind tunnel tests are required. Since the improvement of performance due to turbulators is questionable until experimentally proven for our specific design

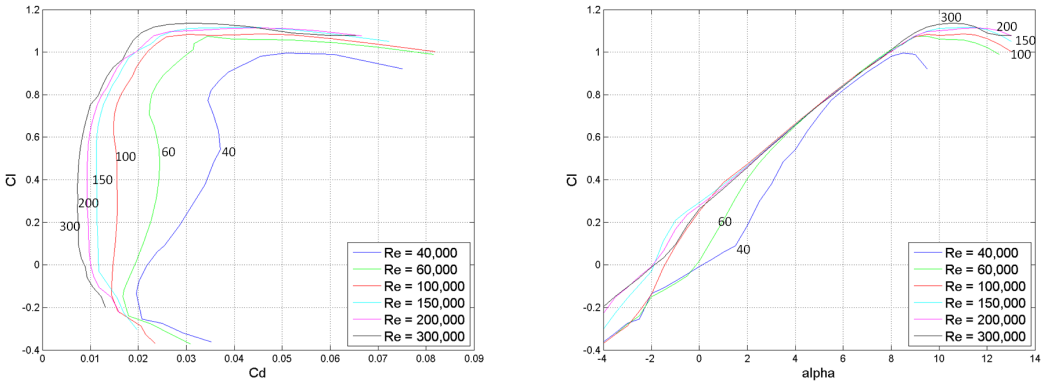

Figure 5.4: Panel method S3016 airfoil $C_l - C_d$ and $C_l - \alpha$ curves

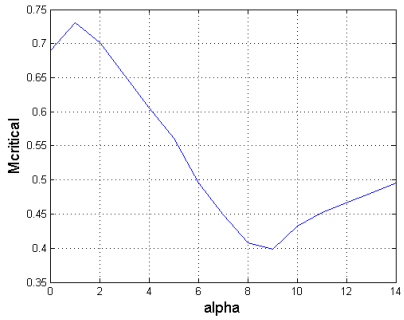

Figure 5.5: S3016 airfoil M_{crit}

and conditions, they are not included in the prototype.

5.2.2 Three dimensional wing

The first step in the three dimensional design of the wing is defining all planform parameters. The wing surface area has been determined with equation 5.3, with a chosen stall speed (V_{min}) of 10 m/s (considering landing requirements) and an assumed $C_{L_{max}}$ of 1. This stall speed is assumed to allow controlled and reasonably accurate landing.

$$S = \frac{2L}{C_{L_{max}} \rho_0 V_{min}^2} = \frac{2 \cdot 9.81}{1 \cdot 1.225 \cdot 10^2} = 0.16 \tag{5.3}$$

This results in a wing surface of 0.16 m^2. The accompanying wing loading is within average range of comparable high speed gliders [24]. Starting from here, first aspect ratio and taper ratio will be chosen, followed by less driving parameters such as incidence, dihedral and twist angle.

Aspect ratio - taper analysis

Theoretically a taper ratio close to 0.4 results in an approximation of an ideal elliptical lift distribution, but also in a smaller tip chord, corresponding to lower local Reynolds numbers and thus to a loss in performance. For aspect ratio there is a similar consideration; higher aspect ratio reduces induced drag, but also decreases chord length and corresponding Reynolds number.

Furthermore, more taper and lower aspect ratio are both beneficial to the structural strength of the return vehicle, resulting in lower mass. To investigate the effect of taper and aspect ratio four XFLR5 3D wing models are produced. These span all possible combinations of aspect ratio 5 and 8, and taper ratio of 0.5 and 0.75. Flow around these wings is computed at the reference altitudes of 0, 10, 20, and 30 km. The graphs for 10 and 30 km are shown in figure 5.6. The wings with taper ratio 0.5 consistently outperform taper ratio 0.75 by a small fraction, for both aspect ratios at all altitudes. The effect of aspect ratio is less clear cut, with aspect ratio 8 being beneficial at 0 and 10 km, whereas at 20 km there is not much difference and at 30 km aspect ratio 5 performs better. Taper ratio is therefore set to 0.5, and aspect ratio will be examined in more detail.

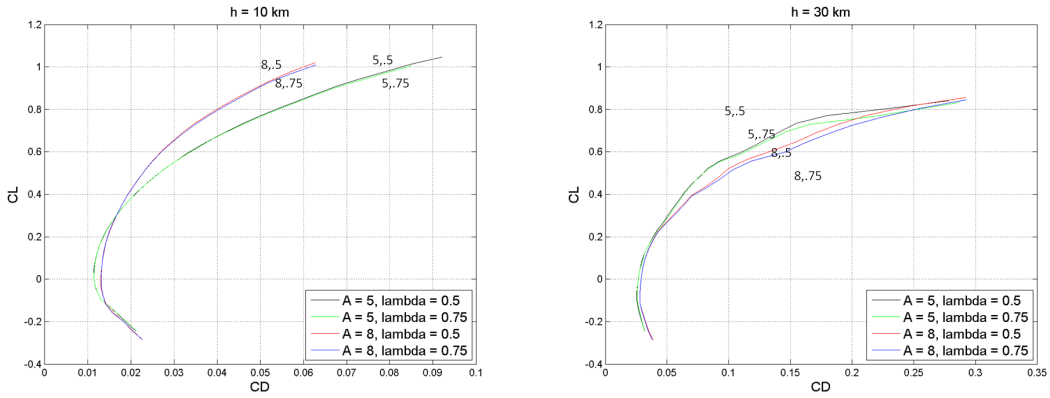

Figure 5.6: Panel method 3D wing $C_L - C_D$, $A - \lambda$ curves at 10 and 30 km altitude

Aspect ratio detail analysis

To make an informed choice for aspect ratio, wings with A = 5, 6, 7, 8, 10, and 12 have been modelled in XFLR5, and airflow at 0, 10, 20 and 30 km is computed. The resulting $C_l - C_d$ curves are illustrated in figure 5.7, in order of ascending altitude.

At altitudes of 0 and 10 km high aspect ratio wings generally perform better. This is expected since Re is still within usual range for aircraft of this size. Only at low α wings with lower aspect ratio perform better, i.e. C_{D_0} is lower, while $C_{D_{induced}}$ increases faster because of the lower aspect ratio. The lower C_{D_0} may be because chord lengths and thus Reynolds numbers are higher. However, since the return vehicle is designed to fly around C_L 0.3 in this regime, higher aspect ratio is better at these altitudes (purely from an aerodynamic point of view). At 20 km a change in this trend is observed though. The $C_L - C_D$ lines of the different wings are much closer together, and more or less linear up to C_L 0.7 - 0.8. Lower Aspect ratios are slightly more advantageous in this regime, most likely because they correspond with higher Reynolds numbers. At 30 km this trend continues more pronounced: lower aspect ratios are more efficient for all angles of attack. Drag to lift relation is more or less quadratic, as it was for 0 and 10 km. This means ideal glide α will be higher at 20 km than at 0, 10, and 30 km. Overall, much higher C_L/C_D values (i.e. glide ratios) are possible at the lower altitudes. This means that the gain from optimising for these regimes is much higher than the gain from optimisation for high altitudes. The aspect ratio is set to 8, as this provides good performance at 0 and 10 km, and is still very close to the optimum at higher altitudes, and is also very reasonable considering structural mass.

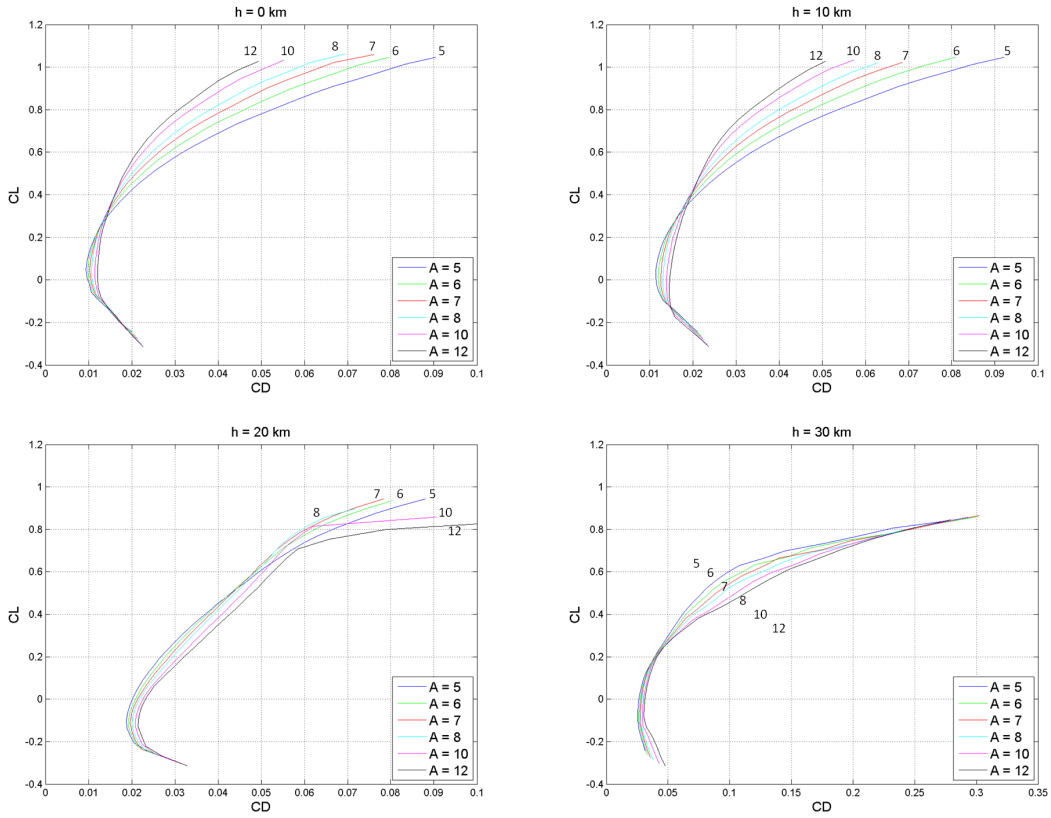

Figure 5.7: Panel method 3D wing $C_L - C_D$, A detail curves at 0, 10, 20, and 30 km altitude, taper 0.5

Secondary parameters

The main reason for adding sweep angle (Λ) is to delay forming of shockwaves over the wing, increasing M_{crit} by a factor $1/cos(\Lambda_{LE})$, both to prevent structural loads from the accompanying shock waves and to increase $M_{drag\ divergence}$. One side effect is a decrease in lift by a factor $cos(\Lambda_{LE})$ [20]. Nominal gliding flight is well below M_{crit}, as can be seen in figure 5.5. Max equivalent dive speed is 81.7 m/s, as computed in section 7.3. This means at sea level the return vehicle will not come close to critical mach numbers in a dive. At high altitude it may however, especially in the freefall phase after detachment from the balloon. The autopilot will attempt to pull into efficient gliding flight as soon as possible however. Therefore sweep will not be needed from an aerodynamic efficiency perspective. It will provide additional yaw stability however, and aid in moving the aerodynamic center backwards, facilitating a more efficiently blended wing - body. Leading edge sweep angle is therefore set to 10°, which is low enough to have no notable effect on lift [13].

Assuming no wind the return vehicle's ideal glide angle of attack will be between 4° and 6° in the lower half of the flight envelope. Headwind, sidewind, and downdraft all require lowering α for ideal performance. Furthermore, the fuselage also has an airfoil shape, albeit a thicker one, meaning it will ideally also be inclined slightly upwards with respect to the airflow, but not as much as the wings. Considering the performance curves 5.11, the incidence angle is chosen to be

2°.

Wings at a dihedral angle provide additional roll stability. Based on common values for reference aircraft [23] dihedral is set to 5°.

Twist can be added to prevent tip stall or to influence pitch stability. Untill actual flight data is known twist is kept at zero.

Ailerons

Ailerons are present to control roll. They are not always present in model aircraft, since roll stability can be achieved by having large dihedral angles. However, with ailerons banking will be easier and more efficient. More importantly they allow spin control in free fall. Pulling up in the wrong direction will decrease the total range of the return vehicle by several kilometers. The ailerons are most effective at the outer edges of the wing. Attention must be paid to preventing tip stall, since this would disable roll control. Historical trends concerning aileron design can be found in figure 5.8. With a $\frac{Aileronchord}{Wingchord}$ of 0.3 ailerons should have a $\frac{Aileronspan}{Wingspan}$ of 0.3 to 0.35. With a total aileron span of 0.4 m at a total span of 1.15 m the ailerons will be sufficiently large. This is advantageous for the roll control in free fall. The hinges of the control surfaces are described in section 7.6.2. The aileron parameters can be found in table 5.3.

Table 5.3: Aileron parameters

Variable	Value	Unit
Aileron-root distance from center	0.3	m
Aileron span (single aileron)	0.2	m
Aileron chord	0.035	m
Aileron surface (single aileron)	0.00676	m^2

Table 5.4: Final wing design parameters

Variable	Value	Unit
Airfoil	S3016	–
Surface area	0.16	m^2
Aspect ratio	8	–
Taper ratio	0.5	–
$\text{Sweep}_{Leading\ Edge}$	10	°
Incidence angle	2	°
Dihedral angle	5	°
Twist angle	0	°
Span	1131.4	mm
Root chord	188.6	mm
Tip chord	94.3	mm

5.3 Fuselage design

The blended wing configuration has an advantage over conventional mid wing configuration. The fuselage can be designed to provide lift while minimizing drag by selecting a low drag airfoil for the fuselage. To fit the payload the fuselage will need to be about 60 mm high. However, ideally the fuselage would be a thin airfoil. This combination results in a large chord length though, which results in a decrease in A. A more slender airfoil for the fuselage would thus result in a

less efficient overall design. To still maintain a high A with reasonably large chord length for the rest of the wing, the fuselage length needs to be as small as possible while still having enough height for the fuselage bay. Therefore a relatively thick airfoil with low drag at low Re needs to be found.

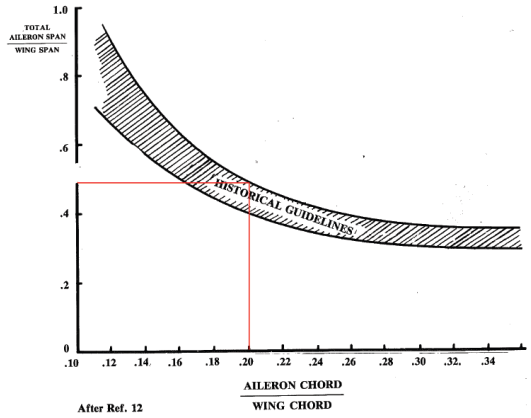

Figure 5.8: Historical trend in aileron size [13]

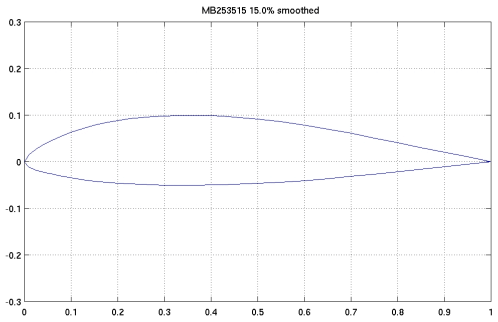

Figure 5.9: The outline of the MB253515 airfoil

The MB253515 (figure 5.9) is an airfoil suited for low Re. The same parameters as for the wing airfoil apply for the fuselage airfoil, except for the thickness requirement. The fuselage part of the blended wing will consist of this airfoil, although it will be scaled to a thickness of 18 % at the center line.

5.4 Tail design

The fuselage mounted horizontal and vertical stabilizer will be used. The advantages over for example the V-tail are the fact that the symmetric and assymetric control are uncoupled, whilst still only requiring two actuators. The return vehicle will also have ailerons, mostly to have control in the vertical spin, but also for efficient turns in the glide phase. The control surfaces are depicted in figure 5.10. Both the horizontal and vertical tailplane surfaces are sized by the volume method [12], displayed in equations 5.4 and 5.5. V_h and V_v correspond to the volumes, S to the wing area, S_h and $S_v$to the horizontal and vertical tail area respectively, l_h and l_v to the distance between the AC of the corresponding surface and the AC of the wing, b to the wing span and $m.a.c.$ to the mean aerodynamic chord length.

$$V_h = \frac{S_h * l_h}{S * b} \tag{5.4}$$

$$V_v = \frac{S_v * l_v}{S * m.a.c.} \tag{5.5}$$

The return vehicle is controlled by 4 control surfaces. Two ailerons are used to provide roll control; the directional stability is controlled with a rudder on the vertical tail plane, and an elevator is mounted on the horizontal tail plane to provide pitch control. The Rudder and elevator are sized by empirical data [14]. They take up 30 % of the chord. The control surface effectiveness will determine whether the size of the control surfaces is indeed acceptable. The tail parameters can be found in table 5.5.

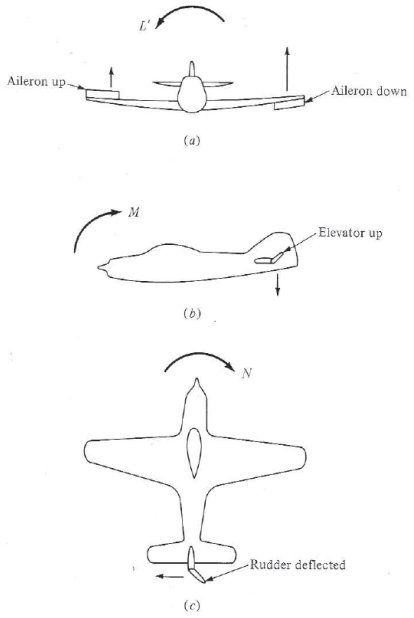

Figure 5.10: Control surfaces [11]

5.5 Drag analysis

The drag of the return vehicle can be separated in different parts. In principle the drag coefficient can be separated in a zero lift drag C_{D_0} and induced drag C_{D_i}, as can be seen in equation 5.6. For an accurate drag prediction, techniques are available to estimate drag for individual components. For this case the parasitic drag is separated into four parts in equations 5.7 and 5.8.

$$C_D = C_{D_0} + C_{D_i} \tag{5.6}$$

$$C_D = C_{D_{i_{wing}}} + C_{D_{trim}} + C_{D_{parasitic}} \tag{5.7}$$

$$C_{D_{parasitic}} = C_{D_{0_{wing}}} + C_{D_{0_{tail}}} + C_{D_{fuselage}} + C_{D_{interference}} \tag{5.8}$$

Table 5.5: Tail parameters

Parameter	Horizontal stabilizer	Vertical stabilizer	Unit
Airfoil	S3016 (upside down)	Naca0010	–
Angle of incidence	-2	–	°
Span	0.34	0.15	m
Root chord	0.12	0.12	m
Tip chord	0.1	0.1	m
Sweep	15	26	°
Control surface span	0.34	0.15	m
Control surface chord	0.035	0.035	m
Control surface area	0.0096	0.00552	m

Lift dependant drag

Lift dependent or induced drag (C_{D_i}) is caused by a tilt in the lift due to the induced angle of attack. It can be reduced by increasing the aspect ratio, approximating elliptical lift distribution or the use of winglets. It must be noted that for MAVs the induced drag is usually not as significant as the parasitic drag. The induced drag of the wing and tail are computed by XFLR5 [10].

Trim drag is the induced drag created by the horizontal tail plane to generate negative lift. It depends on the stability margin required. In table 5.6 the trim drag is computed at ground level. For passanger aircraft a stability margin of 5 % is common, for model aircraft the stability margin should not exceed 20 % [14]. Since initially the exact behaviour of the vehicle is unknown, a large stability margin is desired. The stability margin is set at 15 %. This will be easy to adjust, especially when a decrease is desired, by shifting the payload or adding some (small) mass to the tail.

Table 5.6: $C_{D_{trim}}$ as a function of stability margin

stability margin %	Moment around c.g. –	$C_{D_{trim}}$ –	$C_{D_{tot}}$ %
0	0.0324	0.000582	2.5
5	0.0395	0.000862	3.6
10	0.0465	0.001198	5.0
15	0.0535	0.001590	6.5
20	0.0606	0.002035	8.2

Lift independant drag

The parasitic drag ($C_{D_{parasitic}}$) includes zero lift drag for both wing and tail, fuselage drag and vertical tailplane drag (included in zero lift drag for the tail and the interference drag), as can be seen in equation 5.8. The $C_{D_{0_{wing}}}$ and $C_{D_{0_{tail}}}$ are also found by using XFLR 5. $C_{D_{fuselage}}$ is found using Hoerner, 1965 [15]. Equations 5.9, 5.10, 5.11, 5.12 and 5.13 describe how the fuselage drag is computed. For this($x_{tr}/l*$) can be computed by XFOIL [16] and changes with Re. To use this formula, the fuselage shape was approximated by an elliptical sphere.

$$C_{D_{fus}}/C_{f_{fus}} = 1 + 1.5 * (d*/l*)^{3/2} + 7 * (d*/l*)^3 \tag{5.9}$$

$$C_f = C_{f_{lam}} * (x_{tr}/l*) + C_{f_{turb}} * (1 - x_{tr}/l*) \tag{5.10}$$

$$l*/d_{eq}* = 2 * l*/(b* + h*) \tag{5.11}$$

$$C_{f_{lam}} = 1.328/(Re_{fus})^{1/2} \tag{5.12}$$

$$C_{f_{turb}} = 0.427/(log(Re_{fus}) - 0.407)^{2.64} \tag{5.13}$$

Interference drag

The interference drag is caused by parasitic interference (boundary layer interaction), and induced drag due to changes in lift. The parasitic interference drag of the body is expected to be low. The induced drag due to change in circulation is taken into account in XFLR 5 and is therefore already incorporated. The parasitic interference drag of the tail is of consideration and could be as much as 5 % of the basic tailplane profile drag [15]. Therefore a factor of 1.05 is applied to the C_{D_0} of the tail. It is expected that the parasitic interference drag is greatly reduced for the blended wing compared to a non-blended wing because there are no sharp edges. Because of this no factor is applied to the $C_{D_{0_{wing}}}$.

Wave drag

One might notice that wave drag is not mentioned in the above formulas. Since the mission profile 3.1 states that the flight speed in the normal missions will not reach transsonic conditions, this is not of interest from a glide performance point of view. In case of component faillure, these conditions might be reached and shock waves occur over the fuselage and wing. In this case, glide performance is no longer of interest.

5.6 Vehicle performance curves

Combining the wing, fuselage, and tail aerodynamic data; the performance of the complete return vehicle can be obtained by summing all components. In figure 5.11 the C_L - C_D and the $\frac{C_L}{C_D} - \alpha$ curves are given for the reference altitudes of 0, 10, 20 and 30 km.

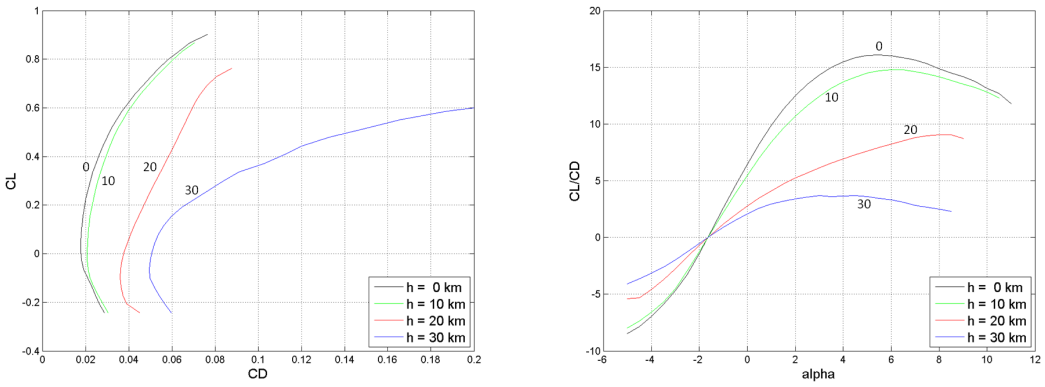

Figure 5.11: Return vehicle $C_L - C_D$ and $\frac{C_L}{C_D} - \alpha$ curves

The $C_L - C_D$ graph shows the magnitude of and relation between the lift and the drag coefficient. The $\frac{C_L}{C_D} - \alpha$ graph shows what the ideal glide angle of attack is, not considering wind or close proximity to stall speed. In addition one can see what glide ratio can be achieved, and how much impact a deviation from the ideal α will have. Both graphs clearly show the decrease in $\frac{C_L}{C_D}$ with altitude.

5.7 Verification and validation

Most of the parameters of the return vehicle are determined by simplified computational optimization. They are based on assumptions and simplifications, which may cause results to lack the desired accuracy. The effect of assumptions in the model can be verified by comparing results

with empirical data or by using more complex computational methods. The tail and control surfaces are checked by comparison with model aircraft to serve as a rough verification. Especially the aerodynamic properties at low Reynolds numbers are very unpredictable. To ensure the required performance of the return vehicle, the entire model must be validated by experiments.

Barring actual flight, aerodynamic validation is best done testing a model in a windtunnel. Since the Reynolds number must be low, the flow needs to be slower or the model must be smaller than the actual return vehicle. The tests will have to take place in a low turbulence wind tunnel (turbulence less than 0.03 %) [17]. The Low-Speed Low-Turbulence tunnel in Delft is suitable [18]. Its turbulence level is lower than required and the cross section is large enough to fit the model. However, a more accurate balance to measure the forces on the model needs to be used.

5.8 Technical Risks

This section gives a brief list of identified elements, technologies, characteristics and conditions posing a risk or uncertainty with respect to the nominal operation of the design. Extensive testing of the functionality of the parts associated with these points is necessary.

- Low Reynolds numbers make flow harder to predict, and while research is gradually taking off in this area [17], it is still in its infancy. Specifically control surface functionality in these conditions is an important point, since these are vital in recovery from unexpected situations.
- Software limitations resulting in inaccurate approximations of airfoil or wing data. Specifically XFLR5 [10], which is in turn based on Xfoil [16] has been used extensively for both verifying experimental airfoil data, and modelling wing performance.

Chapter 6 Stability

In this chapter the stability of the designed return vehicle is discussed. The body fixed reference frame is used, and is displayed in figure 6.1. In section 6.1 the stability during the release of the balloon at an altitude of 35 km is discussed. Thereafter the static and dynamic stability of the return vehicle is discussed in section 6.2 and 6.3 respectively. At last the verification and technical risks are elaborated in section 6.4 and section 6.5.

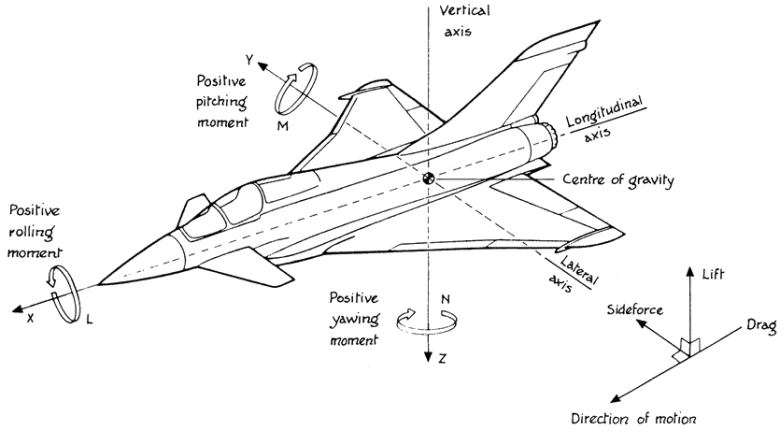

Figure 6.1: The body fixed reference frame [26]

6.1 Free fall stability

The free fall phase is the least predictable phase in the mission profile. Due to the low density at 35 km altitude and low speeds at the begin of the descent the return vehicle has to rely on its natural stability. As the return vehicle speeds up, the Re over the wing will become higher and the autopilot can take control. The natural stability is guaranteed by having the center of pressure placed behind the center of gravity, which is also the case with rockets. Figure 6.2 visualizes natural stability for a rocket. This will ensure spin stability about the y and z axes. The spin about the x axis, or roll spin is determined by other parameters. In normal flight, the return vehicle is spirally stable due to wing dihedral. The CG is positioned lower than the AC, and therefore the vehicle will not roll in the static case. In the nose down free fall this is not the case. A slight difference in lift on one of the wings (or one side of the tail) can cause the return vehicle to spin. Assuming an imperfection, there is a maximum spin for which the moments are in equilibrium. Any disturbance in lift may temporarily speed up the rotation, but the return vehicle will always return to this initial spin.

The roll can be controlled by the ailerons. However, there is a maximum roll rate that can be observed by the sensors on board. The sensors on board of the return vehicle saturate at a spin of 6 rotations per second. A model is made to investigate the spin of the return vehicle.

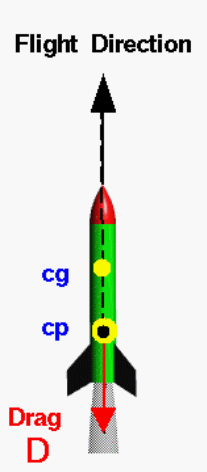

Figure 6.2: Stability in rockets is achieved by placing the CG in front of the CP [27].

A simplified model of the return vehicle can be used to determine statically stable spin assuming an imperfection in the production, and a statically stable spin due to a large difference in lift over the wings (in case of separation or shock wave). The spin due to an imperfection will certainly occur, the spin due to a large difference in lift may occur, although not in a static case.

The assumptions made in this model are:

- The roll spin is not coupled with the spin around any other axis
- The difference in lift coefficient due to an imperfection will not be larger than 0.1 .
- The lift of the wing acts at a distance of 0.3 m from the center of the x axis.
- The velocity due to spin at 0.3 m from the x axis is much smaller than the free fall velocity, such that small angle approximation is valid.
- The C_{L_α} is 4 rad^{-1}.
- The maximum difference in C_L due to disturbance is 0.4.

The imperfection in lift is equal to 2 times the lift coefficient slope times the apparent angle of attack, indicated in equation 6.1. The apparent angle is a function of the spin velocity and the free fall velocity, equation 6.1 holds.

$$\Delta L = 2 \cdot C_{L_\alpha} \cdot \alpha_{app} \tag{6.1}$$

$$\frac{\Delta C_L}{4 \cdot C_{L_\alpha} \cdot 0.3 \cdot \pi} \cdot V_{fall} = \dot{\theta} \tag{6.2}$$

Now inserting the imperfection and the different free fall velocities, we obtain the rotations as can be seen in table 6.1. The sensors have the possibility of getting saturated due to a disturbance as the free fall velocity passes 225 m/s, with the stated assumption. Altough it is not expected that this speed will be reached in operation, it might occur in case of a control error. If this is

Table 6.1: Rotations due to imperfection and disturbance for different free fall velocities

Free fall velocity	$\Delta C_L = 0.1$	$\Delta C_L = 0.4$
m/s	rps	rps
50	0.33	1.33
100	0.66	2.66
150	0.99	3.98
200	1.33	5.31
250	1.66	6.63

the case the rotation sensor might need to be replaced by a more sensitive one. However, it is expected that such speeds will not be reached, and that the difference in lift between the wings will never be this large.

6.2 Static stability

The definition of static stability is that all the forces and moments are in equilibrium. Longitudinal stability is of interest, since lateral static stability is easily achieved for a conventional configuration. The stability is achieved by having the CG in front of the AC . The distance between the CG and the AC is called the static margin σ . A large static margin indicates a large static longitudinal stability. However, stability comes at the cost of control and efficiency. The moment created by having the CP far behind the CG will have to be compensated by negative lift from the tail. Negative lift creates more drag by the tail and requires extra lift from the main wing also increasing drag. This drag has been computed for different static margins in section 5.5. A visualization of the forces in static stability can be found in figure 6.3.

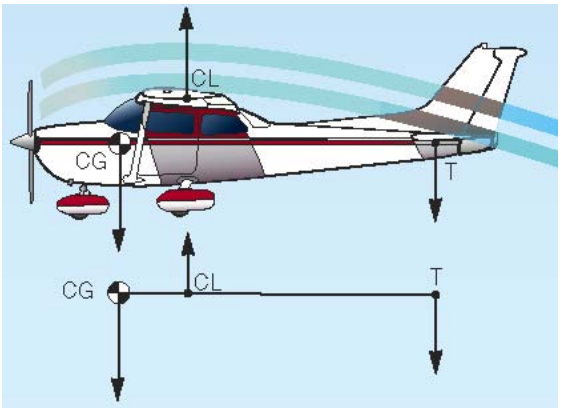

Figure 6.3: Static stability of conventional aircraft. Gravity acting on the CG, Lift (depicted as CL) on the AC, and negative lift (depicted as T) on the tail. [28]

Typical values for σ are in the order of 5 to 15 % of the MAC . Figure 6.3 shows the moment equilibruim equation about the CG. Since a large stability margin is prefered, 15 % is selected. The resulting distance between the AC and the CG can be found in table 6.2. When the stability margin needs to be altered, it is easier to make it smaller than it is to make it larger, since adding mass to the tail has a larger contribution than adding mass to the nose. More on this can be found in section 6.5.

$$C_{m_{cg}} = C_{mac} + C_{N_w} \cdot \frac{\sigma}{c} + C_{N_h} \cdot \frac{x_{cg} - x_h}{c} \tag{6.3}$$

For static stability the C_{m_α} should be negative at $C_m = 0$. This means that in steady flight conditions the aircraft, in response to a disturbance in α, will have a natural counteracting moment. The aircraft is dynamically stable when the overshoot is smaller than the initial disturbance, and the aircraft returns to its original angle of attack.

Table 6.2: Static stability margin

σ in %	$x_{A.C.} - x_{c.g.}$ in m
15	0.021

6.3 Dynamic stability

To determine whether an aircraft is dynamically stable the equations of motion are analyzed. They are separated in the symmetric and asymmetric motions. Stability derivatives need to be computed for the return vehicle. From the EOM the responses of the aircraft to certain inputs can be determined. Determining stability derivatives is usually done by a combination of computational and experimental data. In a short timespan a prediction can be done using computational simulation. It must be stated that these are not very reliable. Testflights are required to determine their validity. The software used to determine the stability coefficients is a MATLAB [29] based Vortex Lattice Method VLM called Tornado [30]. The coefficients can be found in table 6.3.

Table 6.3: Stability derivatives determined with Tornado [30]

Asymmetric		Symmetric	
C_{Y_β}	-0.311	C_{X_α}	0.1162
C_{l_β}	-0.084	C_{Z_α}	6.648
C_{n_β}	0.179	C_{m_α}	-4.159
$C_{Y_{\dot\beta}}$	0	$C_{Z_{\dot\alpha}}$	-2.80
$C_{n_{\dot\beta}}$	0	$C_{m_{\dot\alpha}}$	-4.67
C_{Y_p}	-0.011	C_{X_U}	-0.042
C_{l_p}	-0.543	C_{Z_U}	-0.6
C_{n_p}	-0.09	C_{m_U}	0
C_{Y_r}	-0.464	C_{X_q}	0.2553
C_{l_r}	0.051	C_{Z_q}	16.54
C_{n_r}	-0.284	C_{m_q}	-30.29
$C_{Y_{\delta a}}$	-0.049	$C_{X_{\delta e}}$	0.0116
$C_{l_{\delta a}}$	0.2892	$C_{Z_{\delta e}}$	0.467
$C_{n_{\delta a}}$	0.0107	$C_{m_{\delta e}}$	-2.273
$C_{Y_{\delta r}}$	-0.21		
$C_{l_{\delta r}}$	0.0075		
$C_{n_{\delta r}}$	-0.137		

From these derivatives, responses to inputs as gusts or sudden movements of control surfaces can be simulated. Preferable the change to its new equilibrium position takes place without excessive oscillations.

Dynamic modes

By using the stability coefficients in the symmetric and asymmetric EOM, 5 oscillatory modes can be identified. The symmetric modes are the short period and the phugoid mode. The short period mode is a fast oscillation but highly damped. The phugoid is a very slow weakly damped oscillation, but easily corrected. The first asymmetric mode is the aperiodic roll, an also easily corrected mode. This leaves the spiral mode and dutch roll mode. These mode stabilities can be computed by the Routh Hurwitz stability criteria (E and R) for asymmetric motion [36]. They are computed from the coefficients in table 6.3. Table 6.4 shows the values of E and R computed for the return vehicle. Figure 6.4 shows the trade-off between stability coefficients and the spiral and Dutch roll stability.

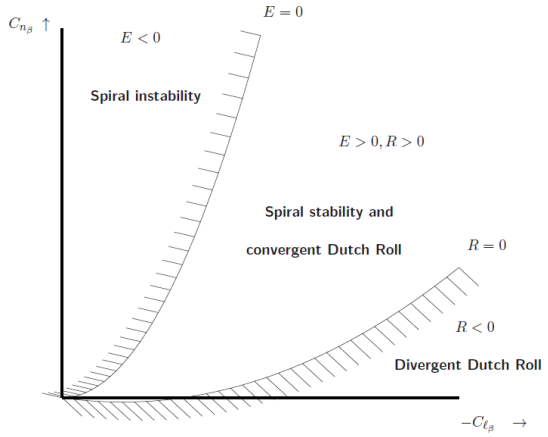

Figure 6.4: Routh Hurwitz stability criteria for asymmetric motion [36]. From the figure it is found that for a spiral stable and Dutch roll convergent aircraft the E and R values have to be positive.

Table 6.4: Obtained R and E values. Dutch roll and Spiral stability criteria are met.

E	$5.70 * 10^{-3}$	≥ 0
R	$2.28 * 10^{-4}$	≥ 0

From the figure it is found that for a spiral stable and Dutch roll convergent aircraft the E and R values have to be positive. Since they are positive for the return vehicle it is stable in both dutch roll and spiral mode. Too much spiral stability will make banking corners difficult. A small spiral instability is allowed according to regulations, since the spiral mode is slow and easily corrected.

6.4 Verification and validation

The accuracy of the stability coefficients derived in section 6.3 is questionable. Some verification has taken place, by checking coefficients of comparable aircraft (which are computed the same way) and by checking with larger aircraft for which the coefficients have been computed by flight tests [36]. This comparison showed that the coefficients are of the right order of magnitude, but this is by far no guarantee that the coefficients accurately describe the stability of the return

vehicle. Therefore a flight test is required to experimentally determine these coefficients, and check the validity of the computational VLM results.

6.5 Technical risks

The return vehicles dynamic stability depends on many factors. The non-dimensional coefficients can be applied in different airspeeds and densities. However, due to non-linear viscous effects these coefficients might not be very accurate at low Re numbers. The method used to calculating these coefficients uses a VLM, which does not take into account viscosity. This assumption of inviscid flow is estimated to be valid for RE above 500000, which is not the case for the return vehicle. More complex methods or validation tests will be necessary if more accurate coefficients are desired. Moreover, the disturbance in free fall is unknown. If the disturbance is larger than assumed the freefall spin will be faster than the IMU can observe. Freefall spin was modelled based on assumed lift and moment discrepancies between different parts of the return vehicle 6.

Shifting the CG

The choice was made to have a σ of 15 %. It is expected that during the flight test a verdict can be reached on whether this much stability is desirable. Perhaps the aircraft will be too stable to be controllable and stability margin will have to be altered. If σ needs to be halved, the CG will need to shift backwards by approximately 0.01 m and the incidence angle of the tail needs to be changed. This is all possible within the current design. The payload compartment is large enough to shift heavy components backwards, and in the worst case a small mass can be mounted near the tailplane.

Chapter 7 Structures & materials

Nowadays composites are widely used for lightweight applications. Their superior performance compared to steel and aluminium can be used to save up to 80% in component mass and reduce the overall mass by 50%. A composite material is shaped by combining two or more materials. For structural purposes the composite material is often formed by reinforcing the fibres with a matrix resin, continuous or short fibres can be used. In the mid-term report several options for these fibres were presented, namely carbon, glass and aramid fibres. These different fibre material options will be further discussed in this chapter.

The available materials are researched in more detail in section 7.1 and a material choice is made in section 7.2. With the material known the loads are calculated in section 7.3, 7.4 and 7.5 for both the wing and the tail. Analytical and numerical methods are used in these sections. Finally more detailed design is done on the control surfaces in section 7.6 and manufacturing methods and a production plan are explained in sections 7.7 and 7.8.

7.1 Material options

In this section the material choice for the skin, as well as the core material will be discussed. This choice will result in a final core and skin material suitable for our design.

7.1.1 Skin material

The reinforcement fibres used for the skin material provide the strength and stiffness to the laminate, where the matrix material ensures rigidity and environmental resistance. The properties of the laminate depends on the way the fibres are orientated in the composite. The fabrics are offered in different orientations and weave patterns. The four main orientation categories are Uni-Directional (UD), 0/90, multi-axial and random orientation. All of these orientations have their advantages and disadvantages regarding different applications.

From the design choices in chapter 2 it follows that the 3 different materials suitable for the skin material are aramid, glass and carbon fibres. These fibres were chosen for their good structural properties and they are commonly used in the aerospace and UAV industry. Other options like the Spectra 1000 375 denier fibres are discarded because of the fact that it is only used for non-structural applications. Furthermore the plastic covering skin with a balsa wood core is discarded due to the fact that it does not offer a lot of impact resistance, especially during landing. The last option that was present is the UHMWPE fibre. It has the lowest density compared to all the other fibres. However, this option is discarded due to the fact that the fibres have difficulty mixing with a resin matrix, therefore they are mostly used for non-structural parts and tend to have problems regarding creep. In the rest of the section the material properties, advantages and disadvantages of the three fibres are discussed.

Aramid fibres

The aramid fibre chosen is the Kevlar 49 high-modules type fibre as shown in figure 7.1 which is primarily used in fibre optic cable, ropes, cables, and composites for marine sporting goods and aerospace applications. Aramid fibres have the highest tensile strength-to-mass ratio among fibres. Additionally, Kevlar shows high energy absorption and ballistic properties, which makes it highly suitable for impact resistance applications. They are readily available in a variety of woven cloth, knits, braids, and stitched fabrics for composite applications. Most commercial matrix resins can be used with aramid fibres, although fibre wet-out is more difficult than with fibreglass or carbon fibres.

Figure 7.1: Kevlar 49 high-modulus fibre sheet.

The main advantages and disadvantages of aramid fibres are summed below:

- Advantages

  Great impact resistance

  High tensile modulus, comparable to glass fibres

  Low density

  Unchanged properties from - 50 to 130 degrees Celsius (thermally stable), small property changes at more extreme temperatures

  Solvent resistance, is unaffected by organic solvents and bases

  Abrasion resistant

  Excellent cyclic stress performance

  Best dampening characteristics

  Best toughness compared to carbon and glass fibres

- Disadvantages

  More expensive than glass and carbon fibres

  Fabric is difficult to cut

  Fibres absorb moisture; can result in freezing problems

  Low compression and shear properties

Glass fibres

Glass fibres which are shown in figure 7.2 can be divided into groups according to their chemical composition. Well known are A-glass, C-glass, S-glass and E-glass fibres, of which only the last two are widely used in aerospace applications. Glass fibres have a high tensile strength, but do not perform as well as carbon fibres. The main advantages and disadvantages of glass fibres are summed up below:

Figure 7.2: Glass fibre fibre sheet.

- Advantages
  - Significantly lower cost
  - Chemical or galvanic corrosion resistant
  - High electric conductivity
  - Wide range of applications
  - Positive thermal expansion
  - Easily machinable
- Disadvantages
  - High thermal expansion coefficient (CTE) compared to carbon fibres
  - Low E-modulus compared to carbon fibres and aramids.
  - Low stiffness and short fatigue life
  - Poor thermal conductivity

Carbon fibres

Carbon fibres, shown in figure 7.3 are high strength, high stiffness fibres that are used for a large variety of structural and electrical applications. Compared to aluminium, carbon fibres have the advantage of being 8 times stronger and 2 times stiffer. When combined with a plastic resin and wound or moulded it forms carbon fibre reinforced plastic (often referred to as carbon fibre) which has a very high strength-to-mass ratio, and is extremely rigid although somewhat brittle. However, carbon fibres are also composed with other materials, such as with graphite to form carbon-carbon composites, which have a very high heat tolerance. The main advantages and disadvantages of carbon fibres are summed below:

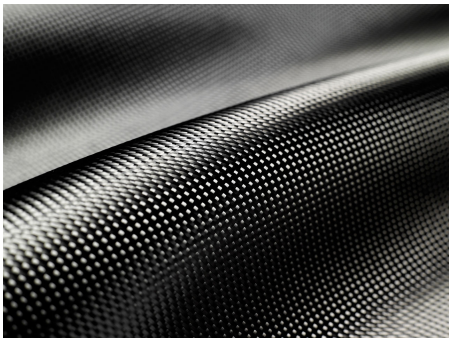

Figure 7.3: Carbon high-modulus fibre sheet.

- Advantages
  - Superior fatigue properties
  - With the right resin, most corrosion resistant material
  - Good thermal stability and high electrical conductivity
  - Good moisture stability
  - Relative high compression strength
  - Good strength-to-mass ratio
  - Best machineability
- Disadvantages
  - relative brittle fibres
  - relative high cost
  - Block communication signals

7.1.2 Core material

This section discusses different core materials. Core materials are used in a sandwich structure, an example of which is shown in figure 7.4, to give a rigid shape to a structure while keeping the top and bottom layer separated from each other. The main load bearing parts are the top and bottom layer which allows for a lightweight core material. Sandwich structures are lightweight and stiff which makes them excellent for the return vehicle. Most cores for UAVs are made of foam.

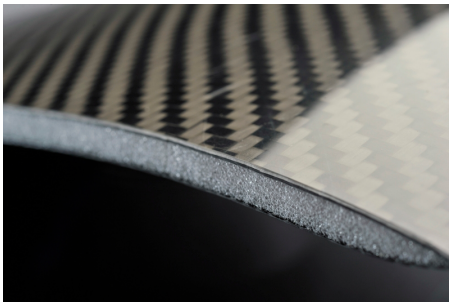

Figure 7.4: Rohacell foam core with a carbon fibre skin

The advantages of foam is the fact that it is extremely lightweight and easy to manufacture. By selecting the right foam, excellent structural properties can be achieved. In the case that these structural properties might appear insufficient it is possible to fortify the foam using composite layup methods, this will be discussed in section 7.2.1.

Other core materials such as cork, balsa wood and aluminium foam were considered. However, they are still considerably heavier than foam, and are therefore not suitable. Honeycomb core material is also discarded because it needs a lot of processability and is hard to incorporate in the wing and fuselage.

7.1.3 Matrix material

To have a good insight in the options for matrix materials the different types of matrix materials and the importance of fibre volume fraction is looked into. Different kinds of fibres also need a resin to form a composite. The first choice that needs to be made in the selection of a resin is whether a thermoset or thermoplastic resin will be used. Most traditional fibre reinforced polymer composites use thermosetting resins. Common thermosetting resins are:

- Polyester resin
- Vinyl Ester resin
- Epoxy
- Phenolic
- Urethane

These resins are easy to use because they are in a liquid state at room temperature. Using a vacuum pump it is easy to remove all air during the process rapidly. The main properties of thermosetting resins are a good fatigue strength, tailored elasticity and excellent adhesion. The downside of a thermosetting resin is that once it has formed a solid state it can not be reformed. This makes the recycling process difficult.

Thermoplastic resins on the other hand are reformable under high temperatures. This should not be a problem as no extremely high temperatures will be reached. Thermoplastic resins also show a much greater impact resistance compared to thermosetting resins. The main downside however is that these resins are in solid state at room temperature. This means the manufacturing process becomes much more complicated and special tools and equipment must be used, which are more expensive. Because of the ease in manufacturing of thermosetting resins these will be favoured over thermoplastic resins. The major advantages of thermoplastic resins are not needed in particular for the return vehicle which implies this resin will not be considered.

7.2 Material trade-off

For the material trade-off different skin, core and matrix materials are considered. In order to determine which material is used for the design, an iterative selection process is used. Since it is important to have a lightweight return vehicle to achieve a high altitude or to be able to take more payload along, the mass is the main design parameter for the material trade-off. A sandwich structure is chosen, this is beneficial because the foam has a low mass and the heavier fibres increases the moment of inertia of the cross section and by doing so reduces the stress. In table 7.1 and 7.2 the material properties of both the fibres and foam are given.

Table 7.1: Fibre properties

fibre	Density $[g/cm^3]$	Tensile strength $[MPa]$	Tensile modulus $[kPa]$	Coefficient of thermal expansion $[10^{-6}/°C]$
E-Glass	2.5	2600	72	1.6
S-2 Glass	2.48	4800	85	0.48
Carbon fibre high modulus PAN	1.84	4209	437	-1.1
Carbon fibre high modulus pitch	2.12	2622	635	-1.45
Kevlar 49 1420 Denier	1.44	2926	109	-2.7
Kevlar KM2 850 Denier	1.44	3429	75	-2.2
Spectra 1000 375 Denier	0.97	2829	103	-
Twaron 1000	1.44	3498	65	-2.2

Table 7.2: Foam properties

Type	ρ $[kg/m^3]$	E_{11} $[MPa]$	E_{22} $[MPa]$	E_{33} $[MPa]$
Spyder Foam	36.84	-	27.57	47.57
Spyder Foam	37.80	8.39	23.15	48.44
Hi-Load 60	36.04	7.58	23.44	41.36
Hi-Load 60a	36.84	8.47	19.43	42.83
Hi-Load 60b	36.84	9.73	19.91	44.20
Foamular 250b	26.11	16.75	13.59	17.07
Foamular 400a	31.71	19.22	20.31	20.27
Foamular 400b	31.71	20.13	21.29	21.28
Foamular 600a	48.69	33.97	33.97	35.21
Foamular 600b	48.69	32.51	33.14	36.20
Stylite a	30.91	12.94	20.03	24.05
Stylite b	30.91	12.73	19.67	23.55
Rohacell 31	30.43	35.30	35.30	35.30
Rohacell 51	49.65	68.60	68.60	68.60

To start the iterative design, Kevlar 49 is chosen because it has a low density and a Rohacell 31 core is selected, since this will result is the lowest possible mass for the return vehicle. For the first iteration a Kevlar 49 1420 Denier woven fibre is chosen with a thickness of 0.071 mm, the lowest thickness available. Another reason why the Rohacell 31 core is chosen is because it protects the return vehicle during a belly landing. Furthermore Rohacell RIMA series are developed to reduce the amount of absorbed resin by the foam, which is beneficial for the total mass of the return vehicle.

7.2.1 Orientation and placement of fibres

For the orientation and placement of the fibres Kolibri [32] is used. This program is used as a design and analysis tool for composite materials and structures, plates and beams can be analysed by defining the core as well as the skin material's mechanical properties. When the plates mechanical properties and the dimensions are defined, the edge of the beam is clamped to represent a cantilevered beam. A report can be generated showing the complete laminate stiffness summary, the displacements, strains and curvatures and the forces and moments the beam can withstand, but also eliminates unwanted bending coupling. By having a balanced layup stretching/shearing coupling is eliminated.

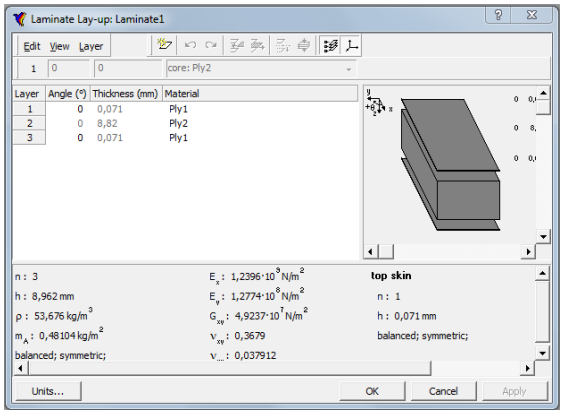

Figure 7.5: Kolibri interface, displaying lay-up of the laminate, ply orientations and laminate properties

Figure 7.5 shows the mechanical properties of the entire laminate, after the individual mechanical properties of the Kevlar 49 fibres and the Rohacell 31 foam are inserted. Furthermore it shows the orientation angle of the layers, as well as their thickness. A balanced and symmetric laminate is chosen because the symmetry prevents internal stresses which can cause delamination. The same method is applied for the spars and bulkheads.

7.2.2 Final Material selection and loads

To conclude the return vehicle will be produced from a Kevlar 49 fibre in a [0/90] degrees orientation, a Rohacell 31 foam core and will be bonded with an epoxy resin. The driving factor behind this material choice is the design for the lowest possible mass.The maximum stress this composite laminate can withstand is $1240MPa$ where the required stress the wing need to withstand is 164.4 MPa which exceed the required strength broadly. The spars and bulkhead will be produces by also using the Kevlar 49 fibers and the epoxy resin. The orientation of the fibres are [$\pm$ 45, 0/90, $\pm$ 45], this means that the spars and stringers can withstand a shear force of 252.81 MPa. This is expected to be high enough to take up the loads.

From Hookes law (equation 7.1), elongation is linearly proportional to tensile stress σ by a constant factor, the inverse of the modulus of elasticity E.

$$\sigma = E \cdot \epsilon \tag{7.1}$$

Furthermore we have the stress equation for bending:

$$\sigma = M_x \cdot y / I_{xx} \tag{7.2}$$

Knowing from equation 7.2 and the data from aerodynamics that $\sigma_{max} = 5.77\ MPa$ and the maximum elongation for both the foam and the kevlar 49 fibres is 3.5% at break, the needed minimum stiffness of the laminate is 164.86 MPa. The only unknown in formula 7.1 is the minimum stiffness our laminate needs to withstand the maximum force. The layup and E-modulus is found using Kolibri, which has been further discussed in section 7.2.1

7.3 Structural loads

To ensure structural integrity for several flights a maximum load factor needs to be determined from the mission profile. There are uncertainties that make this determination difficult and require a large safety factor. This risks the structure to be too strong and thus too heavy. The possibility of breaking the sound barrier is present, leading to complex flutter behaviour. Exact structural loads accompanied by this are difficult to predict and are again taken with a considerable safety factor.

7.3.1 Loading diagrams

In this section the flight loads for the return vehicle are examined. Based on a Vn-diagram, shown in figure 7.6, the maximum allowable load factors and design speeds are determined. These load factors will be used throughout the detailed design. The Vn-diagram, and thus the flight envelope, is limited by the maximum amount of lift that can be produced by the wings, the stall speed, the maximum dive speed and the gust loadings that can be expected.

The first curves on the Vn-Diagram, indicated in figure 7.6, are the ones that are based on the maximum amount of lift that can be produced by the aircraft at each flight speed. Either the maximum upward or maximum downward is considered. The load factor versus flight speed is given by equation 7.3.

$$n_{stall} = \frac{\frac{1}{2} C_{L_{max}} \rho V^2 S}{W} \tag{7.3}$$

This equation is filled out for sea level conditions and a $C_{L_{max}}$ of 0.7 for the positive lift case and $C_{L_{max}}$ of -0.5 for the negative lift case. The surface area and mass are taken from section 2. These lift curves are shown in figure 7.6 as dotted curved lines starting at the origin.

The next line in the diagram is the dive speed. The dive speed is the maximum speed that can be achieved under any condition during the flight. This dive speed is assumed to be equal to the terminal velocity of the return vehicle in a straight down dive. In this situation the drag is equal to the weight and the drag coefficient is equal to the zero lift drag coefficient. This terminal velocity and thus dive speed can be found using equation 7.6

$$D = \frac{1}{2} C_D \rho {V_D}^2 S \tag{7.4}$$

$$V_D = \sqrt{\frac{2D}{\rho S C_D}} \tag{7.5}$$

$$V_D = \sqrt{\frac{2W}{\rho S C_{D_0}}} \tag{7.6}$$

The dive speed is found by filling out the weight, surface area and air density as given before and an assumed C_{D_0} value of 0.015. The next curves on the Vn-diagram are the gust loading

lines. These equations are taken from CS-25 regulations and are presented in equations 7.7 through 7.9.

$$n_{gust} = 1 + \frac{\rho V a K_g U_{de}}{\frac{W}{S}} \tag{7.7}$$

where,

$$K_g = \frac{0.88\mu_g}{5.3 + \mu_g} \tag{7.8}$$

and,

$$\mu_g = \frac{2\frac{W}{S}}{\rho \overline{C} a} \tag{7.9}$$

Where the air density is taken at sea level, a is the lift curve slope and is taken to be 4.2 rad^{-1} and U_{de} is either $\pm$ 7.62 m/s or $\pm$ 15.24 m/s. With these four values for U_{de} four different lines can be plotted. The final variable needed is the MAC which is given as 0.141 m. The four gust loading lines are given in figure 7.6 as dot-dash lines where the gust lines with the higher values of U_{de} are the steeper lines. The maximum load factors, both positive and negative, are found by finding the intersection point between the dive speed and the 7.62 m/s gust lines. At the intersection points the load factors are 23.1 and -22.1.

Another important speed is the manoeuvring speed (V_A). This is the highest speed for which $C_{L_{max}}$ can be used without exceeding the maximum load factor. Equation 7.11 can be used to calculate the manoeuvring speed.

$$n_{maxload} = \frac{\frac{1}{2} C_{L_{max}} \rho {V_A}^2 S}{W} \tag{7.10}$$

$$V_A = \sqrt{\frac{2 n_{maxload} W}{\rho S C_{L_{max}}}} \tag{7.11}$$

The intersection points of the dive speed and the 7.62 m/s gust lines and the intersection points of the manoeuvring speed and the stall lines are connected with a horizontal line. This together with the stall lines and a stall speed of 12 m/s form a closed contour in the diagram which is the flight envelope (shown in a thick line). Note that the 15.62 m/s gust lines are outside of the flight envelope, this means that such a gust would make the return vehicle stall. The complete Vn-diagram is shown in figure 7.6. The major outcomes of this diagram are summarised in table 7.3

Table 7.3: Flight loads summary table

Parameter	Value	
Max load factor	23.1	
Min load factor	-22.1	
Dive speed	81.7	m/s
Stall speed	12	m/s
Manoeuvring speed	57.5	m/s

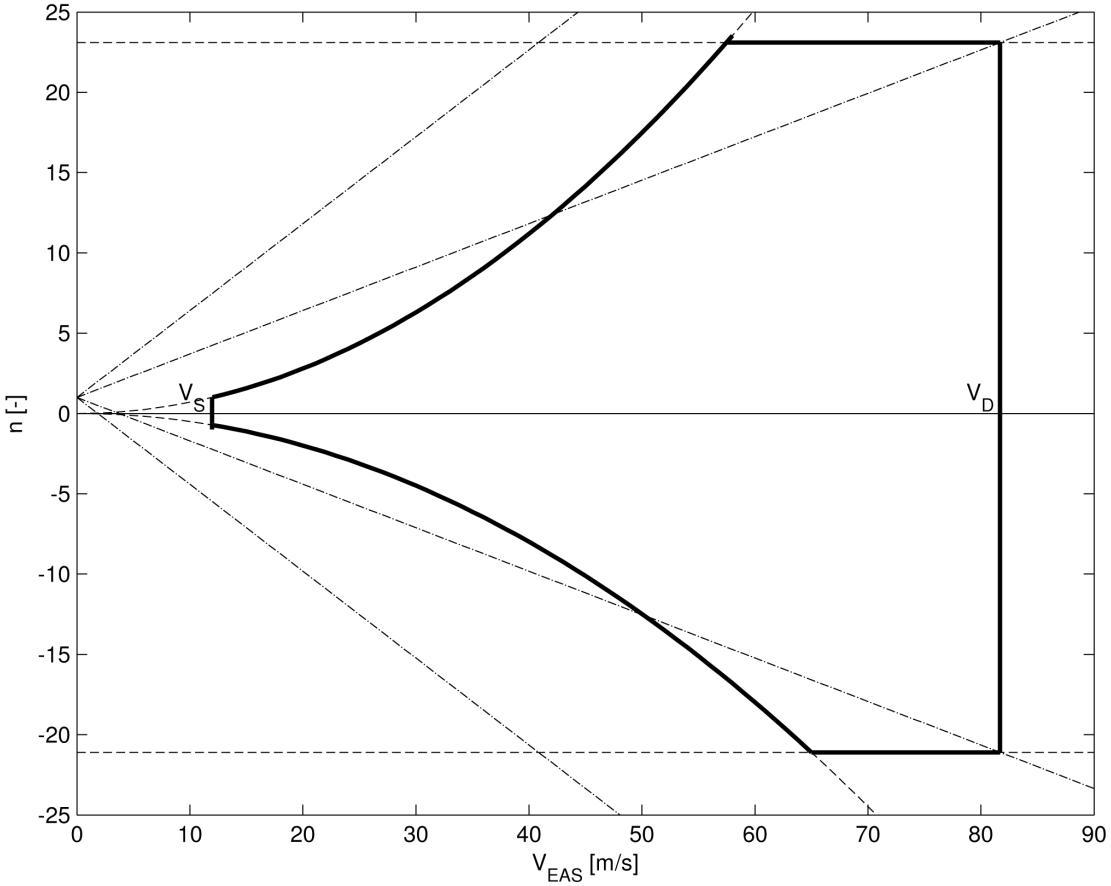

Figure 7.6: Complete Vn-diagram, indicated on the horizontal is the airspeed and on the vertical axis the load factor. Gust lines are the dashed-dotted lines, starting at n=1 and V=0. The maximum dive speed Vd is indicated with the thick vertical line at an airspeed of 81.7 m/s. The stall speed is indicated with the thick vertical line at an airspeed of 12 m/s. The aircraft should stay within the thick lined region to fly within the structural limitations.

7.3.2 Bending stress

To calculate the effects of the force on the wing induced by the lift force a stress analysis has been performed. In order to do this the bending moment calculated in the mid-term report has initially been used. After doing preliminary stress calculations with this load case a lift distribution from the aerodynamic design has been taken to compare with the theoretical elliptical lift distribution. The goal of this section is to provide a maximum stress resulting from a bending moment. Also the location where this maximum stress occurs will be found.

Firstly the distributed load imposed on the wing has been assumed to be the main force experienced by the wing. Integrating this distributed force with respect to the y-axis according to the F_B reference frame [36] gives the shear force experienced by the wing. Integrating again along the same axis gives the moment along the wing.

From the moment distribution the stress distribution can be calculated using equation 7.12 [37]. In this equation the x- and y-axis are again oriented according to the F_B reference frame. Along with the moment distribution the moment of inertia about the x-axis is also needed for

this calculation. This moment of inertia can be approximated using equations 7.13 - 7.15 where K_I is a constant equal to 0.036 for conventional airfoils [33].

To calculate the moment of inertia a linearly varying chord length has been used and the airfoil parameters for the S3016 airfoil have been used for the thickness (τ) and camber (ϵ). For the fuselage a chord of 300 mm has been used while still assuming an airfoil shape, hence the moment of inertia of the fuselage is also calculated using equation 7.13. Also in equation 7.12 the value used for y is equal to half of the airfoil thickness as the neutral bending line has been assumed in the middle of the airfoil. In reality the neutral line is slightly higher because of the camber which is present in the airfoil.

$$\sigma_z = \frac{M_x}{I_{xx}} z \tag{7.12}$$

$$I_{xx} \approx K_I c^2 \tau (\tau^2 + \epsilon^2) \tag{7.13}$$

$$\tau = \frac{t}{c} \tag{7.14}$$

$$\epsilon = \frac{h}{c} \tag{7.15}$$

From these calculations the stress distribution has been obtained. It is plotted in figure 7.7 along with the moment, shear and load distribution which were calculated earlier. The maximum stress location is found at the root of the wing. Because the center line has been assumed in the middle of the airfoil the compressive stress is equal to the tensional stress.

As can be seen the simulation data and the XFLR 5 data are relatively close to each other. This means the initial assumptions made in the baseline report resemble reality quite well. In reality the neutral line is not on the centerline of the airfoil which causes a large difference between the simulated data and the XFLR 5 data. The XFLR 5 data gives higher values, and for safety this will be used for future reference. The simulation data has been plotted for verification purposes.

Furthermore the plots show a major jump in the shear stress diagrams. This occurs because the moment of inertia of the fuselage is much greater than the moment of inertia of the wing. The maximum stress was found to be 5.77 MPa from the XFLR 5 data. Because the step size used for the aerodynamic data is rather small the jump occurs too early, therefore the maximum stress will be slightly higher in reality but the safety factor accounts for this.

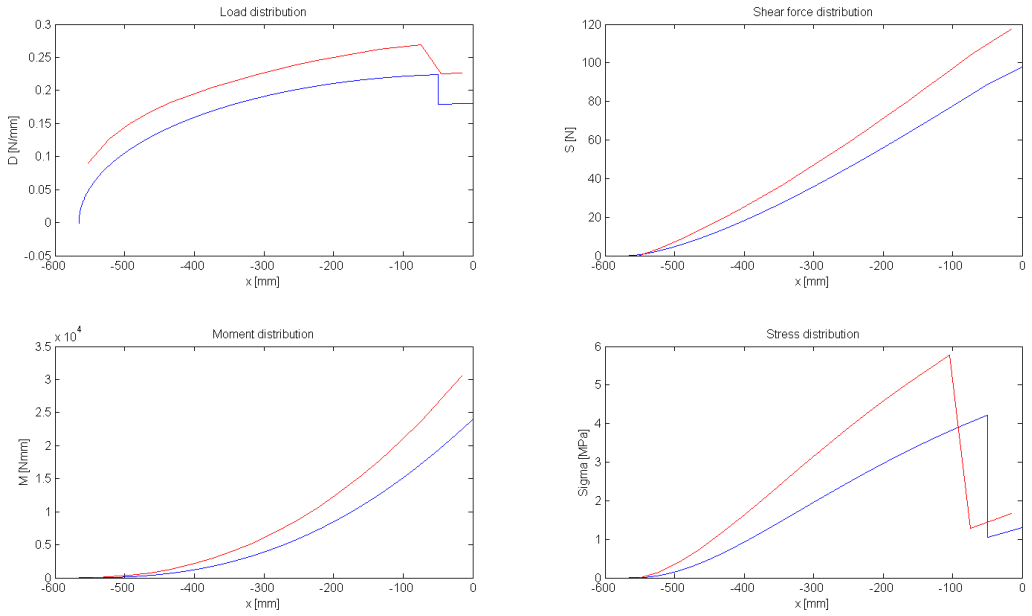

Figure 7.7: Load, shear, moment and stress distribution from wing tip (x=-b) to center line (x=0) for simulation data (lower line) and XFLR data (upper line). The plots are symmetrical with respect to the left and right wing.

7.4 Design loads

The design load is the maximum load the return vehicle is designed to withstand. Table 7.4 shows the maximum loads the return vehicle will experience in its lifetime. Where the third column shows the maximum loads the return vehicle is designed for to withstand.

Table 7.4: The calculated maximum loads the return vehicle will experience and the maximum loads the structure can withstand

Property	Max experienced	Max withstand
Maximum load factor	23.1	
Maximum bending stress $[MPa]$	5.77	43.37
Maximum shear force $[N]$	117.5	2153
Maximum bending moment $[Nmm]$	$3.055 * 10^4$	$3.98 * 10^4$
Wing eigen frequency $[H_z]$	24.8	72.34

After the entire return vehicle is drawn in Catia V5, as can be seen in chapter 9, a Finite Element Method is used to perform a complex structural simulation. The structural simulation shows a detailed visualization of where the structure will bend or twist and shows the values of distribution of the stresses and displacements. Catia V5 has an integrated tool to perform this structural analysis and is used to see whether structure and material can safely withstand

the specified forces and find the critical stresses in each part. Figure 7.8 shows the structural analysis of the return vehicle, where the wing is split into two parts and clamped in the middle of the fuselage to have a representative case. The material properties of the laminate are inserted as defined in section 7.2.1.

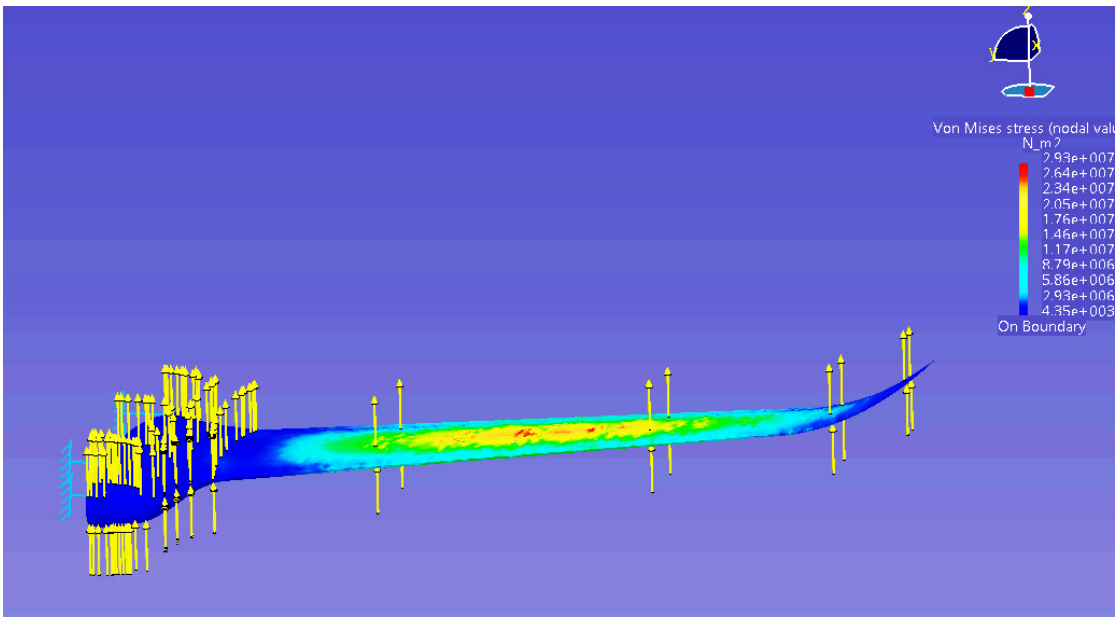

Figure 7.8: Fem analysis of the right wing. The magnitude of the von Mises stresses (N/m^2) on the wing are indicated in the colorbar in the top right of the figure. Model generated in Catia

As can be seen in the figure 7.8, the largest stresses occur around the middle of the wings. The maximum stress is 29.3 MPa. The stress is lower near the root of the wing due to the fact that more material is present to take up these loads. The lower stress near the tip is due to the fact that a lower wing loading is acting on the wing tip, because an elliptical wing loading is assumed. Further the maximum wing tip deflection is 6.57 mm upwards as can be seen in figure 7.9.

7.5 Carbon Tube

The bending loads imposed by the tail surfaces on the carbon tube, which serves as a tail, have been calculated. In order to do this the wing loads on the vertical and the horizontal tailplane have been taken in nominal flight conditions as $F_v = 1.05\ N$ and $F_h = 2.2\ N$ from the aerodynamic design. Applying the maximum load factor $n = 23.1$ gives a maximum load case of $F_{v_{max}}$ and $F_{h_{max}}$. Using the method of Pythagoras, a safety factor of 1.5 and a tail length of 500 mm the moment was obtained using equation 7.16. Furthermore the moment of inertia of a hollow tube is defined in equation 7.18. Subsequently the stress as a result of this moment is found using equation 7.17.

$$M_{tail} = SF \cdot l_t \sqrt{{F_{v_{max}}}^2 + {F_{h_{max}}}^2} \tag{7.16}$$

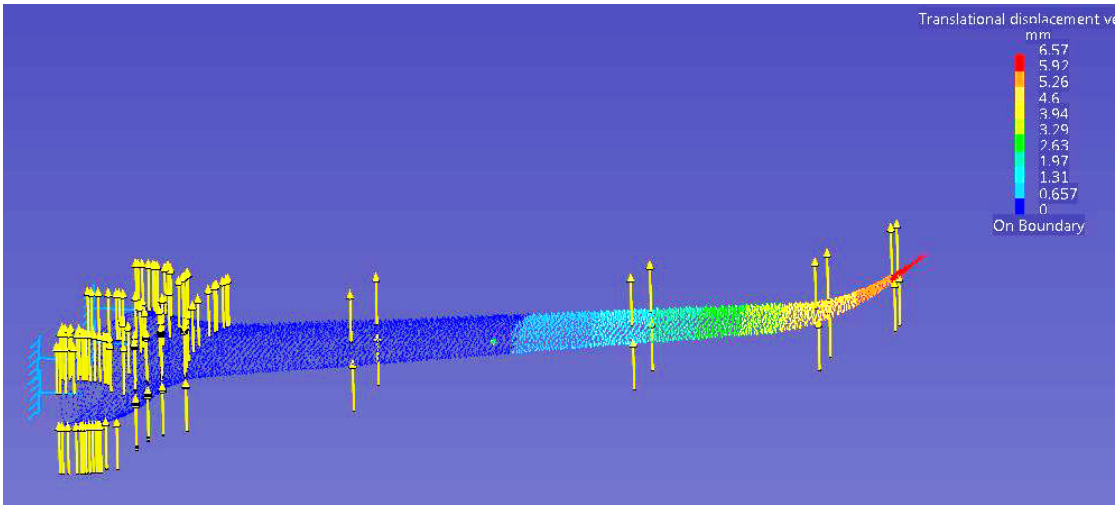

Figure 7.9: Displacement (mm) of the wing tip (upward positive). Magnitude indicated in the colorbar on the top right of the figure. Model generated in Catia

$$\sigma_{tail} = \frac{M_{tail}}{I_{tube}} r_o \tag{7.17}$$

$$I_{tube} = \frac{\pi}{4}({r_o}^4 - {r_i}^4) \tag{7.18}$$

In these equations M_{tail} is the moment imposed on the tail, r_o is the outer radius of the rod and r_i is the inner radius. From these calculations the maximum stress is found at the body. It is calculated to be 341 MPa. The failure stress is calculated using equation 7.1 and is found to be 14.45 MPa. Therefore it can safely be said that the carbon tube can carry the loads implied by the tail.

7.6 Control surfaces

The control surface design will be elaborated in this section. First the servo torques needed for the different control surfaces are calculated. Second the flaps are designed and the different parts needed for the control surface configuration are listed. Finally a figure showing the control surface layout wis shown.

7.6.1 Servo torques

To calculate the servo torques first the control surface layout needs to be known. This has been found in section 5.4 and is summed up in table 7.5

Table 7.5: Control surface dimensions

Control surface	Chord [cm]	Length [cm]	Maximum deflection [$\circ$]
Ailerons	3.5	20	20
Elevator	3.5	34	20
Rudder	3.5	15	20

These values have been used to calculate the torques needed for the servos. The torques have been calculated using a workbook frequently used for radio controlled aircraft [34]. The assumptions used were:

1. The angle of attack of the wing is zero
2. Angular velocity and acceleration of the aircraft is zero
3. Air flow may be modelled using the concept of dynamic pressure
4. Conditions are: sea level and zero humidity
5. Control linkages have zero offset at hinge line and are perpendicular to horns at neutral
6. Control mechanisms are frictionless and surfaces are mass-balanced
7. The wing and control surfaces are thin, flat slabs
8. No aerodynamic counterbalances are used
9. The push rods are significantly longer than the servo and control horns

Torques were calculated using equation 7.19, the symbols used are explained in table 7.6.

$$T_{servo} = \frac{sin(\delta_{cs})\frac{tan(\delta_{cs})}{tan(\delta_s)} M_a P {c_{avg}}^2 l V^2}{4 R_g T} \tag{7.19}$$

Table 7.6: Symbols used to calculate servo torque

Symbol	Unit	Description
δ_{cs}	$^\circ$	Control surface deflection
δ_s	$^\circ$	Servo arm deflection
M_a	g/mol	Molecular mass of air
P	Pa	Air pressure
c	cm	Average chord length
l	cm	Average control surface length
V	m/s	Velocity
R_g	$Pa \cdot cm^3/mol \cdot K$	Ideal gas constant
T	K	Air temperature

Using this method the control torques needed are computed and listed in table 7.7. The table lists the torques needed for different flight speeds up to the terminal velocity of of 81.8 m/s . From these calculations the maximum torques are 0.7 $kg \cdot cm$, 1.3 $kg \cdot cm$ and 0.6 $kg \cdot cm$ for respectively the aileron, elevator and rudder. Using these values the servos have been selected. They will be listed in this section along with the other components needed for the control surfaces.

Table 7.7: Servo torques needed for different flight speeds and control surface deflections

	$\delta_{a,e,r}$ [○]	δ_{servo} [○]		T_{servo} $[kg \cdot cm]$						
			V $[m/s]$:	20	31	41	51	61	72	82
Ailerons	20	40		0.0	0.1	0.2	0.3	0.4	0.6	0.7
	17	33		0.0	0.1	0.2	0.3	0.4	0.5	0.7
	14	27		0.0	0.1	0.1	0.2	0.3	0.5	0.6
	11	21		0.0	0.1	0.1	0.2	0.3	0.4	0.5
	8	15		0.0	0.1	0.1	0.1	0.2	0.3	0.4
	5	9		0.0	0.0	0.1	0.1	0.1	0.2	0.2
	2	4		0.0	0.0	0.0	0.0	0.1	0.1	0.1
Elevators	20	40		0.1	0.2	0.3	0.5	0.7	1.0	1.3
	17	33		0.1	0.2	0.3	0.5	0.7	0.9	1.2
	14	27		0.1	0.1	0.3	0.4	0.6	0.8	1.0
	11	21		0.1	0.1	0.2	0.3	0.5	0.6	0.8
	8	15		0.0	0.1	0.2	0.2	0.3	0.5	0.6
	5	9		0.0	0.1	0.1	0.2	0.2	0.3	0.4
	2	4		0.0	0.0	0.0	0.1	0.1	0.1	0.2
Rudder	20	40		0.0	0.1	0.1	0.2	0.3	0.4	0.6
	17	33		0.0	0.1	0.1	0.2	0.3	0.4	0.5
	14	27		0.0	0.1	0.1	0.2	0.3	0.3	0.4
	11	21		0.0	0.1	0.1	0.1	0.2	0.3	0.4
	8	15		0.0	0.0	0.1	0.1	0.2	0.2	0.3
	5	9		0.0	0.0	0.0	0.1	0.1	0.1	0.2
	2	4		0.0	0.0	0.0	0.0	0.0	0.1	0.1

7.6.2 Control surface layout

With the servo torques known firstly two types of servos have been selected. The selected servos are a 0.8 $kg \cdot cm$ servo for both of the ailerons and the rudder and a 1.5 $kg \cdot cm$ servo for the elevator. A full list of components needed can be seen in table 7.8 and the control surface layout can be seen in figure 7.10. This layout uses nylon clevis to connect control rods to the control surfaces.

A rocker is present in the main wing cut-out, allowing the control rod to transfer push and pull forces around the corner in a frictionless way. Other considered methods were to guide the control rod in a curved fashion along the wing and to use a push-bar instead of a rod which is inflexible and provides a direct link to the ailerons but does so at an angle less than perpendicular to the aileron. However the first option provides a large increase in friction and the latter option is highly inefficient because of the small angle under which the bar can be placed with respect to the aileron.

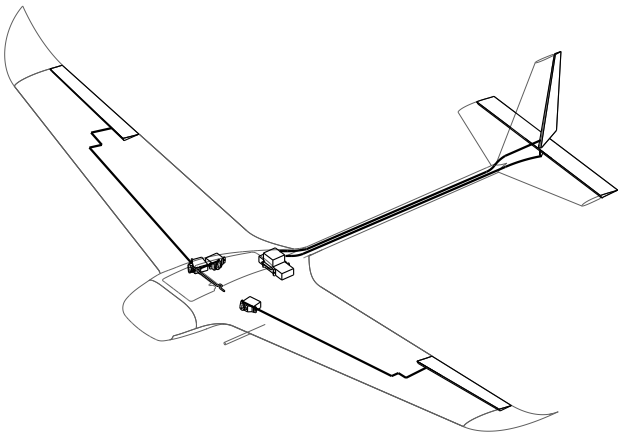

Figure 7.10: Control surface layout showing the servos, control rods, aileron, elevator, rudder and parachute release bar. The kings in the rods present in the wings are rockers, allowing forces to be transferred around the corner in a frictionless way

Furthermore the way in which the ailerons and elevator will be created can be seen in figure 7.11. These control surfaces will be produced by simply cutting off a piece of the wing and then removing the corner pieces, leaving a small triangular cut-out which allows the control surface to rotate. The cut-out will be made at the bottom of the airfoil because this is where the aerodynamic shape will be affected least. As a hinge the aramid fibres will be used. This hinge is created by breaking the resin on the hinge line, allowing for rotation.

For the rudder a slightly different approach will be used because it has to be symmetric. The rudder layout is also displayed in figure 7.11 and has a triangular cut-out at both the top and bottom of the airfoil corner. The hinge line will be placed in the middle. It will use off-the-shelf hinges instead of the hinge technique that will be used for the aileron and elevator.

Table 7.8: Control surface parts list

Part	Amount
Hinges	4
Aileron servo (0.8 $kg \cdot cm$)	2
Rudder servo (0.8 $kg \cdot cm$)	1
Elevator servo (1.5 $kg \cdot cm$)	1
Control horn	2
Servo arm	4
Nylon clevis	4
Control rod	6

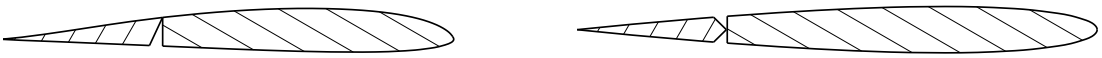

Figure 7.11: Cross section of aileron/elevator (left) and rudder (right)

7.7 Manufacturing methods

This section describes the manufacturing methods used for the materials and structures. Different manufacturing methods presented in the mid term review were considered and a choice on the method to be used is made. It focuses on production of the first prototype which will be done by the team itself using TU Delft resources. For the units which will be produced after this first prototype a different production method will be used. These will not elaborated upon in detail.

From section 7.1 the main materials to be used for the structure have been determined: Rohacell 31 foam, aramid 49 fibers and epoxy resin. For these materials appropriate manufacturing methods were decided upon in order to achieve the desired shape while staying within the available resources.

An important criteria in the selection process is the knowledge and experience of different team members on the field of production techniques. The reason for this is that a first prototype needs to be finished for the symposium which concludes the DSE. Therefore the factors workload and chance of failure were also important in the selection of a suitable production method.

Factors which influence the trade-off to a lesser degree are cost and quality. While these factors are certainly important they are not considered a major issue if they are not optimal because factors mentioned earlier were deemed more important. For a later stage, after the first prototype, these criteria will become much more important.

7.7.1 Foam

For the foam three different manufacturing methods were considered: Hot wire cutting, which can be done using a CNC cutter and a manual cutter, and structural foam moulding. The main difference is that for the hot wire cutting process it is possible to create a desired shape which can also be used as a mould for the fibre layup. For the structural foam moulding process a mould is needed in advance which adds complexity, the mould also needs to be of high quality to ensure smooth propagation of the foam throughout the shape. This method has a high chance failure, therefore careful planning and practice are required.

The main advantage of the CNC hot wire cutter is the fact that it is available at the TU Delft MAVlab and ready for use for the team. The team also has experience in using the CNC hot wire cutter from a previous prototype. This means this method is inexpensive and reliable. A downside is the fact that the desired shape can not be cut from a single block of foam so it needs to be constructed from different parts which need to be glued together. This method induces weak spots in the structure, however these weak spots are not expected to reach a critical level. For these reasons the CNC hot wire cutting method will be used.

For a later model structural foam moulding can also be used but this is too expensive and not readily available for a first prototype. In a later stage this will become less of an issue and the advantages of this method are significant.

7.7.2 Composite

For the composite layup four processes were considered: Resin transfer moulding (RTM), prepreg layup, wet layup and spray-up. Firstly the spray-up method was eliminated because this method provides poor structural properties due to its fibres being oriented in a random orientation. Also it is difficult to control the thickness of a sprayed layer of composite. Expertise is needed to achieve a constant fibre-volume fraction using this method, making the possibility of errors significant for the team as this expertise is not present.

Secondly the prepreg method has been omitted. It is very similar to wet layup, the main difference is that prepreg sheets are harder to preserve as they need a specific temperature and the hardening process also needs specific temperature and pressure conditions. This adds extra complexity and cost to the design but the gain in quality is significantly better. Prepregs will give a higher volume fraction but this difference is not extremely important compared to the complexity and cost. Furthermore a decent fibre-volume fraction can also be achieved with the wet layup process by an experienced manufacturer. Since some team members have experience in working with composites, it must be possible to achieve a reasonable result with this method.

The remaining processes, RTM and wet layup are both suitable for the return vehicle. RTM yields a higher fibre-volume fraction than wet layup so in terms of quality this method is preferred. However the chance of failure is also larger and needs to be minimized using trail and error. More preparation is also needed than when using the wet layup method. The wet layup process is preferred by the team for these reasons. Also the team has more experience using this method which further reduces the possibility of failure, which was deemed one of the most important trade-off criteria.

For a later model the wet layup process will not be used because cost and complexity will be less important. The team will consider RTM and prepregs for this stage.

7.8 Production plan

This section describes a detailed production plan for the first prototype. The section first presents a part production plan for the required parts that need to be produced. After this an assembly plan is shown which presents a step-by-step approach towards building a prototype. The production plan for a later model will look slightly different as different production techniques will be used, also mentioned in section 7.7. This stage is not explained in detail in this section and will be part of a post-DSE plan.

7.8.1 Parts production

Because the design philosophy has been from the start to use as many off-the-shelf products as possible there are relatively few parts that the team needs to produce. This is beneficial in terms of production time and reduces the chance of failure. The parts that need to be produced before assembly are the framework, top skin, bottom skin and foam cores. These parts need to be produced in a specific order and the details will be outlined chronologically in this section. First the Foam core will be explained, secondly the composite parts are manufactured and finally cut-outs in the foam core and skin can be made.

Foam core

The foam core is the first part that needs to be manufactured. It is important that this is done first so the foam can be used as a mould in a later phase. The foam core will consist of seven parts for the body and two parts for the tail, these parts will be cut using the CNC hot wire cutter at the TU Delft. It was decided to split the foam body core into seven pieces because this fits best in the structure of the vehicle, the CNC cutter is also unable to cut the entire geometry

at once. The layout of the seven pieces can be seen in figure 7.12. The horizontal and vertical tail cores will be cut from a single piece and are shown in figure 7.13.

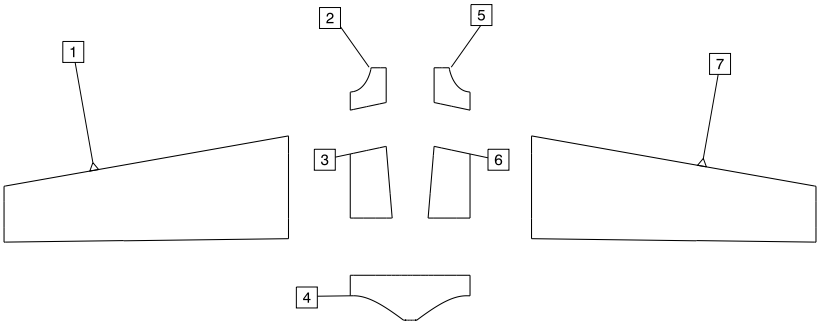

Figure 7.12: Vehicle body foam cores geometry and position layout

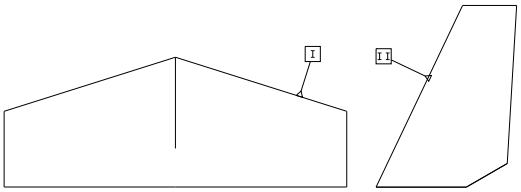

Figure 7.13: Tail foam cores geometry

When producing these parts the wings will be cut from single pieces. The CNC cutter can shape these pieces to approximately the desired geometry so little polishing needs to be done. The fuselage piece needs a different approach. First all the foam pieces (Part 2-6 in figure 7.12) which together form the fuselage will be cut from one piece. Because the CNC cutter is unable to create the exact desired geometry the team will need to polish the foam to the desired geometry. When this is done the wings can be attached to the fuselage using simple epoxy glue to create a so-called foam model. This foam model represents the exact geometry of the return vehicle but consists purely of foam. It is used in the following section.

Composite parts

The foam model will function as a plug for the top and bottom skin. Because it has the exact dimensions of the final shape it can be used to create a glass fibre mould to use for the laminating process. When the laminating process is finished a top and a bottom skin will be created. The detailed production steps for the moulds are outlined below:

1. Place the plug on a clean working surface
2. Cover the plug with primer
3. Polish the primed plug to create a smooth surface
4. Apply release agent to the plug

5. Place glass fibres on the plug. Layers can be added in different directions to achieve the desired stiffness
6. Apply resin on glass fibres, applying too much or non-uniform amount of resin is allowed as this is only a mould
7. Fold vacuum bag sheet to close off the entire shape
8. Apply an air outlet to the vacuum bag
9. Seal vacuum bag using tacky tape
10. Seal the outlet using extra tacky tape
11. Create vacuum in the bag using a vacuum pump
12. Check for air tightness of the bag
13. Wait for the composite to cure, approximately 24 hours at room temperature
14. Remove the vacuum bag
15. Repeat process for bottom skin mould

Next the actual skin needs to be produced from aramid fibres:

1. Clean the glass fibre mould using acetone
2. Apply a release agent to the mould
3. Impregnate the aramid fibres using epoxy
4. Layup the fibres in the 0/90° orientation
5. Use a roller to remove excess resin
6. Insert a bleeder to allow excess resin to flow out
7. Seal the structure using peel ply
8. Apply tacky tape to the edges of the mould,
9. Insert an air outlet
10. Apply extra tacky tape at the air outlet
11. Close vacuum bag
12. Apply vacuum
13. Check for air tightness of the vacuum environment
14. Wait for the resin to cure, approximately 24 hours at room temperature
15. Remove the vacuum bag
16. Cut off rough edges
17. Repeat process for bottom skin

For the structural ribs a similar process is used. The rib layout can be seen in figure 7.14. The moulds to be used for these parts are flat plates for ribs R1 and R5 and foam plates which were cut in the shape of ribs R3, R4 and R6.

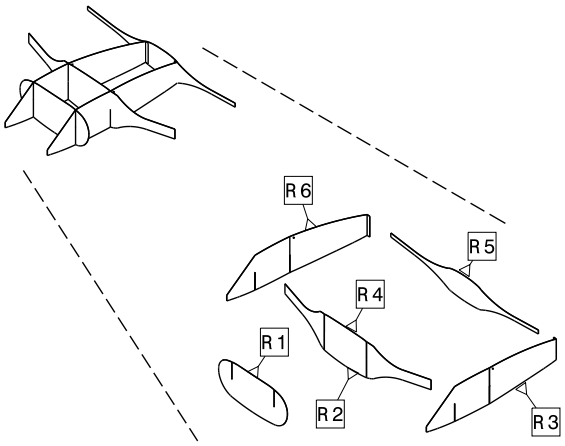

Figure 7.14: Internal frame layout

1. Clean the plate mould
2. Apply a release agent to the mould
3. Apply tacky tape to the edges of the mould,
4. Insert an air outlet
5. Apply extra tacky tape at the air outlet
6. Impregnate the aramid fibres
7. Layup the fibres in the [±45° 0/90 ±45°] orientation
8. Use a roller to remove excess resin
9. Insert a bleeder
10. Seal the structure using peel ply
11. Close vacuum bag
12. Apply vacuum
13. Check for air tightness of the vacuum environment
14. Wait for the resin to cure, approximately 24 hours at room temperature
15. Remove the vacuum bag
16. Cut the desired shapes from the obtained sheets using a Dremel power tool
17. Drill two holes in the ribs oriented in the flight direction to account for the parachute release bar

Foam cut-outs

With the foam cores complete and the plug not needed any more to manufacture composites the foam model can now be shaped into its final layout. To account for the various parts that need to be placed in the wing various cut-outs need to be made. The desired structure with all its cut-outs can be seen in figure 7.15. The cut-outs are explained in table 7.9

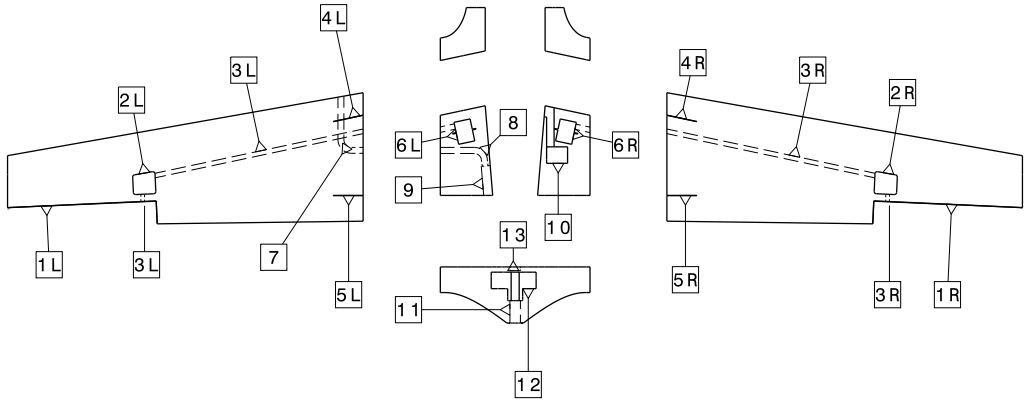

Figure 7.15: Foam Cores with all cut-outs. Dotted lines indicate a cut-out below the surface to accommodate for a rod or a tube. A solid line indicates a cut-out at the surface

Table 7.9: Foam cut-out description

Cutout label	Description
1L, 1R	Aileron
2L, 2R	Control rod hinge
3L, 3R	Control rod gutter
4L, 4R, 5L, 5R	Bulkhead cut
6L, 6R	Aileron servo
7, 8	Pitot tube gutter
9	Airspeed micro sensor
10	Parachute servo
11	Carbon tube hole
12	Elevator and rudder servos
13	Hot wire cutter

The square shaped cut-outs(2L, 2R, 6L, 6R, 10 and 12) will be made using a Stanley knife. This method will be used to cut out a square block from the structure, cutting trough the core from the top skin to the bottom skin. From this block another cut out will be made which has the size of the desired servo. The remaining pieces of foam will be glued back in the return vehicle to serve as respectively a lid and a bottom to seal the servo cut-out. First the bottom will be glued in and the lid will be placed on top of the cut-out in the final stage, before applying the top skin. The only cut-outs without a bottom and a lid are 3L and 3R.

The cut-outs for the push/pull rods are also created using a knife. They are made by cutting out a triangular piece from the top of the wing. After removing this piece the bottom of the triangular shape is removed and the remaining shape is placed back in. This leaves a free space for the rod. A clarifying image can be seen in figure 7.16. The aileron cut-outs were described in section 7.6.2 and will also be made using a knife. A hole also needs to be drilled (11 in figure 7.15) to account for the carbon tube which serves as a tail. This is done using a 14mm drill.

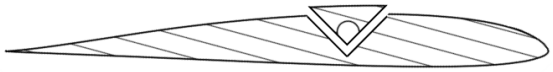

Figure 7.16: Cross section of wing showing a control rod cut-out

To connect all the pieces cable gutters are needed all over the foam core. These will be created using a soldering iron. The soldering iron is heated and used to melt away some of the foam. This has as an advantage that the cut-outs are sealed immediately because of the heat. This method is also used for the pitot tube gutter which is placed at the bottom of the core.

Finally some cut-outs needs to be made in the tail cores to account for the XBee module, carbon rod and control surfaces. A square cut-out is made for the XBee module (T1), also the gutter for the antenna will be melted out using the soldering iron (T6). Gutters are needed for the wiring as well. A 14 mm hole is drilled to account for the carbon rod (T5) and the elevator (T4) and rudder (T3) will be created as explained in section 7.6.2. The exact layout can be seen in figure 7.17.

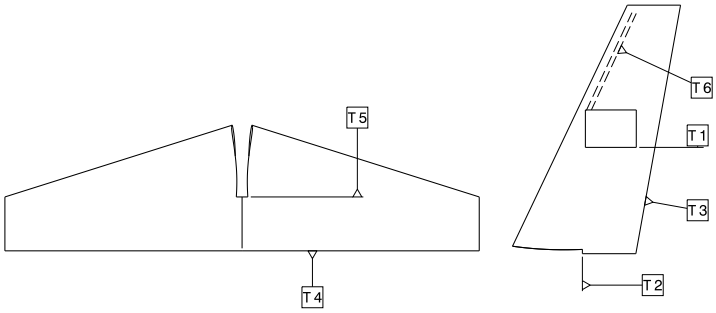

Figure 7.17: Tail foam cores including all cut-outs

7.8.2 Assembly

With the parts produced the assembly can be initiated. This section provides a step-wise assembly plan. First the tail assembly will be discussed and second the assembly of the main body is covered.

Tail

The order of assembly for the tail:

1. Place foam core on a clean surface
2. laminate using wet layup, process is similar to the process described in section 7.8.1
3. Initiate a cut originating at the bottom
4. Cut trough the bottom skin and foam core, leaving the top skin intact
5. Cut off a corner to allow the elevator to rotate
6. Insert a clevis in the elevator, making it stick out at the bottom. See section 7.6.2 for details on the elevator layout.

7. Using a hammer break the top skin connecting the horizontal tailpiece to the elevator. Leave the fibres intact while demolishing the resin. This creates an elevator hinge.

Secondly the vertical tailplane needs to be assembled

1. Place foam core on a clean surface
2. Insert the XBee module in the cut-out made earlier
3. Solder the antenna and the wiring onto the XBee
4. Lay the antenna and the wiring in the gutters which were also cut out
5. Cut off a piece for the rudder
6. Cut off two edges on both sides of the rudder to allow for rotation
7. Glue a clevis into the rudder. The exact layout of the rudder can be seen in section 7.6.2
8. Insert hinges in the vertical tailplane for rudder attachment
9. Laminate the piece, without the rudder, using the wet layup method
10. Glue the foam rudder onto the hinges

Thirdly the Pieces need to be integrated to form the vertical tail.

1. Clamp the carbon rod tightly
2. Drill three holes, 2 *mm* diameter, in the carbon tube for the push/pull rods and the XBee wiring using a pillar drill machine. The holes for the rods are elongated holes. A technical drawing of the carbon rod is shown in figure 7.18
3. Drill a 14 mm diameter hole in the horizontal tail surface to account for the carbon rob.
4. Insert two control rods trough the holes in the carbon tube
5. Insert the XBee wiring trough the remaining hole in the carbon tube
6. Glue the horizontal tail surface onto the carbon tube
7. Glue the vertical tail surface on the horizontal tail surface
8. Glue the control rods onto the wing structure
9. Connect the control rods to the clevis

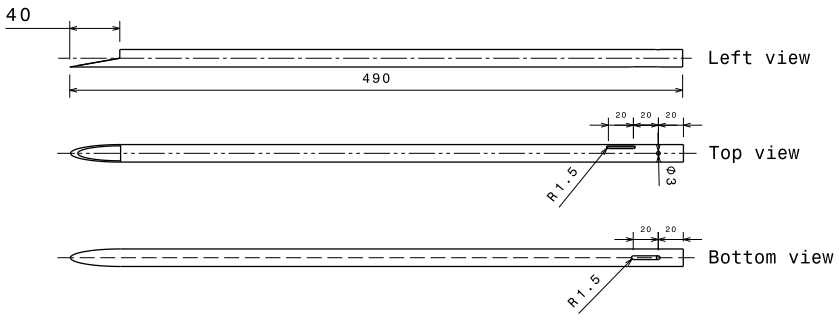

Figure 7.18: Carbon tube technical drawings

Body

This section shows a step wise description of the body assembly

1. Place the bottom skin on a clean surface
2. Make a cut-out in the bottom skin, accounting for the ailerons
3. Assemble the ribs in a puzzle-like way
4. Use epoxy to glue the ribs onto each other and the bottom skin
5. Insert the parachute hatch bar
6. Put the electronics and battery in the front payload compartment
7. Install the pitot tube
8. Install the airspeed micro sensor
9. Connect the pitot tube and the total pressure sensor using the flexible tubes, placing the tubes along the bottom skin. Make sure the tubes are placed accordingly to make them fit in the gutter that was cut in the corresponding foam block
10. Glue the foam cores onto the bottom skin
11. insert the servos for the ailerons, rudder, elevator and parachute in the cut-outs
12. Cut off a piece of the carbon tube, as can be seen in figure 7.18
13. Glue the tail in the foam core
14. Insert the control arms in the designated slots. Use glue to attach them to the bottom skin while still making sure the arms are allowed to rotate
15. Put the control rods in the gutters
16. Connect the control rods to the control arms and servos
17. Apply the wiring of the servos, leading the wires along the top of the foam cores. Make gutters to account for these wires.
18. Test the rudder as well as the elevator. The ailerons can not be fully tested because they require the top skin as a hinge point. However the push/pull mechanism can be tested.
19. attach the parachute release bar to the servo
20. put on the foam lids on all the cut-outs
21. Attach the nose to the vehicle
22. Attach the top skin
23. Make a cut to allow for aileron rotation
24. Use a hammer to break the resin in the aileron hinge section. Allowing for rotation, similar to the elevator mechanism.
25. Insert the parachute in the designated department
26. Close the parachute hatch

7.8.3 Risks

For the materials and manufacturing of the return vehicle, some risks are present. First of all the raw materials may contain small imperfections. These imperfections may influence the strength and stiffness of the material in different directions. Besides that, if no pre-impregnated composite fibres are used, not all fibres may be impregnated with resins resulting in a diminished mechanical quality of the composite. Third, depending on the chosen manufacturing process, small human or machining errors may be present in the return vehicle, also diminishing the mechanical strength of the return vehicle. Because a thin aramid fibre of 0,071 mm is chosen may make the production process more sensitive. Furthermore attention should be paid to the thermal expansion coefficients, choosing the right raw materials, and mould materials in case these are used, to increase the quality and reduce stress concentrations in the final product. Furthermore some risks regarding calculations are present. First no buckling loads are performed, no exact calculations or FEM analysis is performed for the stiffeners in the fuselage, now they are assumed to be full with foam. Lastly it may be the case that loads are higher then expected, or some miscalculations are present.

Chapter 8 Performance

A specific balloon is needed to be able to bring the return vehicle to an altitude of 35 kilometers. The balloon selection is discussed in section 8.1. To analyze the performances of the return vehicle a model is created in section 8.2. With this model the maximum range and maximum endurance is determined in section 8.3. These properties of the return vehicle are used for programming of the autopilot.

8.1 Balloon performance

When selecting a balloon to deliver a payload to a certain altitude, balloon and payload mass need to be considered, as well as a percentage of the total mass (also known as the free lift mass) to actually reach that altitude. If not, equilibrium sets in and the balloon will not rise. Keeping this in mind, the balloon will keep rising at an ascent velocity dependent on the magnitude of the free lift mass. Most balloon vendors are aware of this effect and usually the payload ranges with respective balloon masses to fit an average ascent-rate of about 320 meters per minute (which is about 5.3 meters per second) is specified, i.e. the TOTEX [38] balloons.

At the final stage of the ascent, the balloon will either slow down until it reaches an equilibrium altitude, or keep on climbing until the material is unable to elongate any further (passing its ultimate yield stress), resulting in the burst of the balloon.

8.1.1 Buoyancy theory

Balloons behave according to the Archimedes buoyancy principle [43], where the gravitational force of the displaced air is acting on the outside of the balloon's body. This displacement force equals the gravitational force of the system's mass and the gravitational forces exerted by the buoyant gas acting on inside of the balloon's body, as seen in equation 8.1.

$$F_{displacedair} = (m_{payload} + m_{aircraft} + m_{balloon})\, g_0 + F_{balloon} \tag{8.1}$$

The force exerted by the displaced air is a function of the density of the air, volume of the displaced space by the balloon and the gravitational acceleration. Rewriting equation 8.1 and dividing by the gravitational acceleration yields the following expression shown in equation 8.2.

$$\rho_{air} V_{balloon} = m_{payload} + m_{aircraft} + m_{balloon} + \rho_{gas} V_{balloon} \tag{8.2}$$

Solving equation 8.2 for the balloon's volume yields the following expressing as can be seen in equation 8.3.

$$V_{balloon} = \frac{m_{payload} + m_{aircraft} + m_{balloon}}{-\rho_{gas} + \rho_{air}} \tag{8.3}$$

The density of the balloon gas in equation 8.3 is the only unknown variable and can be found using the ideal gas law.

$$\rho_{gas} = \frac{p_{atm} molmass_{gas}}{LkT_{atm}} \tag{8.4}$$

Having obtained the balloon's volume by combining equation 8.3 and 8.4, where L is Avogadro's number and k is Boltzman's constant. The mass of the displaced air is easily calculated

by multiplying the air density with the balloon's volume. Hence, a mass balance can be created that includes the previously determined mass of the displaced air as can be seen in equation 8.5.

$$mass_{pull} = mass_{air} - \{mass_{balloon} + mass_{payload} + mass_{gas}\} \tag{8.5}$$

When the pulling mass equals zero, the balloon is in theory floating. If this equation yields a negative value, the balloon is descending. And when positive, the balloon is ascending. Multiplying with the earth's standard gravitational acceleration results in an expression for the balloon's buoyant force expressed in equation 8.6.

$$F_{buoyancy} = mass_{pull} g_0 \tag{8.6}$$

With the buoyant force determined in equation 8.6, an expression for the balloon's acceleration is formed as can be seen in equation 8.7.

$$a_{Balloon} = \frac{F_{buoyancy} - F_{aerodynamic}}{mass_{balloon} + mass_{payload} + mass_{gas}} \tag{8.7}$$

As the balloon rises through the atmosphere, aerodynamic drag will grow as the balloon's velocity is increasing. The aerodynamic drag force is a function of the balloon's reference area, velocity, drag coefficient and atmospheric density as seen in equation 8.8.

$$F_{aerodynamic} = 1/2\, C_{D_{balloon}} \rho_{atm} v^2 S_{balloon} \tag{8.8}$$

8.1.2 Lifting gases

The two most common and suitable gases to use in a weather balloon are hydrogen and helium [41]. Hydrogen has the best lifting properties and is the cheapest gas to produce. A disadvantage of hydrogen is that it dissipates through some materials. This is however so slow that it does not influence the lifting performance of the balloon. Furthermore hydrogen is very flammable. For small weather balloons hydrogen is the best fit however, since helium is more expensive. The risks of using hydrogen are small since the gas has much up-draft, it is assumed the gas should mix with air fairly fast. When the gas is ignited most of the reacting gasses will ascent fast, causing no actual damage to personnel. Hence, the gas is only used in relatively small quantities [41].

8.1.3 Balloon mass versus altitude

Trying to get to higher altitudes takes a big balloon with relatively high mass. A positive effect due to the increase in size, is that the mass of payload increases as well. Hence, the larger the balloon, the larger loads it can deliver to higher altitudes.

In figure 8.1 balloon masses for different types of balloons are plotted against their estimated bursting altitudes. Each line in this plot has a maximum payload, the Random Engineering's TOTEX [38] product payloads differ between 250 $grams$ and 1 kg. Kaymont [39] products differ between a 2 and 3 kg payload. Payload data for Random Engineering's Hwoyee [40] model was not available, but it does show it is capable of reaching a high altitude with relatively small balloon mass. It is however not known for which payload mass this balloon is suited.

The best fit for a standard StratoBlimp mission would be Random Engineer's TOTEX [38] balloon, with a balloon mass of 1.250 kg. According to figure 8.1, this balloon can deliver a payload of 1 kg up to altitudes of at least 33 km high. The mass of the return vehicle is close to 1 kg and the mission requires the StratoBlimp to reach an altitude of at least 30 km. Which should ensure the delivery of the StratoBlimp up to the required altitude to be possible.

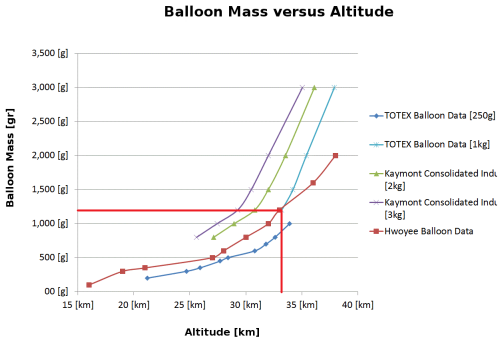

Figure 8.1: Mass of high altitude weather balloons designed for an indicated payload versus altitude. On the y-axis the mass of the balloon is stated, on the x-axis the altitude that can be reached. The best fit is the TOTEX [38] balloon with a mass of 1.200 kg, suited for a 1 kg payload, and reachable altitude of 33 km.

8.1.4 Balloon performance calculations

Taking into account the balloon fit discussed in subsection 8.1.3, the balloon has a mass of 1.250 kg. The assumed payload mass, which in this case spans the total StratoBlimp return vehicle mass (payload included), is set to be around 0.800 kg. Using the buoyancy theory discussed in subsection 8.1.1 with Hydrogen as the buoyant gas of choice; calculation can be done to determine the time it takes to reach a certain altitude, calculate the rate of ascent and determine the average rate of ascent as can be seen in figure 8.2.

With respect to Dutch regulations for ballooning, no more then a maximum of 4 m^3 gas volume is allowed at sea level. This brings the mass of the gas used for this calculation down to approximately 0.340 kg. It is assumed that; the balloon material can stretch infinitely long (meaning that the balloon will keep on rising without burst). The aerodynamic drag coefficient is set to have a value of 0.6 (meaning the balloon will endure some resistance due to aerodynamic drag).

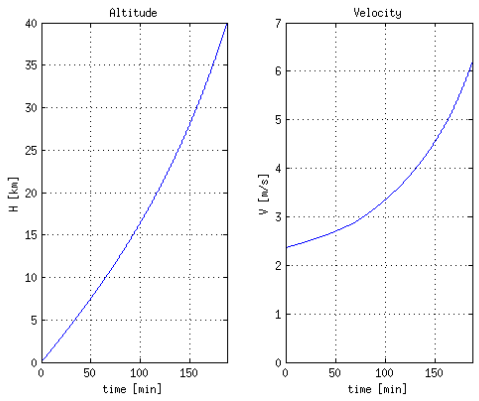

Figure 8.2: Altitude and rate of ascent versus time, where the balloon is assumed to be able to stretch infinitely long, thus speed will increase while time elapses.

With use of the calculations that provided figure 8.2, an average theoretical rate of ascent is calculated to be around 214 m/min. In theory the balloon should take about 187 min to reach an altitude of 40 km.

The balloon's volume and radius increase rapidly, as can be seen in figure 8.3, when the balloon picks up speed and starts to enter the less dense parts of earth's atmosphere. Volume of the balloon at 40 km is increased by a factor of approximately 318 of the starting volume at sea level.

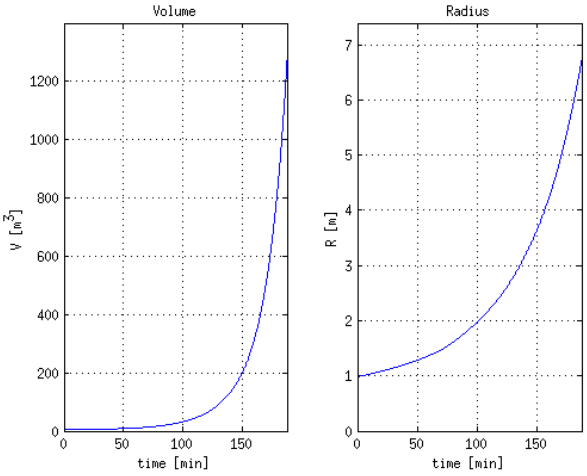

Figure 8.3: Balloon volume and radius versus time

8.2 Return Vehicle Model

The aircraft model is based on the forces in the x_a and z_a direction of the axes of the aircraft, as indicated in figure 8.4. It is assumed that the aicraft is descending at a constant speed, so the sum of all the forces is zero. From this model the equations 8.9 and 8.10 are determined [42].

$$-D - W \cdot sin(\gamma_d) = 0 \tag{8.9}$$

$$L - W \cdot cos(\gamma_d) = 0 \tag{8.10}$$

From figure 8.4 also the glide path angle can be determined, indicated in equation 8.11.

$$RoD = V \cdot sin(\gamma_d) \tag{8.11}$$

The airspeed can be obtained by combining the lift equation with equation 8.10. The equation is defined by equation 8.12.

$$V = \sqrt{\frac{W}{S}\frac{2}{\rho}\frac{1}{C_L}cos(\gamma_d)} \tag{8.12}$$

Using equation 8.9 and 8.10 equation 8.13 can be derived.

$$tan(\gamma_d) = \frac{C_D}{C_L} \tag{8.13}$$

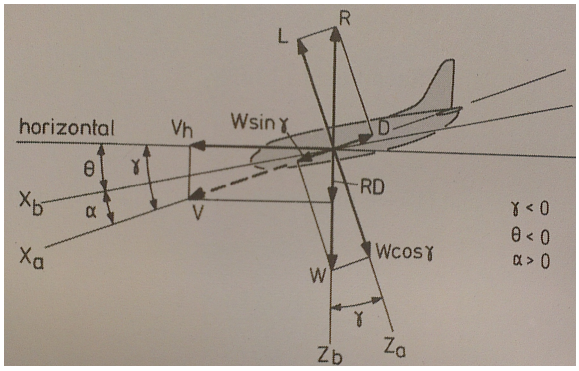

Figure 8.4: Model axis definition for an aircraft in gliding flight. The aerodynamic and body axes are defined by the subscripts a and b respectively. Figure obtained from Ruijgrok [42]

8.3 Range performance

To travel a maximum horizontal distance the return vehicle should fly at specific angle of attack or corresponding airspeed. The calculation and determination of this attitude is elaborated in this section. The maximum range is reached for the minimal downward flight path angle (γ_d). The flight path angle has been calculated from equation 8.13, and is given by equation 8.14 [42].

$$\gamma_d = tan^{-1}(\frac{C_D}{C_L}) \tag{8.14}$$

From equation 8.14 it can be seen that for a minimum downward flight path angle a maximum $\frac{C_L}{C_D}$ value is needed. With the data found in chapter 5.6 a matlab simulation is performed. The maximum $\frac{C_L}{C_D}$ value is determined for different altitudes, namely 0, 10, 20 and 30 km. The corresponding airspeed, rate of descend and flight path angle is calculated with formulas 8.12, 8.11 and 8.14 respectively. This data is given in table 8.1 [42].

Table 8.1: Required flight parameters for maximum range at different altitudes.

Altitude km	Optimal $\frac{C_L}{C_D}$	RoD m/s	$\gamma_d deg$	Airspeed m/s	α°
30	3.69	32.01	32.01	122.24	4.5
20	9.07	4.91	4.9	44.8	8
10	14.8	1.57	1.57	23.2	6
0	16.09	0.87	0.87	14.0	5.5

With the data obtained in table 8.1 the maximum range can be calculated by using equation 8.15, with h being the applied height range for the specific maximum $\frac{C_L}{C_D}$.

$$range_{max} = h \cdot \left(\frac{C_L}{C_D}\right)_{max} \tag{8.15}$$

The range from an altitude of 30 km is found to be 338 km. It should be noted that this model is idealized; wind is not taken into account.

Chapter 9 Component selection & layout

In this chapter the selection, configuration and layout of the components within the return vehicle are determined. In section 9.1 components to be used are selected. The layout of these components within the structure of the return vehicle is explained in section 9.2. In section 9.3 the mass and position of all components is taken into account to determine the total mass and balance of the vehicle. In section 9.4 the power required by all components is examined and whether the selected battery will be sufficient for the mission duration is checked. At last, in section 9.5 a cost budget will be given on prototype and mass production.

9.1 Component selection

This section deals with the selection of autopilot and accompanying hardware platform, standard on-board sensor suite, and the battery.

9.1.1 Autopilot platform selection

The brain of the return vehicle is the autopilot. The selection of this component directly influences the capabilities of the vehicle. Several autopilots are available on the market for example micropilot, Ardupilot, kestrel, etc. Many of these autopilots are open source, like openpilot and Paparazzi, and most of them have a good community supporting its continuous development. Almost all of these autopilots have enough features to support our basic needs for navigation and gliding. The team chose to work with Paparazzi for several important reasons. Paparazzi is an actively maintained open source project with many new features added all the time. Two important developers or teams are working on this autopilot, one at l'cole Nationale de l'Aviation Civile in France and one at the MAVlab of the Delft University of Technology. Having Paparazzi experts nearby at the university can be key to getting all the features the team wants to work on the return vehicle. Next to the available expertise Paparazzi is a very flexible platform allowing for almost any type of hardware to be connected and used in cooperation with the autopilot. Many possible hardware boards are already available to choose from and these board designs are also open source. On top of that, most of the popular hardware designs are available assembled and ready to use for a very reasonable price. The Paparazzi ground station interface is displayed in figure 9.1.

9.1.2 Autopilot hardware selection

When looking at the available options for a hardware platform to run Paparazzi on, two main categories are available. The NXP LPC2100 based micro controller with an ARM7 CPU and the ST microelectronics STM32 based micro controller with a Cortex-M3 cpu. Talking to developers in the Paparazzi community quickly led the team to disregard the LPC2100 micro controllers as they barely have enough processing power to run all the advanced features of the autopilot. To be able to run all current and future features the team opted for a STM32 controller.

Not many autopilot boards with an STM32 controller exist but only one good one is needed. The Lisa and Krooz are possible options here. The Lisa series are boards that are actively maintained by Transition Robotics, the company behind Quadshot. The Lisa/M v2.0, seen in figure 9.2 is the smallest and most used of this series. The Krooz autopilot is a lot bigger and has some features that will never be used on the return vehicle like Bluetooth and Wi-Fi. For these reasons the Lisa/M v2.0 is selected. Hardware features of the Lisa/M are given in table

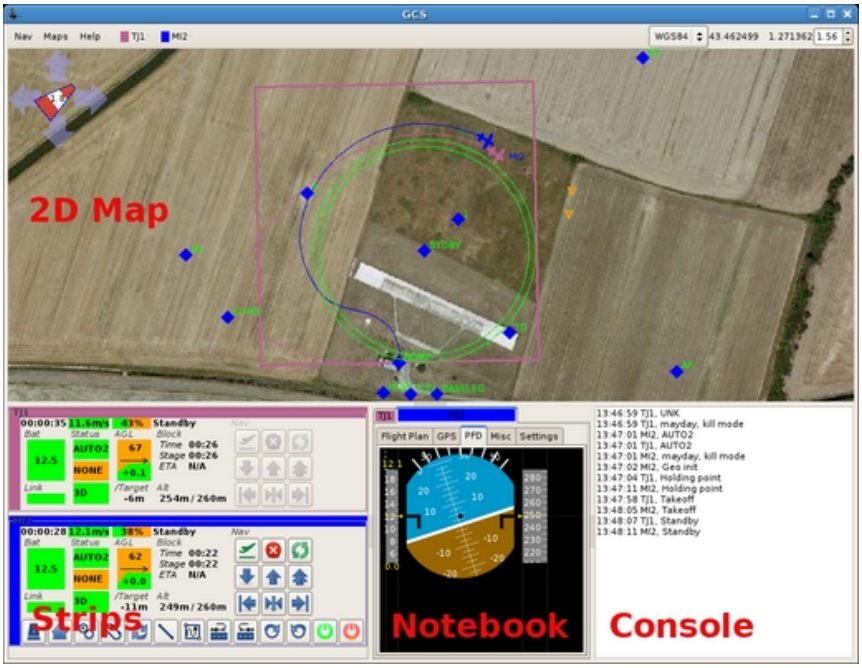

Figure 9.1: Paparazzi Ground Control Station for live tracking and simulation of flights

9.1. Next to the Lisa/M an IMU board is needed. Also here a couple of choices are possible but the Aspirin, seen in figure 9.3 is by far the best option as it can be mounted directly on the Lisa, is actively maintained and has a lot of features within a small volume.

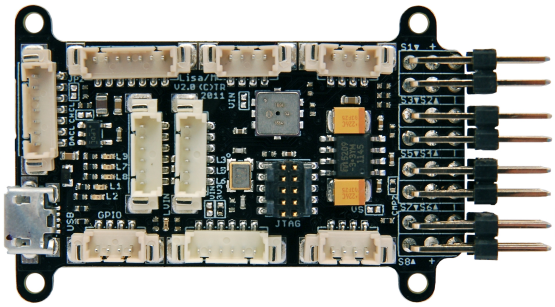

Figure 9.2: The Lisa/M v2.0 autopilot board developed for the Quadshot project

9.1.3 Sensor and battery selection

The return vehicle will be equipped with a standard set of sensors. The Aspirin IMU already takes care of some of this need. It has a 3 axis accelerometer, 3 axis gyroscope and 3 axis magnetometer on board, as well as a pressure sensor. The only things missing are a temperature, humidity sensor and an airspeed sensor. The extra sensors can very easily be connected to the spare ADC ports on the Lisa/M. The 12 bit ADC in the micro controller allows for a resolution of 4096. This allows for a difference of 805 uV to be measured on the 3.3 V channel. Using a standard K-type thermocouple would be a good solution but is not precise enough with a difference of 41

Table 9.1: Features Lisa/M v2.0 autopilot hardware

1 x STM32 microcontroller STM32F105RCT6 with 256kB flash and 64kB RAM
7 x Analog input channels
3 x Generic digital in-/out-puts
2 x 3.3V TTL UART (5V tolerant)
8 x Servo PPM outputs (only 6 if second I2C (I2C1) bus in use)
1 x CAN bus
1 x SPI bus
1 x I2C bus (2 x when using only the first 6 Servo PPM outputs)
1 x Micro USB
4 x status LEDs with attached test point
10.8 grams (with Aspirin IMU mounted)

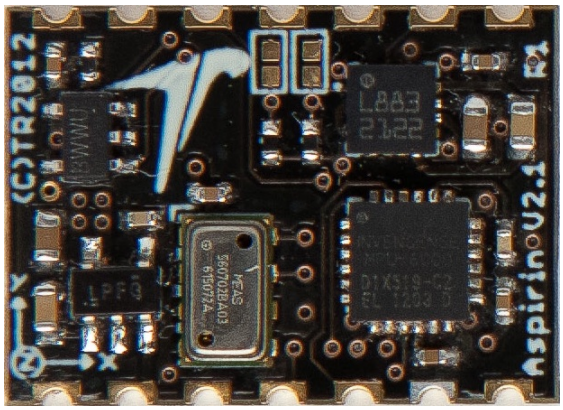

Figure 9.3: Aspirin IMU module with 3 axis accelerometer, magnetometer, gyroscope and a barometric pressure altitude sensor

$uV/°C$. Adding some amplification would solve this problem but this adds extra components. A thermister might therefore be a better solution as it generally has a smaller operating range and a bigger resistance deflection per centigrade. It is also a simple small and robust design but slightly heavier than the K-type thermocouple. Therefore a thermister is selected.

To measure the airspeed an Eagletree MicroSensor V3 is selected, as it is often used in cooperation with Paparazzi. There also exists a lot of documentation on the coupling of these two devices shortening the development time considerably. The sensor data ranges from 15 km/h up to 563 km/h with a resolution of around 1.6 km/h. The SM Modell Bau Speed Sensor was also considered. It has a comparable range of 0 km/h to 450 km/h and has only a slightly higher mass of 6 g compared to the 4 g of the Eagletree sensor. Since the Eagletree sensor is more often used with Paparazzi and since has bether performances this sensor is selected

Two types of humidity sensors exist, resistive and capacitive. Capacitive sensors are the most common, but not many go as low as -60 $°C$. They do exist however, for example the UPSI G-US.12, which goes as low as -90 $°C$, and is both very small and, priced around 5 euro, fairly cheap. Therefor a capacitive sensor is selected.

The barometric sensor on the Aspirin IMU ranges from 10 $mbar$ up to 1200 $mbar$. A pressure of 10 $mbar$ equals an altitude of about 26 km this means that above 26 km no accurate pressure

readings will be available and altitude must be determined using GPS. This is however a very accurate sensor in its range and still the most suitable choice, as no replacement with the same accuracy and a range that goes below 10 *mbar* is found.

For test flights, manual landings, and when the autopilot fails in short range, a standard satellite receiver for remote control will be included in the return vehicle. The OrangeRx R100 is lightweight (4 g) and suitable for short range purposes.

Finally the battery is selected. It was opted to use a lithium polymer (LiPo) battery since these are widely available and provide the highest energy density. The required voltage for powering the Lisa/M is 5 Volts, so a 2cell LiPo is selected which provides 7.2 V. The typical current draw is estimated to be 1 ampère. For a 4 hour mission this requires a capacity of 4 Ah. The selected battery is the Turnigy 4000mAh Spektrum DX8. in section 9.4 a check will be performed to make sure that the battery complies with all requirements. If not a lighter or heavier battery will be selected.

9.2 Layout and integration of components

In the previous section the components needed to perform a successful mission were selected. In this section all of these components are put together inside the airframe and integrated with the structure which will be further explained in chapter 7. Starting from the list of components and the shape and volume of the return vehicle, the location of each component was determined.

In section 9.2.1 the general return vehicle layout is explained and the location of the separate compartments is given. In section 9.2.2 the payload compartment is looked at in more detail, followed by the electronics compartment in section 9.2.3. In section 11.1 more information on the parachute compartment is given. In section 9.2.4 the positioning of the servos, control surfaces and actuation mechanisms are illustrated. Finally section 9.2.5 the integration of the sensors into the airframe is explained.

9.2.1 Return vehicle layout

The general layout of the return vehicle, the location and size of the wing, tail and fuselage, was determined based on the aerodynamic calculations found in chapter 5. The final shape of the vehicle, as can be seen in figure 9.4, is slightly altered, to facilitate production, to allow for the structure and internal components to be implemented, and for aesthetic reasons. These alterations include: increased wingspan, straight trailing edge of the horizontal tailplane, added wing tips. Note that despite these adaptations the changes in aerodynamic properties are minimal.

It was decided to divide the return vehicle in a couple of compartments, separated from each other by bulkheads which also transfer the loads from one side of the return vehicle to the other. These compartments are:

- *Payload compartment* - Contains the payload together with all the supporting equipment required such as batteries and data loggers.
- *Electronics compartment* - Contains most of the electronics required for the operation of the return vehicle such as autopilot board, GPS module, satellite receivers, data logger, and battery.
- *Parachute compartment* - Contains the parachute canopy, lines, and connections to attach the lines to the structure of the return vehicle.

Figure 9.5 shows a close up of the fuselage and indicates the location of each compartment and the location of the bulkheads as thick lines

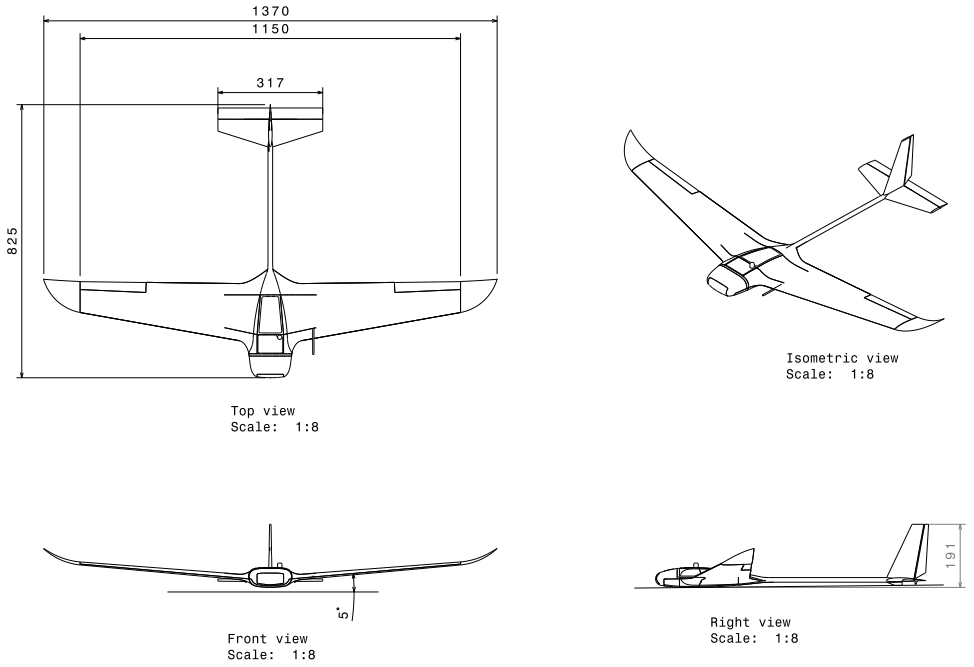

Figure 9.4: Final return vehicle shape and dimensions in *mm*

9.2.2 Payload compartment

First the position of the payload was chosen. It was decided that the payload-compartment could best be placed in the nose of the return vehicle. An easily detachable and replaceable nose section is advantageous to fit many different types of payload into the vehicle. This leads to a system where depending on the payload type to be taken aloft a different nose section can be installed. in Figure 9.6 one of these nose section types is shown: this particular nose section can be used for aerial photography with a camera in the payload compartment filming forward. Other options are: a transparent section near the bottom of the nose to film downwards, cut-outs in the front or side of the nose to insert measurement equipment, etc.

9.2.3 Electronics compartment

The electronics compartment is situated just aft of the payload compartment and contains the major electronics controlling the return vehicle and the data logging equipment.

Against the front bulkhead the battery is installed in an upright position. It is positioned in such a way that the connectors from the battery to the rest of the return vehicle can easily be accessed when the hatch on top of the compartment is opened. The battery is attached to the front bulkhead by means of Velcro strips applied to both the bulkhead and the battery. These Velcro strips are able to handle the flight loads and it makes it easy to remove the battery during maintenance.

The Lisa/M autopilot board is attached to the backside of the battery. The mass of the

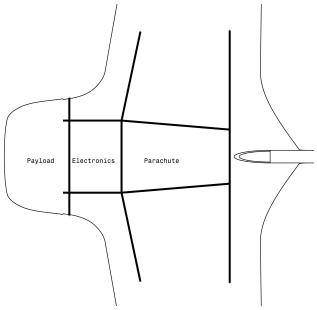

Figure 9.5: Compartment layout in the fuselage

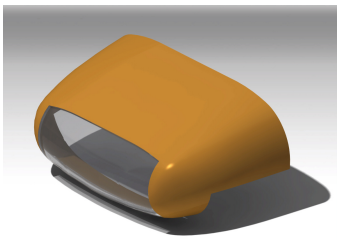

Figure 9.6: Nose section example

battery and its Velcro connection should eliminate most unwanted vibrations which could affect the accuracy of the accelerometers in the Aspirin IMU. Connection pins (M2 bolts) can be glued onto the back of the battery onto which the attachment points on the Lisa/M can be placed. What this will look like in practice is shown in figure 9.7.

Against the front spar bulkhead (between the electronics and parachute compartment) on the left side of the return vehicle the GPS module is installed. It is positioned in such a way that the helical antenna sticks out of the return vehicle at the top. The point where the antenna exits the vehicle is also used as the mount point. An example of how the antenna is used to mount the GPS module is shown in figure 9.8.

The data logger is also installed on the front spar bulkhead, to the right of the GPS module. The easiest way to install this component is to glue it into place. Note that it is installed in such a way that the micro SD card on the Data logger can be easily replaced in between missions.

The last components in the electronics compartment are two satellite receivers. These can be installed at the bottom of the compartment and glued into place. Note that the antennas coming out of these components are also glued into place on the bottom of the compartment. An overview of the entire compartment is given in figure 9.9

9.2.4 Control mechanisms and actuation

Since the available space in the wings and tail is very limited all of the servos that control the deflections of the control surfaces are placed in the fuselage, just outside of the predefined compartments. Using the components close to each other also prevents freezing of parts; the servos for example.

The servos controlling the ailerons are placed on either side of the parachute compartment close to the front spar bulkhead. From the servo a flexible control rod is integrated into the foam

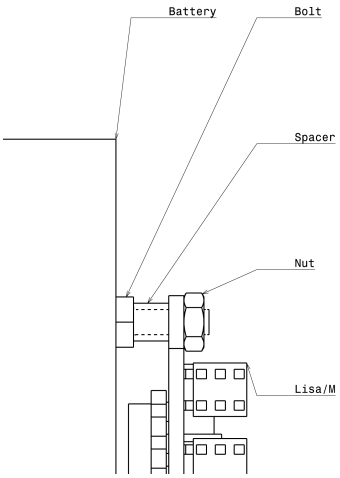

Figure 9.7: Autopilot mounting to the battery

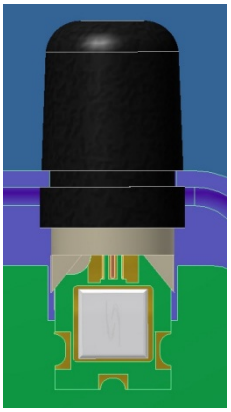

Figure 9.8: Mounting of the GPS module example, showing the antenna sticking out of a device and the antenna sleeve acting as mount point

cores of the wing. These rods transfer the motion of the servo to the outsides of the wing where they are transferred onto the aileron by means of a rocker.

For the elevator and rudder controls the servos are placed just aft of the parachute compartment. From these servos flexible push rods are guided through the carbon tube in the tail. These flexible push rods are connected directly to their respective control surfaces.

One last servo is used to deploy the parachute. It is placed on the right side of the vehicle next to the parachute compartment close to the aft spar bulkhead. Tt connects to the locking mechanism that keeps the parachute hatch in place and releases it when activated.

In figure 9.10 the position of all the servos in the fuselage is shown. The complete control mechanism is shown in section 7.6, figure 7.10.

9.2.5 Sensors and XBee integration

The sensors on board of the return vehicle are an airspeed sensor, temperature sensor and humidity sensor. These sensors together with the GPS module, the Aspirin IMU and the transceivers (satellite receivers and XBee) provide all the data to the autopilot.

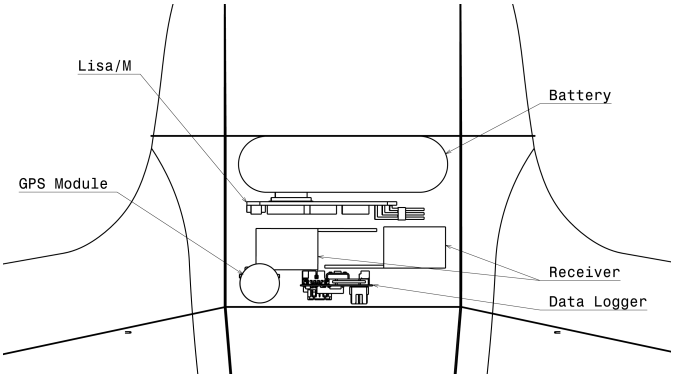

Figure 9.9: Overview of the electronics compartment

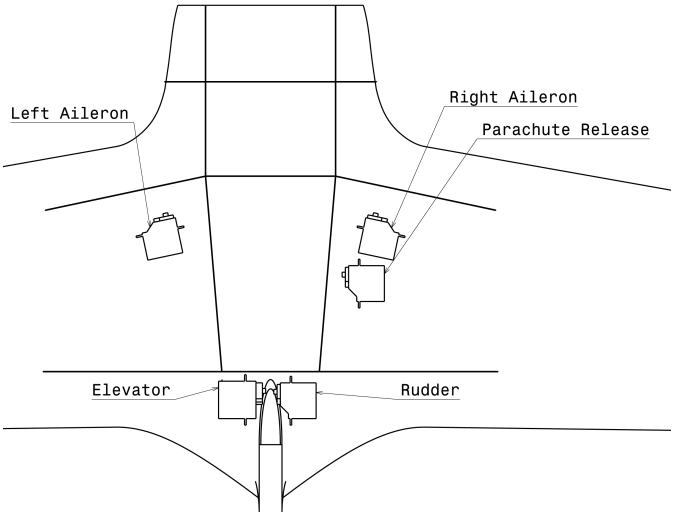

Figure 9.10: Placement of the servos within the fuselage

The airspeed sensor is installed to the left side of the parachute compartment, close to the aft spar bulkhead and is glued in place. In order for the sensor to work it has to be connected to the pitot tube. This pitot tube is installed in the left wing root, and is attached to the front spar bulkhead. the connection between the pitot and the sensor is ensured by means of flexible tubes which are embedded into the foam core of the wing.

The humidity and temperature sensors have to be installed on the outside of the vehicle, preferably far away from any objects radiating heat as to not affect the measurements.

The last component that has to be installed into the return vehicle is the XBee module which takes care of all the data received from and transmitted to the ground station. It was decided to place the XBee module in the vertical tail plane together with the antenna, as these have to be as close as possible to each other to reduce losses. The entire module will be inserted into the foam core of the tail plane and covered with aero-tape to make it easier to remove or replace the component.

9.3 Mass Budget

One of the major limiting factors for the return vehicle is its mass. In this section the mass and corresponding centre of gravity are determined based on the mass and position of each individual component.

The origin of the reference frame for these calculations was taken on the nose of the aircraft. The axis system used is: X-axis positive pointing back, Y-axis positive to the right and Z-Axis positive pointing up. From CAD drawings the location of the centre of gravity of each component was determined and using equations 9.1 - 9.3 the CG of the entire aircraft was calculated.

$$\overline{x} = \frac{\sum x_i \cdot m_i}{\sum m_i} \tag{9.1}$$

$$\overline{y} = \frac{\sum y_i \cdot m_i}{\sum m_i} \tag{9.2}$$

$$\overline{z} = \frac{\sum z_i \cdot m_i}{\sum m_i} \tag{9.3}$$

The results of these calculations are shown in table 9.2. A 5% increase in mass, without changing C.G. location, is added as margin for wiring, and small components such as hinges and control rods. The final mass of the prototype will however exceed this estimate since deficiencies during production will surely lead to extra mass being added.

The total mass of the aircraft is estimated to be 797 $g \approx 800$ g. Keeping in mind that for the prototype this is likely to be approximately 50 to 100 g more.

9.4 Power budget

The power budget is a check to see whether the battery which was selected in section 9.1 has enough power stored to keep the return vehicle running through the length of the mission. In table 9.3 the maximum and typically expected powers of the electrical components is given. Note that for the servos their typical power is estimated as being 20 % of their maximum power since they are not active all the time and do not require their full power during most of the manoeuvres. For the Lisa/M, GPS module and XBee communication module a test set-up was made to measure the typical power. A 10% margin is taken on top of the total power to account for unforeseen power drains.

Using equation 9.4, and knowing that the battery supplies a voltage of 7.4 V the maximum and typical current are calculated to be 3.75 A and 0.91 A respectively. Since the battery has a capacity of 4 Ah the maximum battery life is estimated to be 4 hours and 25 minutes. This battery lifetime should be sufficient with a maximum mission time of 4 hours.

$$P = U \cdot I \tag{9.4}$$

Table 9.2: Center of gravity calculation based on component mass and location

Component		Mass $[g]$	CG location		
			x $[mm]$	y $[mm]$	z $[mm]$
Electronics					
	Battery	133.0	106	0	11
	Lisa/M + Aspirin	10.8	120	-9	18
	GPS module	9.4	146.5	-6.5	18
	Data logger	10.0	147.3	-2	22
	XBee Pro 868	10.0	795	0	68
	Satellite receivers	8.0	130	0	-6
	Airspeed sensor	4.0	252	-37	2.3
Airframe					
	Carbon tube tail	32.5	546	0	0
	Bottom skin	16.4	228	0	14.6
	Top skin	15.1	234	0	29.4
	Hatches	4.2	232	0	29.8
	Internal frame	14.0	166	0	9
	Foam cores	61.0	222	0	23
	Vertical tail	11.1	798	0	76
	Horizontal tail	15.4	790	0	1.4
	Nose Cover	24.6	42	0	8.2
	Pitot Tube	20.0	135	-130	20
	Left Aileron Servo	5.0	193.5	-66	7.5
	Right Aileron Servo	5.0	193.5	66	7.5
	Elevator Servo	10.0	293.6	-17	0
	Rudder Servo	5.0	294.0	18	0
	Parachute Release Servo	5.0	220.0	59	7.5
Parachute					
	Canopy + wires	59.0	215 0	5	
	Parachord	19.0	160	0	9
	Rubber bands + liner	2.0	230	0	20
Payload		250	60	0	10
Total		760	170	-4	20
	+ 5% margin	797	170	-4	20

Table 9.3: Power budget estimations

Component	maximum power $[W]$	typical power $[W]$
Lisa/M + GPS + Comm	unknown	5.03
Servo left aileron	0.82	0.16
Servo right aileron	0.82	0.16
Servo Elevator	2.20	0.44
Servo Rudder	0.82	0.16
Servo parachute	0.82	0
Wire cutter	14.8	0
Total	25.3	6.1
+ 10% margin	27.8	6.7

9.5 Cost budget

This chapter will discuss the cost of building a prototype and estimated costs of building a small series for potential first costumers.

9.5.1 Prototype

During prototyping overhead is big because small quantities that need to be delivered in a short time frame are ordered, resulting in high shipping costs. In many cases it is not possible to order from the cheapest supplier in order to get the needed parts fast enough to avoid production delay in the critical prototyping phase. An overview of the prototyping costs can be seen in figure 9.11.

Income	Budget
Student start kapital	€ 600.00
Delft Robitics Laboratory	€ 2,694.96
Approved budget	€ 2,694.96
Total	€ 3,294.96

Expenses	Budget
Student start kapital	€ 600.00
Paparazzi electronics	€ 590.92
Groundstation	€ 286.60
Parachute	€ 22.11
Airframe	€ 199.03
Production materials	€ 567.29
Production tools	€ 190.76
Payload	€ 838.25
Total	€ 3,294.96

Figure 9.11: Summary of the budget for building a prototype

Labour costs 100 units	Time (days)	Cost
Lamination of shell	25.00	€ 6,000.00
4 at the same time		
Cutting carbon tubes	2.00	€ 480.00
Airframe assembly	15.00	€ 3,600.00
Electronics assembly	25.00	€ 6,000.00
Testing	12.50	€ 3,000.00
Delays	7.95	€ 1,908.00
10% of total production time		
assuming labour costs of 30 euro/hour		
assuming 1 work day = 8 hours		
Total	87.45	€ 20,988.00
Cost per unit	0.8745	€ 209.88

Figure 9.12: Labor costs for 100 units

Expenses per unit when producing 100 units	Budget
Paparazzi electronics	€ 300.00
Parachute	€ 20.00
Airframe	€ 200.00
Production materials	€ 400.00
Total	€ 920.00

Figure 9.13: Estimated build costs when building a small series of 100 units

The production materials are a big part of the total expenses. This is because the available materials are sufficient for about 2 prototypes. Buying extra aramid fibers for approximately 50 euros would allow for a second shell to be produced. The additional material also gives some margin in case some of the products need to be reproduced. The category production tools are a one time investment. For example aramid cutting scissors, a vacuum pump and soldering equipment are all listed in this category. The payload cost is relatively high for the prototype because of the need for a radio transmitter and receivers to manually control and test the return vehicle. A motor to propel the return vehicle during initial tests, a battery pack to supply the motor and a standard GPS-GSM tracker for recovery in the event of a failure are also listed next to a high quality and extremely durable HD camera to film the entire flight. Filming the flight could help understanding what the aircraft does at high altitude. It also is great material to promote the company and boost initial sales. This results in a total cost of about 2700 euros to build a prototype. If the return vehicle is not lost during testing then the electronics could be reused. If everything goes well during production it will be possible to produce a second body for little extra cost. An overview of the ordered parts used for production can be found in Appendix B. It is split up in the cost for the return vehicle, ground station, payload and production. The cost given is the amount paid for each part, excluding shipping cost and import tax. To have an idea of the shipping costs and possible import tax, about 25 % of the order cost is budgeted.

9.5.2 Series production

A single return vehicle will cost less than 1000 euros in material costs when produced in larger quantities, not taking into account the initial costs to produce moulds for core material forming and lamination of the skin. Assembling a single return vehicle could take about 3-4 days because of curing times, but several vehicles could be assembled at the same time. This means that a single return vehicle in series production will take up an average of 7 work hours to complete. Time estimates for producing 100 return vehicles can be found in figure 9.12. Taking into account company overhead, start up and further development costs would make a single return vehicle cost approximately 2000 euros to produce. Figure 9.13 shows the estimated build cost per unit when building 100 units.

Chapter 10 Aircraft systems

The aircraft systems chapter is divided in three main sections; namely the flight systems avionics in section 10.1, where all hardware related systems are discussed. The autopilot in section 10.2, where all software related systems are discussed respective to return vehicle control, navigation and simulation. And concluding the communications in section 10.3, where all related hardware and software systems respective to return vehicle to ground communications are discussed.

10.1 Avionics

In this section the electronic hardware required for flight and avionics is discussed. Special attention is paid to the integration and compatibility of all components in section 9.2.

The major electrical component is the Lisa/M autopilot board. This board processes the data from the sensors and sends it either to the data logger for storage or to the XBee module to be transmitted to the ground station. The datalogger is linked to the SPI 1 port while the XBee transciever is connected to the UART 2 port. The sensors the Lisa/M receives data from as well as the ports they should be connected to are:

- *Aspirin IMU* - The Aspirin IMU is a sensor pack which contains a 3 axis gyroscope, 3 axis magnetometer, 3 axis accelerometer and a barometric pressure sensor. This sensor pack comes with the Lisa/M and is mounted on the back of the autopilot. The gyroscopes have a range of $\pm 2000\ ^\circ/s$ with a resolution of 16.4 $LSB/^\circ/s$. For the magnetometers the accuracy is 10 $milliGauss$. The accelerometers can handle accelerations up to 16 g with a resolution of 2048 LSB/g. Finally the resolution of the barometer is about 0.012 $mbar$.
- *EagleTree Airspeed Microsensor v3* - This sensor is connected to the I^2C 2 port and sends (indicated) airspeeds, which it calculates from a pitot tube, to the autopilot board. The accuracy of the airspeed is about 0.3 km/h on a speed range of 15 km/h till 564 km/h.
- *GPS Module* - This component consists of a Ublox MAX6 GPS chip and a Sarantel helical antenna. The module is attached to the UART 3 port and outputs the GPS position with a position accuracy of 2.5 m. This GPS module is chosen for its altitude maximum of 50.000 m and its speed range of 500 m/s. The helical antenna has a wide receiving angle of 135 degrees and can handle accelerations up to 4g. It can be used at an operating temperature higher then -40 degrees.
- *Temperature sensor* - A thermistor will be connected to the ADC port of the Lisa/M. The slightest difference in resistance can be measured by the ADC port, therefore the accuracy is dependant on the resolution of this port. The resolution of the ADC port is 4096 steps (12-bit) which can be evenly distributed over a temperature range of -100 $^\circ C$ to 100 $^\circ C$, which gives a resolution of 0.05 $^\circ C$.
- *Humidity sensor* - The G-US.12 humidity sensor is selected and should be connected to one of the ADC ports of the Lisa/M. This humidity sensor has an operating temperature from -90 degrees till 85 degrees. With a resolution of 5

As a backup and in case manual flight intervention is required a pair of satellite receivers is added. These receivers allow the return vehicle to be controlled by means of a remote control from the ground when it is in close range. Both of these receivers are connected to the UART 1/5 port of the Lisa/M.

Control over the moving parts of the return vehicle (control surfaces and parachute hatch) are controlled by the servo ports on the autopilot board. The servos are arranged as follows:

- *Servo port 1* - Left aileron
- *Servo port 2* - Right aileron
- *Servo port 3* - Elevator
- *Servo port 4* - Rudder
- *Servo port 5* - Parachute release
- *Servo port 6* - Left open
- *Servo port 7* - Left open
- *Servo port 8* - Left open

In table 10.1 the chosen servos can be found according to the required torques which can be found in table 7.7. Both servos work on an operating temperature of -30°C to 60 °C.

Table 10.1: Required and applicable moment by servo.

Control surface	Servo	Required moment	Applicable moment	Speed
Aileron	HXT500	0.7 $kg \cdot cm$	0.8 $kg \cdot cm$	0.09 $s/60°$
Elevator	HKSCM9	1.3 $kg \cdot cm$	1.4 $kg \cdot cm$	0.10 $s/60°$
Rudder	HXT500	0.6 $kg \cdot cm$	0.8 $kg \cdot cm$	0.09 $s/60°$

When the return vehicle has to be released from the balloon, a wire cutter will heat up and melt the wires that connect the return vehicle to the balloon. This wire cutter release mechanism is powered by the battery and gets its signal from one of the ADC ports on the ANALOG 1 connector. Finally the autopilot is powered from the battery through the I^2C CAN 1 bus. The total hardware diagram is shown in figure 10.1.

10.2 Autopilot

In this section the autopilot system, control theory, simulation and navigation is discussed. The autopilot is an important and integral part of the design and plays a key role in performing a successful mission. Within the scope of the StratoBlimp project a few constraints were implemented with respect to the hardware selection and software used [1]. Subsection 10.2.1 will only discuss the Paparazzi autopilot and will not consider any other types of available systems. The control theory used by the autopilot is explained in subsection 10.2.2. Subsection 10.2.3 discusses the various methods available to the autopilot. In subsection 10.2.4 a virtual representation of the return vehicle is created with the use of JSBSim [45], where a set-up is created which will allow the autopilot to be tested in a virtual environment and in future design to accurately estimate autopilot parameters. Autopilot systems and simulations have risks and these are discussed in subsection 10.2.5.

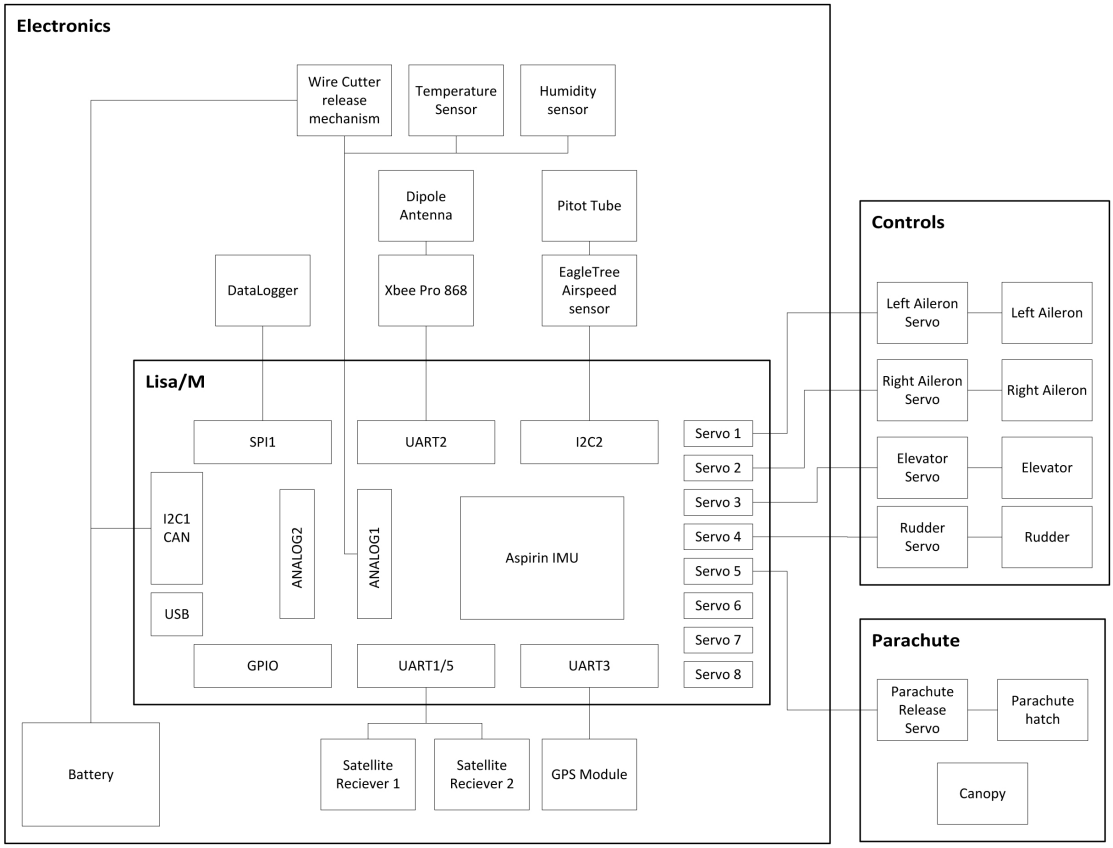

Figure 10.1: Hardware diagram
showing all the electrical components in the return vehicle and their connections.

10.2.1 Paparazzi

Paparazzi is a complete autopilot system which can be used for autonomous flight. It consists of the autopilot hard- and software in the return vehicle and the ground control software. It was originally designed for powered fixed-wing aircraft, but since it is open source in can also be used for a glider [44].

A general overview of the interaction of the software files and the hardware is given in figure 10.2. The most important part for the software are the XML files. These are used together with the source code to generate code which can be loaded on the controller board. The controller board gets input from the sensors and the users to generate the right output for the actuators and the telemetry link back to the user. The XML files are described in the following list. A simulation can be made to check the behaviour of the aircraft in autonomous flight [44]. The XML files are used for easy configuration. The XML files are used with the source code in the Paparazzi center to build firmware for the controller board. The content of each file is described shortly.

Airframe - In the airframe file the settings of the aircraft are described. This file contains information about the type of aircraft, which controller board is used, the different input sensors and actuators of the aircraft and the used control loops. Also the radio control

specifications are defined in this file.

Flight plan - The flight plan file is used to define the different waypoints of the aircraft. Blocks are created to define what the aircraft will do in which order. The order of these blocks can be changed during actual flight, also a specific block can be activated. The aircraft can be told to circle slowly down in case the GPS signal is lost or fly to a specific location in case the communication with the ground station is lost for a certain amount of time.

Radio - In the radio file a description of the radio control signal is described. The different functions on the radio controllers are defined with the corresponding output on the aircraft.

Telemetry - The telemetry file describes which data has to be sent back to the control station. Examples of this are the airspeed, GPS location and signal, battery level and attitude.

Settings - In the settings file different variables used in the graphical user interface of the ground control station are stated. Also the range and step values of these variables are defined here.

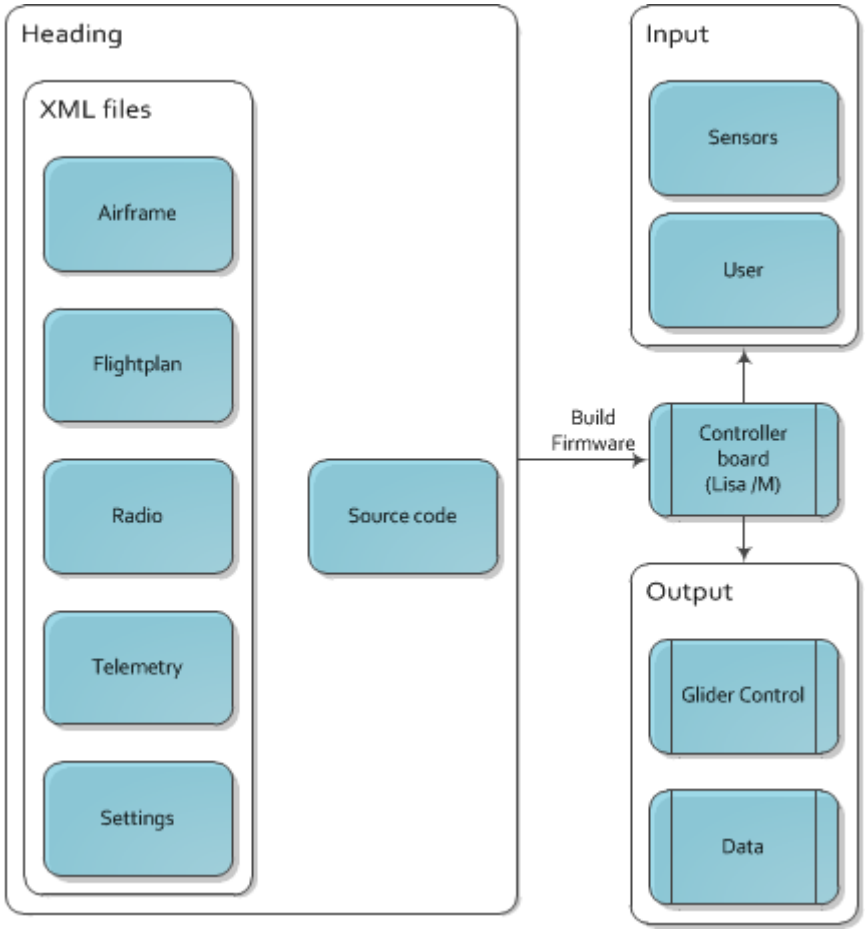

Figure 10.2: Overview Paparazzi software. The XML files are used with the source code and loaded to the controller board of the return vehicle. The controller board uses the input from the sensors and the user to control the control surfaces of the return vehicle and send back data to the user.

10.2.2 Control theory

The control loops used by Paparazzi [44] span a wide range of applicable uses for powered flight. Because the return vehicle does not have any type of propulsion system, it can only make use of a few control loops. Hence, these loops need to be appended and some need to be disregarded entirely since they do not serve any purpose.

Paparazzi distinguishes between two types of aircraft, namely the fixed wing and rotor craft. In the case for the return vehicle, it will be using the fixed wing controls for guidance and attitude control. These control loops are embedded in the Paparazzi's source code and can be changed to fit the mission requirement.

For gliding flight the return vehicle needs to be controlled about it's three axes; the pitch, roll and yaw axis. These axes determine the return vehicle's speed respective to pitch, attitude respective to roll and course respective to yaw. No propulsion is present, making it impossible to use any type of altitude hold control.

Using the Paparazzi autopilot, slight modifications need to be made in order to compensate

for the missing engine. This can be done on an XML configuration level or by modifying the code. Both methods eventually yield the same result, where modifying the source code can permit loops of higher complexity. This will be described in deeper detail in the next paragraphs for pitch, roll and yaw control loops.

Pitch (speed) control loop

When gliding, the aircraft's true airspeed is an important variable. Staying close to predetermined desired true airspeed, will allow the return vehicle to fly close to an optimal flightpath. This optimal path theoretically should result in a situation where the lift over drag ratio has the highest possible value respective to the aircraft's theoretical aerodynamic model. The range will, as a result of this type of control, be extended to its theoretic maximum range.

The pitch control loop, which is a typical modified P+I control loop (integration branch starts after the proportional gain). As can be seen in figure 10.3, this loop starts with determining the error between the actual true airspeed and the desired true airspeed. The error is multiplied with a proportional gain. Next in the loop the error is integrated and multiplied with it's gain integration value. Summing these values results in a limited value for the elevator command. In Paparazzi this is a normalized value that ranges from -9600 to +9600.

Because Paparazzi predominantly deals with aircraft that have a propulsion system installed, the pitch loop had to be modified to fit the aircraft's gliding characteristic, where the throttle command is replaced with an elevator command. The original loop used throttle to maintain speed, while the elevator command was used to maintain altitude. In figure 10.3 can be seen that the throttle command has been substituted for a pitch command. The pitch command will therefore control the return vehicle's flying speed.

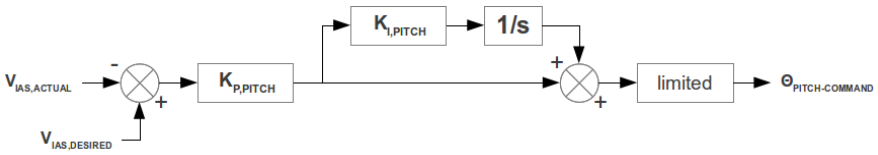

Figure 10.3: Pitch control loop

Roll (attitude) control loop

The roll control loop as seen in figure 10.4 determines the aircrafts attitude and changes the attitude if roll is used to make a turn.

This loop basically sets a desired roll angle and commits to holding this angle. Summing the desired roll angle and the actual roll angle results in an error that can be multiplied with the proportional roll gain, forming the proportional part of the roll control loop. Paparazzi adds an additional element to the loop that includes the roll rate multiplied with a specific roll rate gain. The sum of these two elements results in a limited value (±9600) for the normalized roll command which is sent to the aileron's servos.

Paparazzi's original roll control loop includes a correction for throttle. Because a propulsion system is not present in the return vehicle, this element is excluded in the modified roll control loop.

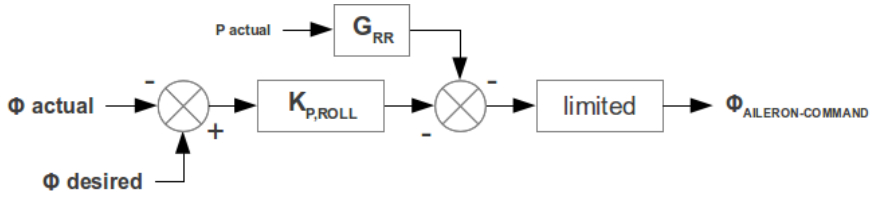

Figure 10.4: Roll control loop

Yaw (course) control loop
A type of control is needed that is capable of ensuring that the vehicle's course is always in the direction of the desired heading. This is established by a course control loop.

The course control loop as seen in figure 10.5, which is a typical modified P+D control loop (differentiation branch starts after the proportional gain), begins by determining the error by summing the actual heading with the desired heading. The error gets multiplied with the proportional course gain. Next the error is differentiated and multiplied with a differential course gain and the proportional course gain. The sum of the proportional part and the differential part forms a limited value which sets the desired roll angle. This instigates a roll up to the point where the error reached a the desired value for the desired roll angle.

The rudder command is not present in the original Paparazzi loop. Paparazzi uses the course control loop's command output as an input for the roll control loop. The use of the rudder is preferred to increase the efficiency of autopilot controlled turns, but is left out to keep the autopilot as simple as possible. This ensures that no heavy modifying of the Paparazzi source code is needed, which could lead to unforeseen time consuming bugs and raise the complexity while a simple solution could suffice.

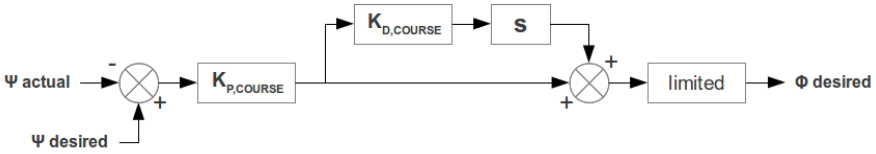

Figure 10.5: Yaw control loop

Gain settings versus altitude
The mission profile states that the return vehicle will be dropped from high altitude and will attempt to find it's way back to the point of origin (designated landing spot). During the flight densities vary greatly and control loop gains need to be adjusted accordingly to ensure the return vehicle's controllability. Paparazzi allows this to be done via its flight plan by specifying at what altitude to choose a corresponding gain value. By setting up specific blocks in Paparazzi's flight planner, it is possible to handle in-flight gain changes with respect to sensor-input from the on-board barometric pressure sensor and GPS. The barometric pressure sensor allows Paparazzi to determine the pressure altitude (atmospheric conditions at 0 m ISA need to be set before flight). GPS is an equal viable option, but it's implementation will be investigated in future autopilot designs.

Other fixed wing control loops in Paparazzi
The fixed wing control loops supplied by the Paparazzi code span several other loops, but have

little use for a gliding return vehicle. Loops for maintaining altitude which delivers output for auto throttle loops can be neglected since the throttle will always have a zero value and does not influence the complete system. The auto pitch and pitch loop are members of the vertical control group. They can be switched off, thus making them non-responsive.

At this point, there is no control that corrects for negative wind speeds, because there is no available aerodynamic- and performance theory that can aid in the design of such a control. This type of control will be part of future parts of the autopilot.

Spin stabilization
The return vehicle is dropped at an altitude of 35 km. Because of the very low densities at these heights, it's easy for the return vehicle to find itself in a stable spin. At this moment Paparazzi does not include any active spin recovery loops. This means no native support from Paparazzi is available and active spin recovery needs to be developed/implemented into the Paparazzi code. Advanced expertise is not available, thus an own version of active spin recovery control needs to be investigated and designed for likely to occur situations. Spins can be virtually created to a certain degree by making use of simulation software like JSBSim or analytical methods.

Future autopilot design
The autopilot design within the bounds of this project is kept as simple as possible respective to the KISS design philosophy. KISS stands for "Keep It Simple Stupid".

Preliminary return vehicle control loops neglect the use of the rudder. This is however not intended for future development of the aircraft. Paparazzi implementation needs to be explored and tested. Testing the Paparazzi hardware will yield a better understanding of the Paparazzi source-code / XML-structure and it will thus be possible to design more complex control loops that can increase gliding efficiency.

Determination of proportional, integrator and differentiator gains can only be found after the vehicle is tested in a real environment (i.e. wind-tunnel) or/and in a computer simulated environment.

10.2.3 Navigation

Navigation is the process of planning, recording and controlling the movement of a craft from one place to another. The planning is done using a flight plan discussed in section 10.2.1. The recording and controlling is handled by Paparazzi which uses the planning as its input. Recording is done by the sensors discussed in section 10.1 and controlling is done by servos connected to the control surfaces. Inbetween these are the control loops discussed in section 10.2.2. The Flight Plan is an XML file that must contain waypoints and blocks, while it can optionally contain sectors and exceptions. The blocks contain different functions or manoeuvres where the waypoints are used as reference. For example a block could contain the manoeuvre to fly circles around a waypoint, or the condition to wait for GPS signal. Using deroute or exceptions the autopilot can jump between blocks, executing one manoeuvre after the other. Changing between blocks can also be done in the ground control center. Sectors are used to create no-fly-zones, using exceptions to deroute when the vehicle is in a sector.

The blocks used in the flight plan for this mission are based on the steps discussed in the mission profile in section 3.1. The different control loop gains required for different altitudes (as previously discusses in subsection 10.2.2) during the descent are in blocks, they are executed when an altitude is reached using exceptions.

10.2.4 Simulation

This subsection of the aircraft systems chapter covers the simulation of the return vehicle. An attempt is made to create a virtual model which allows testing of the vehicle's performance, autopilot navigation and autopilot control loops. JSBSim, an open source flight dynamics library and simulation tool, is used to create and test this virtual model in a simulated environment. This virtual model is also known as a flight dynamic model (FDM); it spans the returns vehicles metrics, mass balance, reactions (external & ground), propulsion, autopilot, flight control systems and aerodynamics.

JSBSim

JSBSim is a flight dynamics library and aircraft simulator, which was originally written by Jon S. Berndt and now is being maintained by a large team of independent engineers active in the aerospace industry and within the academic community. The software package is widely used for academic research and educational purposes. It has been implemented as part of the core simulator for full featured flight simulation like Paparazzi, FlightGear and OpenEagles.

FDM setup, scripting & output

Figure 10.6, describes how an aircraft's flight dynamic model is configured in XML using JSBSim. An event driven XML script controls and plans parts of the simulation, this allows recreating situations and changing parameters respective to certain occurrences, i.e. initial conditions, altitude change, elapsed time, autopilot controls and parameters, etc. All output can be gathered in a CSV file and its contents can be plotted.

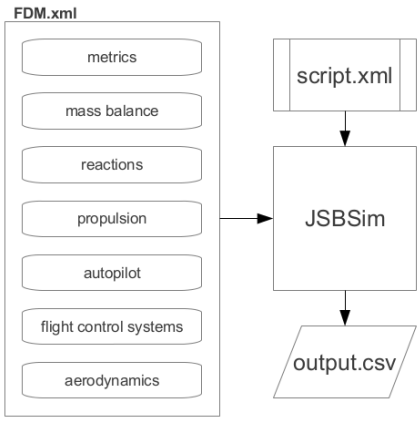

Figure 10.6: JSBSim overview

Paparazzi autopilot testing

Initially, the goal of the simulation will be to test Paparazzi autopilot settings and to gain some insight into the paparazzi control loops. On the long run this goal will change, because the FDM will become more accurate and more situations can be tested. This will aid in the flight planning and design of control loops with higher complexity.

At this point the return vehicle's FDM is far from an accurate representation of the real world model. Implementing an initial mass balance, dimensions and aerodynamic parameters yielded a virtual model which displayed nose heavy stable spins at 2,000 m and 10,000 m which it is

unable to recover from. Because the model is already unstable without any automatic control (ailerons, elevator and rudder in neutral position), its evident to say that no realistic data can be gathered from this virtual model. The model should in theory be stable given that it has a 15 % stability margin, it also has a similar aerodynamic shape as to other RC models in the same weight category.

Comparing and debugging the return vehicle's FDM with other aircraft FDM's, it has become clear that the aerodynamic parameters need be defined with a higher accuracy. Only physical test flights with logged data and wind tunnel tests can validate and thus increase the virtual model's approximation to real world behaviour. Until these tests can be conducted, the return vehicle's FDM will remain in alpha phase and will yield no usable results.

10.2.5 Risk analysis

In case the autopilot fails, some safety features will be incorporated. As discussed in subsection 10.2.3 different modes can be activated in case there is no GPS signal or communication with the ground station for a certain amount of time. Another possibility is that the battery level is too low to keep controlling the return vehicle during the duration of the mission. In that case the return vehicle will switch to a power efficient mode. Also there is the option the autopilot will fail causing no control of the return vehicle. In that case as a last measure the parachute will be activated as described in section 11. An overview of the different risks concerning the autopilot is shown in table 10.2.

Table 10.2: Risk table autopilot. In this table the different modes of failure with respect to the autopilot are listed with the action being taken. Also the probability of such a failure to occur is estimated.

Failure	Probability	Action taken
Total autopilot failure	Very small	Release safety parachute
Loss of GPS signal	Small	Fly holding pattern. In case long time loss of signal activate parachute
Long time loss of communication link	Small to medium	Fly autonomous to predefined location
Landing location out of range	Medium	Change landing location
Programming bugs	Small	Activate parachute from ground station

A verification and validation procedure will be done to the autopilot subsystem. To determine the gains of the autopilot the simulation described in subsection 10.2.4 is used. This simulation is validated by a real flight test at low altitudes. In case there are large discrepancies between the simulation and the actual flight test the simulation will be adjusted. The autopilot flight plan will first be simulated in Paparazzi Center and than validated by a low altitude flight. The input and output of the Lisa/M controller board can be tested on the ground. The attitude of the return vehicle can be adjusted and the output on the ailerons, rudder and elevator checked. Also a failure of the autopilot can be simulated and the parachute release tested.

10.3 Communications

Being able to communicate with the return vehicle is a crucial feature of the StratoBlimp system. The ability to communicate with the return vehicle is not only very useful during testing and

prototyping but it is also a feature offered to customers so they can always track the state of their valuable payload and it adds to the safety and flexibility of the overall system. Section 10.3.1 explains the need for a communication system and what it should be capable of. In section 10.3.2 the different communication frequencies and types are discussed and in 10.3.3 different radio modules are discussed. A link budget is generated in section 10.3.4 and the suitable frequency and radio module are selected. Also the needed gain is determined in this section. A suitable antenna for both ground station and return vehicle are selected in section 10.3.5. Section 10.3.6 goes deeper into the types of ground stations and section 10.3.7 gives a schematic overview on data flow and cooperation between hard- and software. In section 10.3.8 more can be read on the security of the wireless communication system. Finally possible risks have been assessed in section 10.3.9.

10.3.1 Features

During the entire mission a ground station will track the return vehicle. The dataset the return vehicle will send out includes GPS data, airspeed, barometric altitude, battery status and attitude. Knowing these values on the ground is not critical to complete the mission but it certainly helps during testing. It is also a main safety feature to always know the state of the return vehicle and have control over it. These values will be sent at different intervals depending on their importance. The GPS data will be sent with the highest frequency as it ensures the ground station can track the return vehicle, while battery status, attitude and altitude are of bigger importance in the later stages of the flight. The frequency with which this data is sent can then be increased. Besides receiving data from the return vehicle there is also a possibility to send commands. This could be very useful during testing to fine-tune the gains of the vehicle. Also during normal operation this feature might be used to remotely trigger the release mechanism or parachute or even change the landing location in the event of an emergency, for example during extreme weather conditions.

10.3.2 Band selection

Many frequency bands are considered but a couple jump out. The 434 MHz, 868 MHz and 2,4 GHz are all ISM bands and thus have a rather large allowable ERP without the need of a license. The team decided that designing the communication to be usable without the need for a license is preferable. If a higher bandwidth or longer range is needed a license could be acquired at a later stage or by the customer itself. Satellite communication is also an option the team considered. It is actually a very good option but the high recurring costs led the team to prefer direct link communication. Note that when tracking very valuable equipment satellite communication might be preferable as there is no risk of flying out of communication range. Communication will also still be possible when landed at an unforeseen location below the horizon of a normal tracking antenna.

10.3.3 Radio module selection

In this section the radio modules for three different license-free frequencies, namely 2400 MHz, 868 MHz and 434 MHz are discussed. These radio modules with their specifications are listed in table 10.3. The Xbee Pro 868 [47] is a tranceiver, which can both be used for transmitting and receiving. Due to this the XBEE Pro module is ideal for two-way communication. The Radiometrix NTX2\NRX2 [48] package contains a separate receiver and transmitter for the 434 MHz band. For two-way communication one of each type is needed on the ground station and the return vehicle. The XBEE Pro and Radiometrix NTX2 are shown in figure 10.7. For 2400 MHz the XBee Pro ZB is selected. This module is also a transceiver, just like the XBEE Pro 868 module [49].

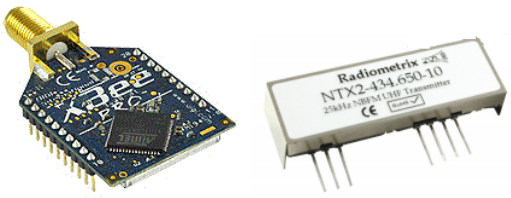

Figure 10.7: Left: The Xbee PRO 868. Right: The Radiometrix NTX2 transmitter

Table 10.3: Radio module specifications [47] [48] [49]

Frequency			
	434 MHz	868 MHz	2400 MHz
Model			
	Radiometrix	XBee Pro 868	XB Pro ZB
Max transmit power $[mW]$	10	315	63
Max transmit power $[dBm]$	10	25	18
Receiver sensitivity $[dBm]$	-118	-112	-102

As can be seen in table 10.3 there is a large difference in the transmit power, especially the 868 MHz module has a high transmit power. The transmit power and receiver sensitivity are used to create a link budget in section 10.3.4.

10.3.4 Link budgets

For three different license-free frequencies link budgets are generated to select the most suitable frequency. The discussed frequencies are 434 MHz, 868 MHz and 2400 MHz [46]. Also the needed gain for the antennas is determined. The selection of the antenna is further elaborated in section 10.3.5. The link budgets for up and down link are elaborated in this section. First an overview is given about the different terms used to make a link budget in table 10.4.

Table 10.4: Different terms in the link budget with unit [50]

Symbol	Unit	Description
$Pout_{Tx}$	$[dBm]$	Transmitting power in dB, depends on radio module
G_{Tx}	$[dBi]$	Transmitter antenna gain in dBi, depends on antenna
$FSPL$	$[dB]$	Free space path loss in dB, depends on distance between ground station and return vehicle
$Otherloss$	$[dB]$	Loss in power due to atmosphere
E_b/N_0	$[dB]$	Required signal to noise ratio in dB
G_{Rx}	$[dBi]$	Receiver antenna gain in dBi, depends on antenna
R_{xsens}	$[dBm]$	Sensitivity of receiver, depends on radio module
$Fademargin$	$[dB]$	Available end power in dB

Now that all the properties for a link budget are known, an uplink and downlink budget are made. There are however some regulatory constrains. The amount of effective radiated power (ERP) to transmit without a license is regulated [46]. The ERP is a combination of the transmit power and the antenna transmitter gain. For example: a transmitter with a power output of 100 mW and a gain of 3 dB has an ERP of 200 mW (3 dB is a factor two) [51]. These limitations

are listed in table 10.5.

Table 10.5: Transmit limitations [46]

Frequency $[MHz]$	Max ERP $[mW]$	Max ERP $[dBm]$	Bandwidth $[kHz]$
434	10	10	740
868	500	27	250
2,400	100	20	83,500

Table 10.6: Downlink budget for 868, 434 and 2400 MHz for a distance of 150 km between return vehicle and ground station.

Symbol	Unit	868 MHz	434 MHz	2400 MHz
$Pout_{Tx}$	$[dBm]$	25	7.85	5
G_{Tx}	$[dBi]$	2.15	2.15	2.15
$FSPL$	$[dB]$	-134.7	-128.7	-143.6
$Otherloss$	$[dB]$	-3	-3	-3
E_b/N_0	$[dB]$	-3	-3	-3
G_{Rx}	$[dBi]$	16.5	11.2	26
R_{xsens}	$[dBm]$	-112	-118	-97
$Fademargin$	$[dB]$	14.9	4.5	-4.4

Table 10.7: Uplink budget for 868, 434 and 2400 MHz for a distance of 150 km between return vehicle and ground station.

Symbol	Unit	868 MHz	434 MHz	2400 MHz
$Pout_{Tx}$	$[dBm]$	10.5	9	5
G_{Tx}	$[dBi]$	16.5	1	15
$FSPL$	$[dB]$	-134.7	-128.7	-143.6
$Otherloss$	$[dB]$	-3	-3	-3
E_b/N_0	$[dB]$	-3	-3	-3
G_{Rx}	$[dBi]$	2.16	2.16	2.16
R_{xsens}	$[dBm]$	-112	-118	-97
$Fademargin$	$[dB]$	0.43	-4.6	-30.4

To check which frequencies can be used, link budgets for the downlink and uplink situation are generated respectively. The downlink budget is shown in table 10.6 and the uplink budget in table 10.7. The values for output power and receiver sensitivity are obtained from the references in section 10.3.3. With the specifications and free space path loss the needed antenna gain is calculated to have a positive fade margin [50]. However, the combination of transmit power and antenna gain for the specific frequency should stay within the ERP regulations stated in table 10.5. Also the antenna gain on the return vehicle is limited to 2.15 dBi since a half-wavelength dipole antenna is used, which will be explained in section 10.3.5.

For the downlink a positive fade margin is found for the 868 MHz and 434 MHz frequencies. A negative fade margin is found for the 2400 MHz frequency, this frequency can't be used within the restrictions of the ground station antenna. For the uplink budget however the only feasible option would be the 868 MHz frequency. This is however a very small fade margin. This margin

is hard to improve, since the sum of the G_{Tx} and $Pout_{Tx}$ value is not allowed to be larger than 27 dBm (see table 10.5) due to restrictions. Also the G_{Rx} can't change, since this is a property of the radio module. Changing the antenna on the return vehicle is also not an option, since a dipole antenna is used (section 10.3.5). An option might be to reduce the range a ground station has to cover, so the free space path loss gets smaller and thus the fade margin will increase. The fade margin for 868 MHz with respect to the ground station distance is given in table 10.8. As can be seen for a smaller distance to cover the fade margin will increase, and thus will increase the radio link performance. This can be reached by using multiple ground stations, as discussed in section 10.3.5.

Table 10.8: Distance in km versus fade margin in dBm for 868 MHz frequency

Distance $[km]$	Fade margin $[dBm]$
50	10
75	6.4
100	3.9
125	2.0
150	0.426

Data rate can be determined from the E_b/N_0 ratio [52], the bandwidth and the signal to noise ratio which is in this case the fade margin. Using the values from table 10.6 and 10.7 for 868 MHz results in a theoretical maximum downlink data rate of 77.60 kB/sec and an uplink data rate of 2.24 kB/sec. The downlink would certainly be sufficient as a GPS coordinate typically takes up between 1 and 8 bytes depending on the coding used and resolution needed. Using Hoffman coding could bring down the size of a GPS coordinate to 4.4 $bits$. As every command takes up a different amount of bits it is difficult to estimate how much uplink speed is needed. But certain is that with a speed of 2.24 kB/sec commands can be send. If this is possible within the standard paparazzi format is still to be determined. But adding a simple coding layer to the communication module to compress the commands could be a solution if the data rate proves to be a problem.

10.3.5 Antenna

This section describes the antenna choice for the return vehicle and ground station. Cost, link quality and flexibility are taken into consideration to make this choice. For the return vehicle the mass of the components has also been considered.

For the return vehicle low mass is the main selection criterion for the antenna. Though the mass of the antenna is very important the radiation pattern and gain of different antenna types are also taken into consideration. High gain directional antennas like parabolic and helical antennas are ruled out because of the high volume and mass. Practical options are a microstrip (patch) antenna (figure 10.8) or a dipole antenna. The mass of both antennas lies around 10 gr but the volume and shape differ. The microstrip antenna is a flat square antenna inside or mounted on a PCB, while the dipole is a metal straight wire or rod. The dipole antenna would be around 165 mm long for a half wave antenna. A full wave dipole would not improve the gain or reliability of the antenna so it is not considered.

When gains of both the antennas are compared the microstrip antenna comes out on top with a gain of about 6 dB while a half wave dipole has a gain of only 2.15 dB. The only property left to select the most useful antenna is the radiation pattern. The radiation pattern dead spots could be countered by using an array of antennas but this isn't considered a good option for this application as this would make the mass of the communication system go up too much or would

Figure 10.8: A microstrip (patch) antenna

require a lot of custom electronics design which isn't possible in the scope of this project.

The microstrip antenna has a radiation pattern in the shape of a half sphere. If the antenna is mounted on the bottom side of the return vehicle facing down it would only be in contact with the ground station when flying in close proximity in normal flight. Mounting the antenna in the nose would also be an option. This configuration ensures contact with the ground station during the ascent and whenever the return vehicle is heading towards a ground station. This has the disadvantage that when the return vehicle is commanded to land at a site away from a ground station (it's heading is more then 90° different from the heading to a ground station) it cannot stay in contact with that ground station. The same is true when the return vehicle is to fly a hold pattern. It would lose its communication for every half circle of the holding pattern, the latest is of less concern as it would come into communication range again shortly while flying the second part of its holding pattern.

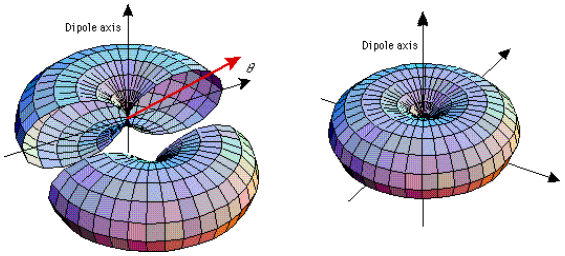

Figure 10.9: Radiation pattern dipole antenna

A dipole antenna does not have a dead zone of half a sphere but on the longitudinal axis of the antenna as can be seen in figure 10.9. The radiation pattern is typically shaped like a toroid with the antenna through its center. Mounting the antenna inside the wing parallel to the return vehicles y-axis (according to the vehicle reference frame F_r [36]) would result in a dead zone to the left and right of the aircraft. When mounted vertically, for example in the tail or sticking out of the aircraft (parallel to the z-axis in the F_r reference frame) as it is just 82 mm tall, would result in a dead zone straight below and above the return vehicle. This is the most preferred pattern as it is very flexible in regards to the heading of the return vehicle. It has the same properties as the y-direction mounting with regards to the ascend part of the mission. Following from the fact that a simple antenna is used on the return vehicle there has to be a high gain directional antenna on an auto tracking set-up at the ground station end of the link. Several options are possible here, a parabolic (dish) antenna, a helical antenna and a yagi

antenna are good options. When looking at the link budget, section 10.3.4, the needed gain can be determined. For the downlink an antenna with a gain as high as possible is required. More gain means a bigger signal to noise ratio which in turn results in a higher achievable data rate. To make the ground station configuration easier one antenna for up and downlink should be used. To stay within the maximum allowed ERP (table 10.5) the gain and transmission module output power should be tuned. It is obvious that a high gain is preferred over a high transmission power since a high gain also improves the downlink data rate.

10.3.6 Ground stations

The link budget in section 10.3.4 is calculated for a distance of 150 km so the first question raised is what the influence of the earth's curvature on the communication range is. When the ground station antenna is at ground level the return vehicle has to fly above 1.7 km at a range of 150 km to have a line of sight with the ground station. This does not take into account buildings and trees obstructing this line of sight. Putting the ground station on top of a tall building could solve this problem.

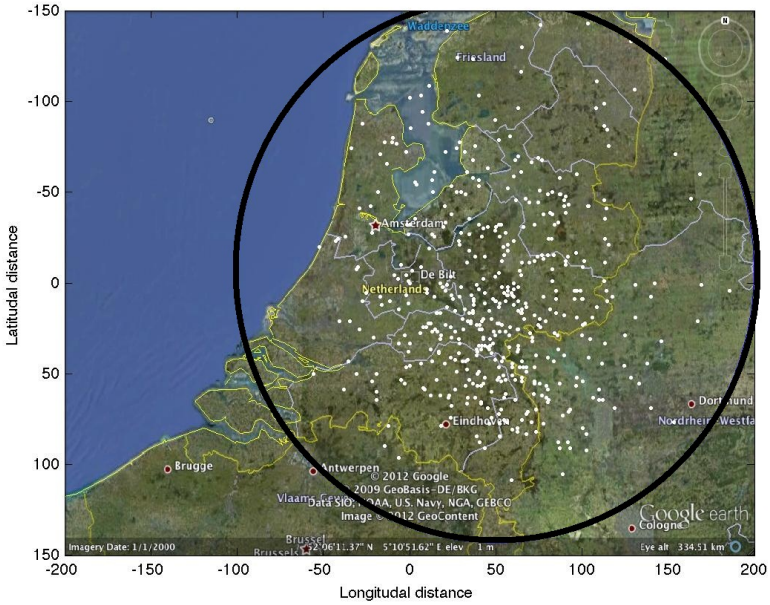

Figure 10.10: Burst location KNMI radio sondes and ozon sondes of the year 2012

According to the link budget there is little room for error in the uplink. When the range of the return vehicle proves to be bigger then 150 km the requirements might have to be adjusted stating that communication with the ground station is not required during the entire mission. As an alternative more ground stations could be added or a mobile ground station could be used. Though using a mobile station ups the operation costs and defeats the purpose of not having to retrieve the return vehicle. More advanced methods like using a relay satellite or launching another aircraft to relay the communications are not discussed as they are a lot more expensive than the proposed systems.

Figure 10.10 depicts burst locations of all KNMI radio sondes and ozon sondes of the year 2012. The blue circle is the communication range with a radius of 150 km with its center at the

KPN radio tower in Ugchelen. This proves that if these radio and ozon sondes would carry the proposed 868 MHz module we could in theory communicate with all but one of them using a directional antenna on the KPN radio tower in Ugchelen.

10.3.7 Communication flow

In figure 10.11 an overview of hard- and software components in the ground control station is depicted followed by 10.12 where a simplified version of the data handling in the ground control station is shown and lastly in 10.13 a simple overview of data handling between components in the return vehicle is shown.

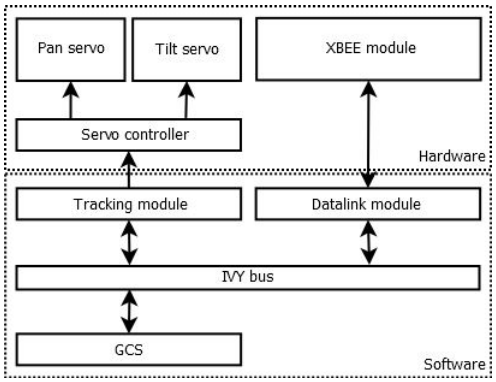

Figure 10.11: Hard and software components in the ground station

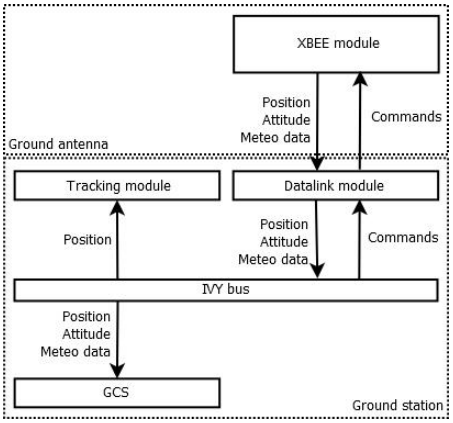

Figure 10.12: Ground control station data handling

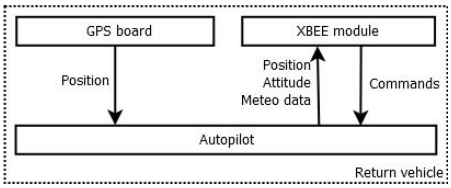

Figure 10.13: Return vehicle control software

10.3.8 Security

The return vehicle is a flying object capable of flying over almost the whole of the Netherlands and the fact that it is controllable with commercially available transmission equipment makes it possible for someone with the wrong intentions to take control over the UAV. To prevent this from happening the XBEE protocol used allows for 128 bit encryption. A 128 bit key is set in the ground station and all return vehicles belonging to a single customer. This immediately solves the problem when working with multiple clients in one area. Ground stations will only be able to track and see return vehicles having the customers encryption key set. One disadvantage is that it is quite easy to capture and copy the encryption key once a return vehicle is captured. People probably are not going to put this much effort into hijacking these UAVs considering the scientific nature of the market we are aiming at. But should the client lose a return vehicle the encryption keys could be changed. The keys could even be rotated on regular bases to increase security.

10.3.9 Risk analysis

A big risk during operation is a component failure or flying out of range resulting in a loss of contact with the ground station. During normal flight this should not be a problem, the craft will automatically return to the base regardless of its communication capabilities. Under exceptional conditions where returning to the launch spot is not possible due to extreme weather conditions or damage to the craft, this could be a problem. Therefore all systems ensuring the survival and retrieval of the return vehicle should not rely on its communication with a ground station. During prototyping and testing a backup communication package might be taken as payload to ensure the retrieval of the vehicle in case of a crash landing. This package could be a self contained communications module that sends its GPS coordinates over the GSM network.

10.3.10 Final selection

The best radio module to use is the XBEE 868 Pro, which uses a binary phase shift keying (BPSK) modulation technique [47] improving on the already tight link budget. It is also capable of AES encryption. This module can be used on the 868 MHz ISM band, where a relatively large ERP is allowed. Paparazzi is also capable of handling the XBEE API and another advantage is that the module can be used two-way; the module is capable of receiving and transmitting, instead of the Radiometrix modules. On the return vehicle the half wave dipole antenna is preferred mounted in the xz-plane tilted slightly forward in reference to the z axis (F_R reference frame) of the return vehicle. One single ground station is preferred for prototyping, this ground station could be mobile. When the range or data rate proves to be insufficient for a commercial application then buying a license might be the best solution as it improves range, and reliability of the data communication. Satellite communication could also be considered for high value payloads but this would require more development to integrate this type of communication with paparazzi.

Chapter 11 Release & safety mechanisms

In this chapter the parachute is selected in section 11.1 It covers the sizing and an analysis of the acceleration of the parachute. The release mechanism is discussed in section 11.2

11.1 Parachute

Due to the regulations, the return vehicle needs to have a parachute, in case of an emergency or malfunction. Also, at the testing phase it avoids the return vehicle from getting damaged. This is why a parachute needs to be installed.

11.1.1 Parachute Sizing

Design criteria

There are a few off-the-shelf products that can be used in the return vehicle. A parachute can be bought from the following manufacturers:

- FruityChutes
  - Classic eliptical
  - Iris Ultra chute
- RocketChutes
- Spherachutes

Since the mass of these parachutes is very high (over 140 grammes for the fruitychutes), it is decided to use a custom made parachute. In the design of the custom parachute the combination of surface area and drag coefficient must result in a maximum descent speed of 5 m/s. A typical drag coefficient for a spherical parachute is 1.5, except for the Iris Ultra chute which has a coefficient of 2.2. For the Rocketchutes and the SpheraChutes, no specific drag coefficient are known. For our typical parachute, we will calculate the area for a mass of 1.5 kg, which gives us a safety factor of 1.5 on the target mass. Using equation 11.1 we can calculate the minimum parachute area required at sea level.

$$D = C_D \cdot \frac{1}{2} \cdot \rho \cdot V^2 \cdot S \tag{11.1}$$

This results in a parachute surface area of S = 0.64 m^2 and for a round parachute a diameter of 90 cm. Following the fruity chutes recovery guidelines [53], the parachute needs the following parameters:

- Shroud line length is 1.15 times the parachute diameter.
- Shock cord is more then twice as long as the wing span.
- Packing volume has no bigger ratio then 1:5 in any dimension.

Next to these requirements, the following requirements were recommended by Sphera chutes [55].

- The parachute needs a spill hole in the middle for stability and to reduce the initial shock.

- The spill hole needs to be reinforced at its edge because of high loads.

Following these requirements, a parachute has been produced. The parameters for the parachute that needs to be produced can be found in table 11.1.

Table 11.1: Parachute production parameters

Parameter	Value	Unit
Diameter parachute	90	cm
Diameter spill hole	18	cm
Amount of shroud lines	8	-
Length of shroud lines	103.5	cm
Shock cord lenght	300	cm

Using the parameters from table 11.1 the parachute was produced. The packing volume and the masses of the shock cord and parachute are obtained and shown in table 11.2. In figure 11.1 the packed parachute is shown.

Table 11.2: Parachute primary parameters

Parameter	Value	Unit
Parachute mass	59	g
Shock cord mass	4.7	g
Packing volume	440	cm^3

Figure 11.1: The packed parachute including shock cord

Especially in mass, there is a big improvement with respect to the heavier designs of Fruitychutes and Rocketchutes.

In theory the custom made parachute will reduce the descent rate to 1.5 m/s. In practice the drag coefficient can differ from the theory, and therefor the parachute needs to be tested. This can be done by doing a simple test by throwing it out of the window. By filming the descent, the descent rate can be determined. In figure 11.2 an example of the test set-up is shown.

From this test it was obtained that the descent rate was 2.21 m/s for a system mass of 0.5 kg. By using equation 11.1 the drag coefficient can be calculated. This test gave a resulting drag coefficient of 2.5, which is 1.0 higher then the design drag coefficient. For this drag coefficient, it can be calculated that the descent rate of a 1.0 kg system would be 3.13 m/s, which is within

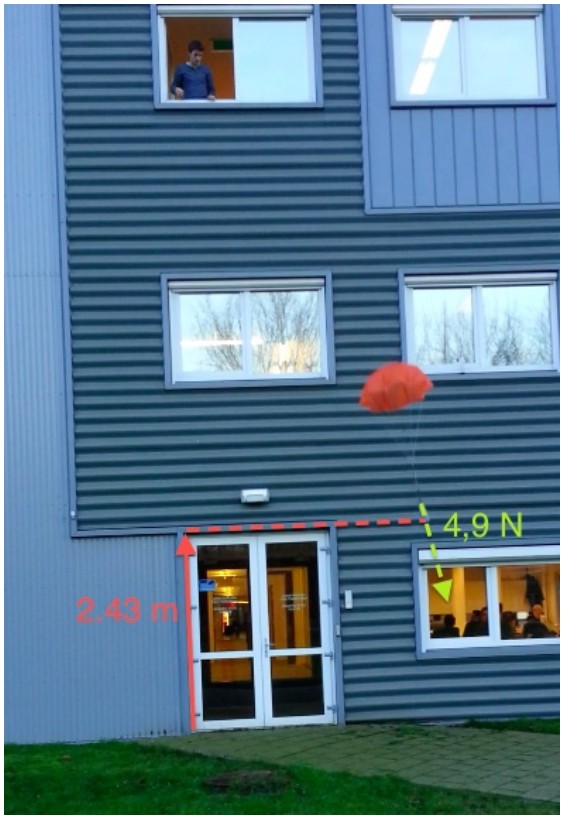

Figure 11.2: Out of the window test for descent rate

the design descent rate. The parachute surface can be reduced, if needed. This would save mass and volume in the return vehicle, and still meet the requirement of a 5 m/s descent rate.

According to the test results, we can resize the parachute. Because the drag constant appeared to be larger, the size can be reduced. Following equation 11.1, the parachute needs a surface of 0.384 m^2, with a diameter of 0.70 m. This smaller parachute will reduce the mass and packing volume. For these parameters, first a new parachute needs to be produced. Within this report the parameters of the parachute with a diameter of 90 cm are used.

11.1.2 Initial shock

During flight, the airspeed of the airplane will be larger than the designed 5 m/s descent speed of the parachute. This means that the drag force of the parachute will be larger. The maximum airspeed the vehicle can reach at sea level is about 90 m/s when pointed nose down. At this speed, a fully deployed parachute with diameter 0.70 m will have a drag force of 4763 N. This is 486 times as high as the drag force for a 1 kg vehicle at constant descent speed, and so the deceleration of the vehicle would be 486 g. The electronics and structure won't be able to withstand this deceleration, so the speed needs to be decreased more gradually. There are several options to cope with this problem. Two possible solutions are discussed below.

Decrease speed before deployment of parachute
To decrease the speed of the vehicle before the parachute deploys, a drag chute can be used with

a smaller surface that slows down the vehicle and also drags out the main parachute. Due to a decreased speed, the shock caused by the main chute will be smaller.

Slow opening of the parachute
Because the parachute needs some time to deploy, the surface at high speeds is low, and the drag force is lower. The parachute will be fully deployed at a later time, when the parachute has already decreased the speed of the vehicle. A system to slow down the deployment of the parachute is a riser. A riser is a ring over all shroud lines and can be pulled up towards the parachute. The shroud lines are smaller so the parachute can't be fully opened. Later on, when the riser will lower, the parachute can be fully deployed. At this moment the speed has been decreased and the shock will be lower.

Both concepts are investigated with respect to the opening shock. The effect of a drag parachute and delayed opening of the main parachute are analysed using a model [56]. The structure is designed to withstand a deceleration of 25 g or 245 N. For the two different systems, the deceleration and speed versus time is shown in figure 11.3 for a drag parachute and figure 11.4 for a slow opening parachute. The drag parachute does not decelerate the return vehicle untill a velocity of 5 m/s is reached, the main parachute still needs to deploy. With a delay of 1 s of deployment of the main parachute, the speed is reduced to 28.15 m/s according to figure 11.3. For this speed, the speed and deceleration with respect to time is calculated and shown in figure 11.5.

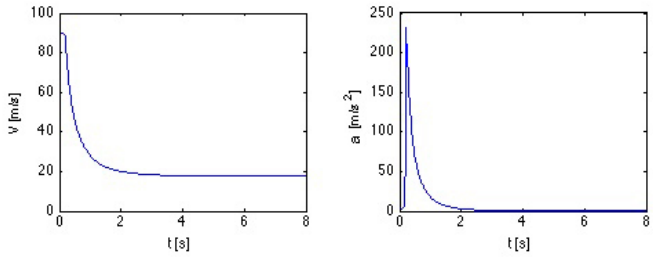

Figure 11.3: Velocity and deceleration using a drag parachute with diameter d = 0.16 m

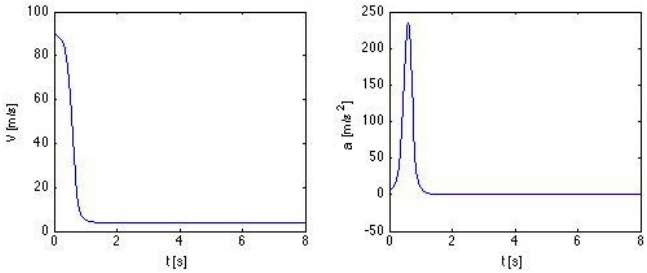

Figure 11.4: Velocity and deceleration using a riser which slows down the opening time to 0.55 s

It is possible to use both systems. Both systems have their advantages and disadvantages. Tests need to point out which system is best suitable for the return vehicle. At this moment, no conclusion can be given. Finally, because the shock acts over a small amount of time, a shock

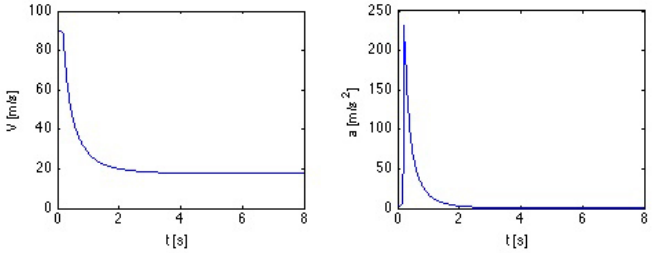

Figure 11.5: Velocity and deceleration using a parachute being fully deployed at 28.15 m/s

cord will be used to lower the shock impact.

11.1.3 Deployment System

The parachute will be folded and held within the fuselage of the return vehicle. The parachute will be double S-folded and the lines will be kept under the parachute, which is different from what is indicated in figure 11.1. Within this deployment system the following parts need to be made:

- Release of the deployment hatch
- Spring system to push the parachute out of the return vehicle
- Prevent obstacles in the compartment

The parachute will be stored in a compartment inside the return vehicle. This box will be closed by a hatch, mounted on top. At the rear this hatch will be held in place by two hooks. This system can be compared to the hatch of the battery compartment of a remote control. The hatch is released at the front of the return vehicle. On this side of the hatch, it also has hooks. The hatch will be hooked to a small bar, but when the bar rotates, the hooks will be released and the deployment hatch will open. The parachute spring system will push the hatch open. The hatch will stay attached to the parachute and function as a drag chute.

To function, the parachute needs to exit the return vehicle. For this to happen, the parachute can be dragged out or pushed out. When the hatch is being released, the parachute needs to push it away. This is why a spring system is being installed along the bottom of the parachute. Elastics will be attached at the top of the box. When the parachute is installed, the parachute will push the elastics down and so the elastics create a force which will push the parachute out of the return vehicle.

The parachute should be in a compartment without any sharp edges to prevent the parachute from ripping open or get stuck behind a part. For this reason, no obstacles may be present within the parachute box. The bar holding the hatch will be made outside this box. One of the major concerns is the tail of the return vehicle. When released, the parachute can get stuck in the tail plane. To minimize this risk, the tail plane has a sweep angle. Because of the sweep angle it is possible that the parachute will get off the tail plane, but further testing has to point out if this is sufficient. Otherwise a deployment bag must be used.

11.2 Release Mechanism

The release mechanism is very important; it separates the balloon from the return vehicle. Because the wire that is connected to the balloon has to be cut at any moment during the

mission, the release needs to be controlled. The wire needs to be cut if the balloons bursts and the descent starts, but also if the drift distance gets to large and the return vehicle needs to be released. It is important that the release succeeds, because wire and balloon debris can get stuck in the tail plane while flying which can make the vehicle uncontrollable. The wire will be at the bottom of the return vehicle, externally because of reduced space inside the return vehicle.

As release mechanism, different systems can be used. Two concepts seem suitable to release the rope:

- **Release by servo**
  This system would move a blade, so the wire connecting the return vehicle and balloon gets cut.
- **Release by heated resistor**
  This system will heat up a resistor which melts the nylon wire.

For both concepts, a trade-off will be made on the advantages and disadvantages of both systems.

11.2.1 Release by servo

A servo or actuator is designed to make a controlled movement. The servo can move a pin so the rope becomes loose or cut the wire with a blade. A servo can directly be connected to the autopilot, so the mass is dependant on the mass of the servo. Also the use of battery power is low, but the release is dependant on a working autopilot. Especially at high altitudes, it is not guaranteed that the electronics will keep working because of low atmospheric temperatures. Furthermore, because the system is external, moving parts can freeze causing the release mechanism to fail.

11.2.2 Release by heated resistor

The wire between the balloon and the return vehicle will be a 1 mm thick nylon wire. Melting temperature of this nylon wire is around 260 $°C$. This temperature can be reached with a resistor by overloading it for a short period. A small resistor with design power and temperature of 0.25 W and 250 °C respectively is used. This means only a small overload is needed to exceed the melting temperature of nylon. By connecting it to the 7.4 V battery, a current bigger then 0.034 A is needed, not causing problems for the battery. For a 10 Ω resistor, a 0.74 A current will be used. This is much higher then the 0.25 W, and an overload of a few seconds is enough to cut through the wire. The current is too high to connect to the autopilot, so a MOSFET needs to be used to activate the connection with the battery.

11.2.3 Trade-off

For the return vehicle, a trade-off is made on which release mechanism to use. It is important to select a design with respect to volume and reliability. Both systems only have a mass of a couple of grams. On volume, the heated resistor is much smaller. Only the electric wire is needed and the MOSFET can be placed anywhere. The servo can also be used, but there is no space for the servo to be placed close to the release hook. This means a mechanism is needed to place the servo somewhere else, resulting in additional mass. With respect to reliability, both systems can be influenced by the cold. The characteristics of the resistor can change, and the resistor may not work in a cold environment, which should be tested. However this system is not influenced by icing. It is a static system, and so no movement can be blocked by ice. The servo can get stuck because of ice. The servo is vulnerable to low temperatures so it should be placed inside the vehicle. This will make it less vulnerable to atmospheric temperature. This advantage however is not consider sufficient, so a heated resistor has been chosen.

Chapter 12 Market analysis

One of the key elements of a successful product is to have a clear overview of potential customers and their needs. Therefore a market analysis is performed.

This chapter consist of a short overview of comparable products and the current market in section 12.1. In section 12.2 the possible growth in the future is shortly described. In section 12.3 a profitability analysis has been done resulting in a profitability diagram. This diagram will be used in the design process as a market tool. At last in section 12.4 different distribution channels are discussed.

12.1 Current market

To have an understanding of the size of the potential market, it is investigated how many balloons are launched on a yearly basis. Also some research will be done to comparable products and the cost of these products.

12.1.1 Potential customers and market

In the Netherlands, twice a day a weather balloon is launched by the KNMI (Koninklijk Nederlands Meteorologisch Instituut) from De Bilt in the Netherlands [58]. The KNMI is responsible for over 700 balloon launches a year. As a comparison, the NOAA does the same in the United States for 70 sites, resulting in more than 50,000 balloon launches each year [59]. It should be noted that these balloon launches are for standard weather measurements with a 50 euros payload. Using a return vehicle for these type of measurements is probably too expensive since the investment of the return vehicle is large with respect to the payload. However, these institutions and other research organizations may be interested in a device which will automatically bring back the payload attached to the balloon.

There should be aimed for the more expensive measurement equipment used in weather balloons. Measurements for ozone concentration, UV intensity and other atmosphere composition typically require this expensive measurement equipment. Therefore there should primarily be aimed for this market segment. Currently this measurement equipment is too large and heavy to be used in the designed return vehicle. More compact measurement equipment could be developed with research institutes. Also no time and money has to be spent to go out and search for the payload. The cost analysis for a payload with a cost of 2,000 euros is elaborated in section 12.3

12.1.2 Comparable products

The most competitive products found are made by a company in New Zealand, called GPS Boomerang. This company builds a glider launched by a balloon, called the DataBird, which can carry a payload up to 330 gram. It can reach a maximum altitude of approximately 35 km. However no proof exists the DataBird ever reached an altitude above 20 km. There are some big performance differences between the DataBird and the designed return vehicle. The DataBird does not allow for any communication from the ground with the glider. It should be noted that the DataBird operates in New Zealand where different regulations for weather balloons and UAVs apply. Also the designed return vehicle is much more likely to get permission to fly in the Netherlands, since it carries a safety parachute and the DataBird does not. Despite these differences, the DataBird should be considered as a very competitive product as it is already on the market [57]. Besides the DataBird no comparable products are found.

12.2 Future market

The growth in need of weather balloon measurements, as performed by the KNMI and NOAA, is considered to be zero. There is no reason to suspect this market in Europe or the United States will expand. A possible growth market could be countries in Asia and Africa, since by growing prosperity in these regions increasing amount of government budget is used for research. Though the current market is not likely to make a large growth in Europe and the US, it is a fact that every day several hundred weather balloons are launched for which a return vehicle potentially could be used, so this might create a very steady demand for the designed return vehicle.

12.3 Profitability analysis

To investigate if the return vehicle is an economically feasible product a profitability diagram is created. This diagram shows the potential profit the designed return vehicle will make in a life cycle with respect to the old situation; not recycling the measurement equipment. This analysis is done by using equation 12.1. This gives an estimation of the potential profit generated when using the return vehicle with respect to the previously used method. A description of these variables is given in table 12.1. The way the diagram should be interpreted is described in the caption of the figures.

$$Prof = Cycles \cdot ((1 - Rec\%) \cdot PLcost + PLRcost) - Prodcost \tag{12.1}$$

Table 12.1: Description of variables in formula 12.1.

Variable	Description
Prof	Profitability of using the return vehicle with respect to using the old method
Rec frac	fraction of recovered equipment using the old method
Cycles	Number of cycles the return vehicle can be used in one lifespan
PL cost	Payload cost
PLR cost	Payload recovery cost using the old method
Prod cost	Initial purchase cost of the return vehicle

The recovery cost is estimated to be 300 euros per mission. These cost consist of the man hour and transport cost. Assumed is a payload with a cost of 2,000 euros which after retrieving could be reused. Examples of such payloads are for example spectrometers, particle density meters and UV radiation meters. The values in table 12.2 are used in equation 12.1 to generate the profitability diagram for a mission with more advanced measurement equipment.

Table 12.2: Used values in equation 12.1 for profitability diagram for mission with expensive measurement device

Variable	Value
Rec frac	0.97
Cycles	Number of cycles the return vehicle can be used in one lifespan, set as variable
PL cost	2,000 euros
PLR cost	300 euros
Prod cost	Initial purchase cost of the return vehicle, set as variable

The profitability diagram is given in figure 12.1 with a top view in figure 12.2. Note that not all of these design combinations are feasible; it is simply not realistic to design a return vehicle at

the lowest price which can be used 100 times. This figure has been used as a guide to determine how many flights the return vehicle could make with corresponding purchase costs to have a competitive product.

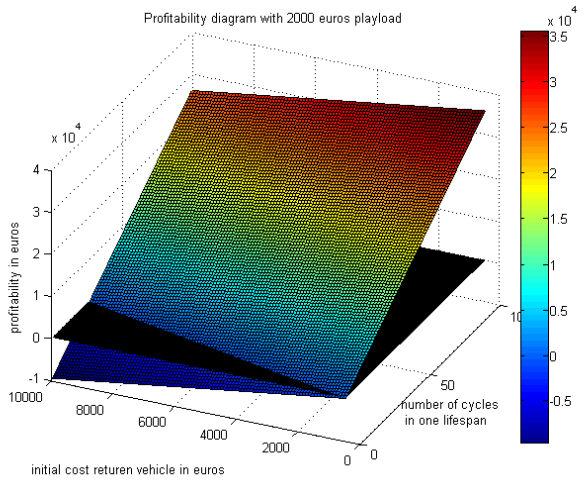

Figure 12.1: Profitability diagram for a mission using a measurement device of 2,000 euros. On the x-axis and y-axis are the initial cost of the return vehicle and number of cycles it can be used respectively. On the z-axis the profit for this combination of initial cost and usable cycles is given.

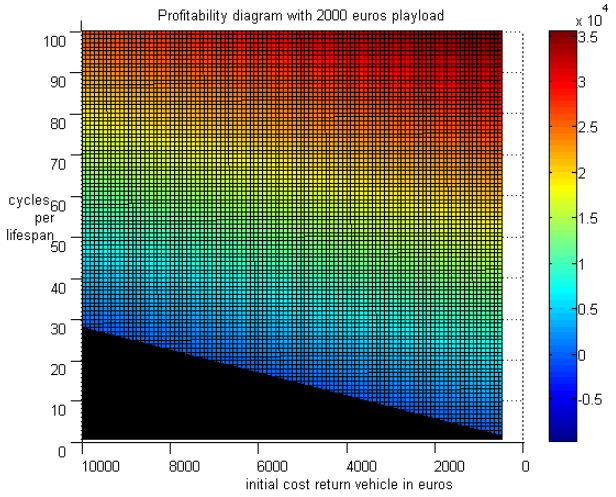

Figure 12.2: Top view of the profitability diagram for a mission using a measurement device of 2,000 euros. The cycles per lifespan are stated on the vertical axis and the cost of the return vehicle on the horizontal axis. Only combinations which generate a profit are shown, with the potential profit indicated in the color bar on the right.

12.4 Distribution channels

The best way to get the product to potential customers is by making contacts at the KNMI and other research institutes which perform measurements in the atmosphere. A first model could be tested by such a research institute. In case the potential customer is satisfied by using the return vehicle it could be recommended by this customer to other potential clients.

Another useful medium to get the return vehicle known by potential customers is the ISARRA, the International Society for Atmospheric Research using Remotely piloted Aircraft. This group discusses all the possibilities to perform measurements at high altitudes using small aircraft. This group already has contacts with potential research organizations which could be interested in an advanced descending vehicle [61].

12.5 Summary

To compete with current weather balloon systems the price of a return vehicle should be kept to a minimum. However it should be as robust as possible so the customer can use it under most weather conditions and it can be used at least 20 times. That is why it is recommended to use very durable and high performance materials, further elaborated in chapter 7. The cost of the materials however are kept in mind. The customer wants the return vehicle to glide back to the launch spot. From chapter 3 it is found most of the weather balloon burst within a 150 km radius from the launch spot. Therefore it is recommended during the aerodynamic design, elaborated in chapter 5 the return vehicle can glide this distance. Besides performance also the reliability and safety of the return vehicle are important factors to keep the payload intact. That is why several safety features are programmed in the autopilot and it is also one of the reasons a parachute is used in the return vehicle.

In the project requirements a maximum price of 10,000 euros per return vehicle was given. There will be aimed for a cost of 5,000 euros to be competitive with for example the DataBird from GPS Boomerang [57]. From the profitability diagram it can be obtained that in this case a return vehicle is still economically beneficial for a payload which has to be recovered. The return vehicle will be too expensive to use for standard weather balloon measurements, since the cost of a payload for a standard weather balloon is only about 50 euros [58] and there is no need for the measurement equipment to be recovered. From a sustainable perspective however using the StratoBlimp system will reduce the amount of waste in the environment.

The return vehicle is more competitive for missions with more expensive equipment. For these missions the risk of loss of the measurement equipment is reduced by using the return vehicle. Besides the risk of loss of equipment also money is saved since no recovery costs have to be made. Currently the return vehicle can only be used for a standard atmosphere measurement as performed by the KNMI. The payload compartment is too small to fit advanced measurement and thus expensive equipment inside the return vehicle. In collaboration with a research institute a more compact measurement could be designed, which can be used multiple times. Using the return vehicle can then reduce the measurement cost significantly as can be seen in figure 12.2 and 12.1.

Chapter 13 Review

This chapter provides a retrospective view of the design process. Section 13.1 gives the compliance matrix which gives an overview of starting requirements met. Section 13.2 contains the feasibility analysis which explains why certain requirements were not met. Section 13.3 deals with reliability, availability, maintainability, and safety. Section 13.4 provides insight in the sensitivity of the design to a change in parameters. Finally section 13.5 contains information about the technical risks in the system.

13.1 Compliance matrix

Table 13.1 gives an overview of the requirements set and whether they are met or not. For those not met the reason is given in section 13.2. At this moment the first prototype of the StratoBlimp return vehicle meets 75 % of the requirements. The system is able to accomplish the project objective: a high altitude weather balloon system that is capable of autonomous return and soft precision landings, within a budget of 10000 euro, designed by 10 students in 10 weeks time. The requirements not met are mostly related to the nonexistence of UAV regulations and restrictions on communication without license.

13.2 Feasibility analysis

This section explains why not all requirements set at the beginning of the project are met. To meet the schedule requirement of the DSE, for efficiency during prototyping, and in one case because it is simply not feasible with current weather balloons, some requirements were considered more important, while some are rescheduled to be fulfilled post-DSE.

Maximum altitude

In discussion with the client the maximum altitude requirement of 50 km was quickly dropped since it was unfeasible within the budget with current weather balloons. The new requirement of 35 km is more realistic, although the burst altitude of commercially available balloons is unpredictable.

Landing range

To acquire a landing range of less than 10 m a highly specialized sensor suite would be necessary. As discussed in chapter 11 with the GPS accuracy a landing range of 40 m can be achieved. This requires a large grass field, but the balloon launch also requires this. Therefore a 40 m requirement is considered sufficient.

Optional and extra dataset

Due to regulations with respect to transmit power, and the large distance to cover, images will not be send to the ground station. If a license is obtained, the transmission power can be 10 times as high and testing will show whether this bandwidth allows for both the meteorological data and the images to be directly sent to the ground station. The current design is not adapted to this, images are stored on an internal SD card.

Regulations

As discussed in section 3.3 the return vehicle is not allowed to perform the entire mission at this moment. Post-DSE the procedure of obtaining permission will be continued. The mission profile

Table 13.1: Compliance matrix

Category	Requirement		Value
Performance	Operate from sea level up to 50 km altitude	✗	35 km
Performance	No power can be used for trust	✓	
Performance	The return vehicle should land with a maximum circular error of 10 m	✗	40 m
Performance	The maximum vertical landing velocity can not exceed 1 m/s	✓	
Performance	The return vehicle has a life time of at least 20 flights	✓	
Science mission	The sensor package includes a standard meteorological sensor suite	✓	
Science mission	At the highest point film the curvature of the earth and the blackness of space	✓	
Science mission	2-way data communication during the entire mission, data shown on ground station	✓	
Science mission	A HD camera system capable of filming the entire mission	✓	
Science mission	Minimum dataset: attitude, altitude, speed, position and battery voltage	✓	
Science mission	Optional dataset: meteorological data	✗	
Science mission	Extra dataset: Pictures from camera	✗	
Safety and reliability	The return vehicle performs precision landing on a predefined landing spot under all weather conditions	✓	
Safety and reliability	The operations should in no way interfere with commercial airline operations	✓	
Safety and reliability	Faillure of the return vehicle should not endanger commercial airline operations	✓	
Safety and reliability	The balloon and return vehicle have to operate within the current local regulations for weather balloons	✗	
Safety and reliability	The settings and gains need to be adaptable during the entire mission	✓	
Sustainability	A lost return vehicle shall not pose a threat to the environment	✓	
Schedule	A mission profile for StratoBlimp will have to be designed	✓	
Schedule	The turnaround time of the weather balloon is at most 1 day	✓	
Schedule	The mission profile should be compatible with current rules and regulations concerning weather balloons	✗	
Cost	The entire system can have a maximum cost of €10,000 per unit	✓	€2500
Additional	Meteorological measurements should be performed during both ascent and descent	✓	
Additional	Autonomous flight, using paparazzi as an open-source autopilot system	✓	

can be adapted, for example to clear military airspace, further contact with the regulator will show to what extend this will be necessary.

13.3 Reliability, Availability, Maintainability and Safety

Within this section, the reliability, availability, maintainability and safety of the return vehicle will be discussed. Every item will be discussed separately.

13.3.1 Reliability

A perfect reliable system would work at all times. The reliability of the return vehicle can be split up in the following parts.

- **Structures & Materials**
  The structure is able to deal with high accelerations by using strong composites. Most of the weight is in the middle of the structure. Furthermore the material will encounter a large temperature range. The strong rohacell core in combination with aramid composite outer layer is able to deal with all flight loads and is impact resistant.

- **Autopilot**
  The functioning of the autopilot is essential for safe return of the return vehicle. To get a reliable system, iron out all human programming errors and obtain the gains necessary for all altitudes, intensive testing will have to be done, both in the Paparazzi simulation and in the air.

- **Environment**
  The environment can have a big influence on the flight of the return vehicle. High wind speeds, gusts and wet weather can cause the return vehicle to change its course. Because the balloon drifts due to the wind, the return vehicle needs to fly back upwind. This reduces the ground speed and the return vehicle can be forced to choose an alternative landing location. To test the reliability, the system will first be tested at calm weather, and without the presence of jet streams. When the drift is too large, the user can choose to release the vehicle or to let it fly to an alternative location.

- **Electronics**
  At high altitudes atmospheric temperature is lower than the minimal operating temperature of the electronics. If the electronics get too cold, they stop working and the vehicle can be lost. On the other side, since all electronics are working, they also produce heat. To prevent freezing all electronics are packed at the isolated core of the body against the battery.

- **Communications**
  The data link between return vehicle and ground station is designed for a maximum range of 150 km. If the link is broken, the vehicle can still complete its predefined mission but the user will not be able to change the mission profile or switch to an alternate landing location. Because an antenna needs to be pointed at the vehicle and weather conditions can reduce the range, the link is only reliable at a percentage of the theoretical maximum range. An increased transmit power can increase the range if needed, but for this a license is required. This problem could also be fixed using multiple ground stations, even extending range and reliability (redundancy) of the overall system.

13.3.2 Maintainability

The maintainability of the vehicle is dependant on the parts that needs to be maintained. Electrical components can easily be accessed by the maintenance hatches on top of the vehicle. The

same is true for the parachute through the same hatch through which it deploys. The only electrical component that is not accessible is the antenna in the tail. If this component malfunctions, the tail plane probably needs to be replaced. The maintainability will be an issue if the structure gets damaged. The whole skin structure is made out of one piece and so a particular part cannot be changed. In case of structural damage, it is not easy to analyze the damage and it will be better to replace the whole structure. This increases costs and will take time, but all internal components will be reusable. During belly landings, the bottom can get damaged. Because the vehicle is painted, damage to the aramid composite will be clearly visible (when paint is gone there may be no damage but the fibers do need to be checked).

13.3.3 Availability

Almost all current components of the return vehicle are off the shelf. When moulds are made subsequent production steps are relatively fast. Therefore the system has a high availability concerning production. Furthermore the system does not need heavy equipment, only a ground station, weather balloon setup, and the return vehicle, which can all be transported by one car. The turnaround time of the return vehicle is dependent on the reliability and the maintainability. As outlined in section 13.3.2, after a normal flight, it is easy to change the battery and put in a new memory card. By using two memory cards and two batteries one can be prepared for the next flight while one is being used. This way the turnaround time can be very close to the actual mission time. What is needed every mission is a balloon and hydrogen gas. For a normal mission, where the return vehicle returns to its launch spot, the availability depends on the availability of these two objects. If the return vehicle is not capable of flying back to the initial launch location. Then an alternative landing spot will be chosen. If the vehicle lands successfully at its alternative landing spot, it needs to be picked up. This will cost time, and so the availability will decrease. This will probably be a consequence of flying with bad weather conditions. Last, it is possible a component malfunctions or the structure gets damaged. This probably resulted in a landing by parachute, which means this component has to be checked for damage and be folded again. The availability, in case of maintenance, is dependent on the availability of the needed components and the type of malfunction, as discussed in subsection 13.3.2.

13.3.4 Safety

If a failure of the system will occur, the system needs to be landed safely. In table 13.3 the possible failures can be found. For every type of failure, the safety measure is described. In case of a failure during flight, it depends on the autopilot if the parachute will be deployed. When the autopilot is working after a failure, it is able to decide whether it is capable of landing the vehicle. When it turns out the vehicle cannot be steered anymore, the vehicle will descend to a height of 1000 m before deploying the parachute. This way, the vehicle will descend faster and the risk of collision with another airplane is reduced. During this descend, it is still possible a fault will be fixed and the autopilot will be able to fly the airplane again. In case the autopilot stops working, the parachute will be deployed after a short period. At this moment there is no additional control board for the parachute on board. Such a system will be isolated so it won't freeze and will take over control of the safety parachute in case the autopilot stops working. It will get its power from a reserve battery pack, so it is not dependant on the power of the main battery.

The design of the parachute and balloon are made following the regulations, with an added safety margin. This law requires a break strength of the rope between return vehicle and balloon of maximum 230 N. For this requirement, a nylon wire with a break strength of $220N$ will be used. Also the parachute is sized big enough to assure a descent speed lower then 5 m/s to assure safety. At last, filling the balloon needs to be done outside, in case hydrogen escapes. This way

Table 13.3: Safety measures in case of malfunction

Failure	Safety measure
Loss of contact	Await connection or safety parachute
Signal or sensor loss	Await sensor signal, safety parachute for critical sensor/signal
Control surface malfunction	Safety parachute
Uncontrollable situation, e.g. spin	Await controllable flight or safety parachute
Release mechanism malfunction	Attempt glide or safety parachute
Freeze of autopilot	Safety parachute
Not enough range to reach target	New destination or safety parachute
Structural break-down	Safety parachute
Struck by object during flight	Disconnect from balloon or safety parachute or crash
Battery out of power	Safety parachute

it will disappear into the atmosphere and will not cause any danger to the person filling the balloon.

13.4 Sensitivity

Changing specific parameters of a system usually influences the rest of the system as well, resulting in more parameters that need to change. This section illustrates the sensitivity of the systems to specific changes. The main concerns in case of the return vehicle are parameters that are related to mass, range or data link. Figure 13.1 shows the system parameters and their primary and secondary consequences on the system design. Following this diagram, extra care was taken to the design of high sensitivity parts, to ensure an efficient process, avoiding unnecessary iterations.

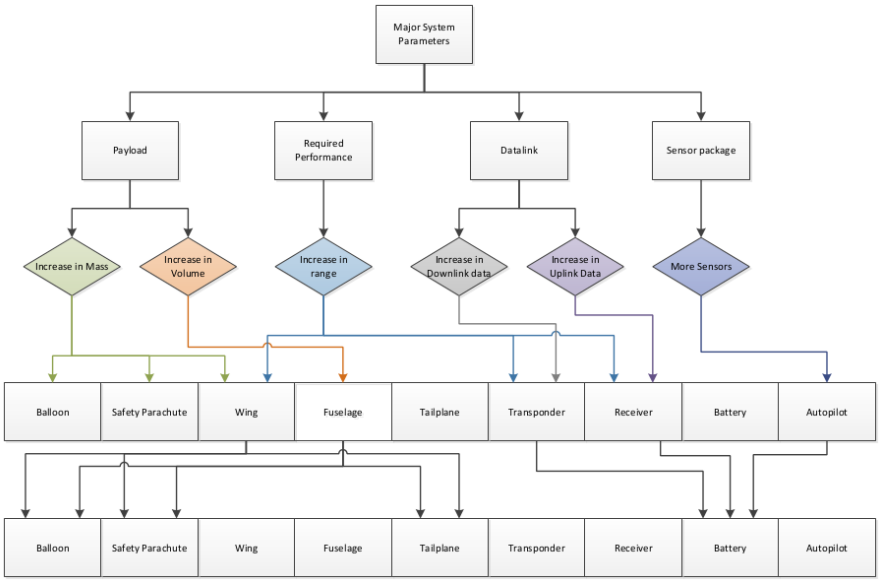

Figure 13.1: Sensitivity diagram on main system parameters

The first system parameter is payload, where the mass and volume can change. If the market

calls for a higher or lower mass or volume of the payload, the vehicle still needs to be able to operate. Concerning payload the system is not very sensitive, because the current payload is around 125 g while the maximum payload is 250 g. If the mass is lower then 250 g, dummy mass will be carried to place the center of gravity at the correct point. Furthermore the payload compartment is only approximately half full with the current payload. Increase above these quantities is possible, but while increasing mass mostly decreases performance (up to being unable to fly), increasing payload further than what fits in the fuselage now will be hard.

The second system parameter that has to be taken into account is range. Not only does the plane have to fly the required distance, the communication also has to have this range. This is why the transmitter and receiver need more power if this parameter increases. For a power increase, a license needs to be obtained.

Third is the data link: it is possible that more information needs to be transmitted to the ground station directly. There is a difference between uplink and downlink, but both call for an increase in power to transmit more data. This will increase the battery power needed. The battery is sized to have an extra 20% of power on board as reliability margin, which could be used, but for an equal level of reliability the battery needs to increase.

If the user requires more or other data than provided by the integrated sensors, these can be put in the payload department, or possibly in the electronics department. The autopilot can receive additional sensor data. In addition to calculating important parameters like attitude, data like weather conditions (humidity, temperature) are examples of data that do not need to be measured for the autopilot to work but for which sensors are installed. Every sensor brings in more mass and uses autopilot computing power. For this, more battery power is needed.

For all system parameters, with a change in mass, the balloon and safety parachute have to be changed. For any increase in power, a higher capacity battery is needed. From the diagram it can be found that the system is most sensitive to an increase in mass and increase of range. This is why special attention has been paid to sizing these parameters, as errors are hard to correct.

13.5 Technical risk assessment

In this section the technical risks, meaning the potential failures of the design, are identified and ranked in probability and severity upon occurrence. The higher these two parameters are, the more attention and resources need to be allocated to solving them. These risks are plotted in a risk map, table 13.4, with probability increasing to the right and severity increasing moving up, i.e. the high risk components are located in the upper right corner.

1. Autopilot

The autopilot works the way it is programmed. If faults have been made on programming, the autopilot will not function as desired. It is assumed most human programming errors can be filtered out through extensive testing. The error impact depends on whether the faults will decrease the performance of the vehicle or will make it uncontrollable. Also, the autopilot can freeze or overheat and stop working. In an uncontrollable situation or if the autopilot shuts down, the parachute will deploy preventing this risk from being catastrophic.

2. Battery

The battery is of high importance, because it has to power all electronics. The battery is therefore critical, and has been sized to carry 120 % of the power needed for a complete mission. Because of the low discharge rate, it is unlikely that the battery will overheat. Also a freeze of the battery is unlikely, because it is well isolated and it is surrounded by electronics producing heat.

Table 13.4: Risk map on probability and severity

	Very improbable	Improbable	Probable	Very probable
Catastrophic	12		8	
Critical	2,11	1,4,7	6	
Marginal		3,9	5,10	
Negligible		13		

1. Autopilot
2. Battery
3. Sensors
4. Actuators
5. Glide factor
6. High altitude stability
7. Control surfaces
8. Parachute
9. Release
10. Data link
11. Structural integrity
12. Collision
13. Payload

3. Sensor

Most of the sensors are sensitive to temperature extremes. The IMU is located in the fuselage though, as is half of the GPS component, meaning both of these are at least partially isolated. Sensors on the outside, such as the pitot tube are more likely to freeze up. Because the autopilot can calculate a lot of values by internal sensors alone, it only leads to a drop in performance, not to catastrophic failure.

4. Actuators

The actuators are placed within the fuselage of the vehicle. This way they are not sensitive to the atmospheric temperature. The risk of failure is minimized because a control surface failure can lead to an uncontrollable situation.

5. Glide factor

The drift of the return vehicle can get high in case of bad weather conditions. For this reason the performance of the vehicle needs to be sufficient to get back to the launch position. If this glide factor is not reached, an alternative landing site needs to be chosen. Because we have no data from flight tests, the glide factors can not be confirmed.

6. High altitude stability

At high altitudes, because of the low density, any dissimilarity can cause the vehicle to start spinning. This spin can cause high g-forces on components, which can cause them to fail. A failure can cause the autopilot to decide to deploy the parachute, meaning the vehicle is not able to fly back.

7. Control Surfaces

The control surfaces are moved by actuators in the fuselage of the vehicle. A rod is used to connect the actuators to the control surfaces. This brings in friction, which can cause the control surface to stay in place. The control surfaces can also freeze up during ascent, making them useless during descent. Depending on which control surface is affected, this can make the return vehicle uncontrollable.

8. Parachute

If any system fails, the parachute is needed to prevent a crash. Since the parachute takes a lot of space in the return vehicle, a lot of things can go wrong. The hatch can get stuck, the parachute can get stuck in the tail and the parachute can fail to open. The parachute will be tested extensively before letting the return vehicle ascend to high altitudes.

9. Release

When the balloon has burst, the vehicle needs to get rid of the wire connecting the two parts. This wire will increase the drag of the vehicle and can potentially get stuck in the tailplane, possibly making the vehicle uncontrollable.

10. Data link

A data link is used to send all parameters of importance. When the communication is lost, the vehicle is still able to fulfill its predefined flight plan. The parameters will also be saved on a data logger. Only in case of an emergency landing by parachute, the search crew will depend on the last moment coordinates that were transmitted.

11. Structural Integrity

Since the vehicle is constructed to sustain high load cases, the risk of failing structural integrity is low. If the structure fails, this will affect the performance of the vehicle and depending on extent of the damage result in a crash.

12. Collision

The return vehicle flies at different altitudes and can cross flight zones of commercial airlines. No-fly zones will be avoided however, so risk of collision is low. In case of a failure, the vehicle will descend to a height of 1000 meters before opening the parachute, to minimize time spent in the air while uncontrollable.

13. Payload

The payload can be found in the nose of the vehicle. The payload is off the shelf and failure will not affect the performance of the vehicle.

Chapter 14 Post-DSE

From the beginning of the DSE it was clear that to produce and test a prototype the timespan of 10 weeks would not be sufficient. Therefore 2 independent goals were set: First to present the prototype design at the symposium and second to perform the actual mission as a demonstration at an event such as the Cansat competition. Figures 14.1 and 14.2 give an overview of the post DSE activities.

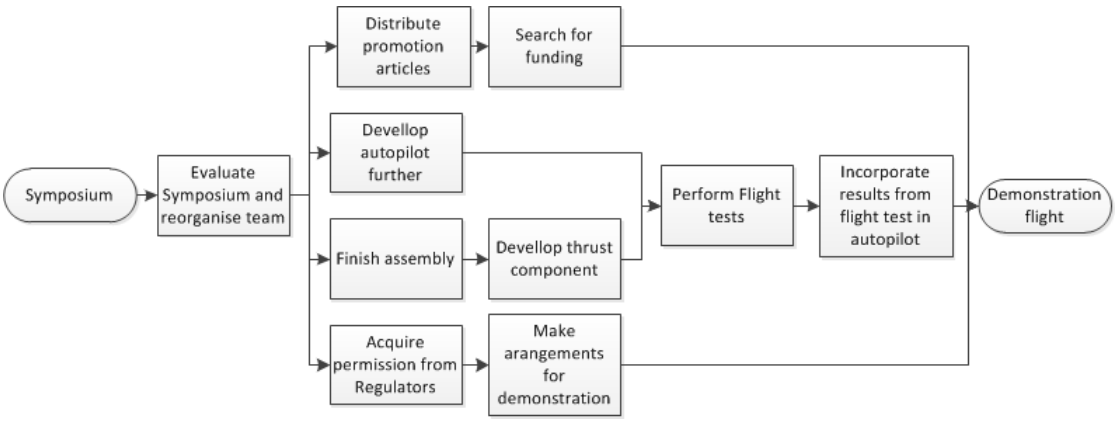

Figure 14.1: Post DSE activities flow chart

Symposium

At the day of the symposium a prototype of the return vehicle and ground station will be displayed. No test flights have been performed up to that point, and little validation experiments have taken place. The main goal at the symposium is to promote the StratoBlimp project and to give an indication of the progress that has been made. A good representation is critical. The symposium is the ideal platform to get the project known to companies, research chairs and fellow students.

Demonstration flight

The demonstration flight should take place at a promotion event to maximize exposure. The Dutch Cansat [62] competition would be the demonstration event of choice. The IMAV [63] would perhaps be more suitable, but it has more strict regulations on the use of airspace.

Post DSE development

At the end of the DSE there is still a lot of development that needs to take place before the full scale flight test can take place. In the first month after the DSE the prototype is further assembled and the programming on the autopilot is continued.

To obtain more accurate flight coefficients and autopilot gains, a flight test will have to be performed. A small propulsion component could be used to gain altitude from which the return vehicle can glide to the ground. The results from these tests can act as a validation of the stability, controllability and autopilot functions of the return vehicle.

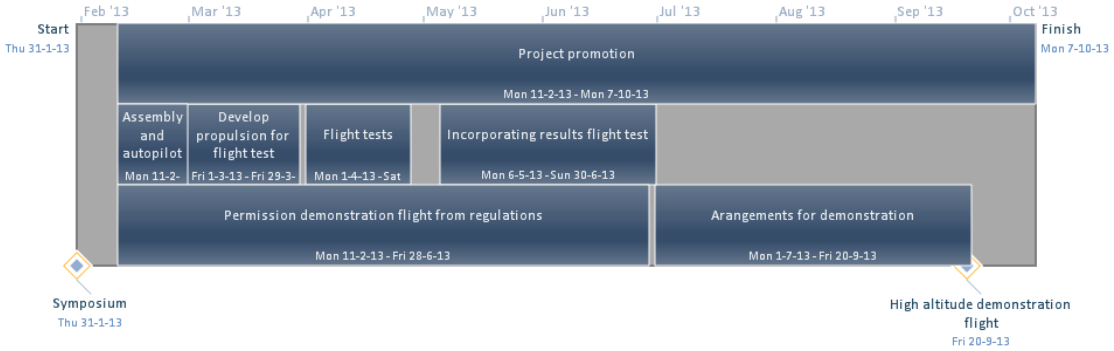

Figure 14.2: Gantt chart for post DSE activities

Further activities

After the symposium there is more time to look for funding. Since the initial budget only considered the construction of the prototype, the project will need more resources to continue its activities for the rest of 2013. This funding is likely to be coupled with promotion of the project. Potential sponsors are usually interested in student projects that generate exposure in the technical media such as national student magazines and the local university paper. Furthermore a permit for the high altitude demonstration flight needs to be obtained from the regulator. Lastly time is reserved to make arrangements for the demonstration.

Chapter 15 Conclusion

The project objective stated in the introduction was to design a next generation high altitude weather balloon system. With the exception of the maximum altitude and the required landing accuracy, the final StratoBlimp design meets all requirements. In order to also comply with the other requirements, a significantly larger budget and more development time is required.

For the current design aramid fibres and Rohacell 31 foam are selected for the materials to construct the body of the return vehicle. With these extremely light materials the total mass of the return vehicle prototype is estimated to be 850 g including 250 g payload, which is slightly lower than initially anticipated. Two way communication will take place by a direct link in the 868 MHz band. The ground station consists of an auto-tracking helical dish antenna connected to a laptop. It needs to be auto-tracking to comply with the European power transmittion regulations for amateurs while still be able to cover the 150 km range. An advantage of the ground station is that it is foldable and is transportable by car.

The autopilot board measures the pressure and location of the return vehicle. Additional Other atmospheric measurements are performed with additional sensors that measure temperature and humidity. To comply with mission requirements the return vehicle is also equipped with a HD camera to film the entire mission. However, the camera is placed in a separate compartment and has a stand-alone battery so it can be replaced easily. An alternative payload could consist of a more elaborate sensor pack, and because of this stand-alone compartment the system is suitable to a broader range of customers. A possible market is the high altitude observations research in particle content and radiation levels in the atmosphere. At the moment ozone sensor packs now have a mass of 1 kg, but they can be further optimized. Research on decreasing the mass of these sensors would allow them to be incorporated in the return vehicle.

The return vehicle is designed to be very stable during cruise flight so that little corrections by the autopilot are required. Due to the broad range of conditions the autopilot will change control gains by switching between modes. Such a mode can be defined by altitude or by flight mode such as the vertical dive at the beginning of drop. A different mode can also be activated by the user with the ground station. In case of a malfunction a parachute automatically deploys and the return vehicle will safely land on the ground. With the GPS coordinates transmitted to the ground station the return vehicle can be easily retrieved, saving labour and transport cost . This will ensure that the StratoBlimp has a significantly lower impact on the environment compared to the current system.

The StratoBlimp team has started building a prototype that will be used for testing. With demonstration flight planned at the 2013 Cansat competition the team wants to prove that atmospheric observations can be done in a more sustainable way and with a smaller budget.

With a prototype cost of €2500, the current design was produced for a quarter of the initial budget. The market price of the StratoBlimp system is expected to be around €5000. By improving the method for observations the StratoBlimp can contribute to a better understanding of the climate on earth and more accurate weather models.

Chapter 16 Recommendations

The StratoBlimp team has worked hard to complete the ground station and return vehicle designs in time so that a prototype could be produced and displayed at the symposium. The main reason for producing a prototype is to allow for testing, section 16.1 covers recommendations on validation methods for the current design.

Depending on the succes of the prototype, a followup vehicle may need to be developed. During the design process choices were made and the options were narrowed down. Many of these choices could not be revisited during the development of a single prototype. Narrowing down after a relatively short design process was necessary to complete the full design in a short time span, therefore new insights may arise about choices made earlier in the process. These new insights are described in section 16.2 , they will form guidelines for the development of a new vehicle.

16.1 Validation of current design

The current design still lacks validation in a number of areas which can be done using tests. None of these tests have been completed during the time of the DSE, but they are essential in optimizing the design and determining its reliability. Table 16.1 sums up the validation tests.

Table 16.1: Recommended validation tests

Vehicle property	Experiment	Improvements possible
Aerodynamics	Wind tunnel test	More accurate performance curves
Stability	Flight test	Better autopilot gain values
Structures	Load test	Find possible flaws in design
Electronics	Vacuum and climate test	Validate reliability in extreme conditions
Parachute	Deployment tests	Determine loads and reliability

Some other parts are still not fully developed. More research on internal temperature control is required. With a more accurate performance curve a better flight simulation can be done, allowing for more options in the flight profile. The autopilot program is in a testing phase and gains need to be determined using trail-and-error. More experimenting with smaller stability margins could improve controllability and glide ratio if it turns out the return vehicle is sufficiently stable. Wind tunnel tests can also be used to experiment with different turbulators, and further optimization of wing tips could improve efficiency.

16.2 Recommendations for a new design

The selection of the return vehicle concept was a difficult one. Since there were many options and little time the trade-off between concepts followed from simple calculations and rough estimations and therefore can be reconsidered. For example, if it turns out the high altitude spins are more easily controllable than expected, the flying wing concept can be reconsidered. The flying wing has advantages for the internal volume, may have a lower mass and does not have the fragile tail. Another concept worth investigating is the variable wing glider. This could be especially useful when it turns out it is difficult to cover ground at jet stream altitudes. Some assumptions concerning wing loading and required glide ratio can be revisited when a more accurate range estimation shows that the return vehicle covers the ground with a lot of altitude to spare. A list of recommendations is given below:

1. Return vehicle concept

   Depending on the mission, the concepts that can be taken into consideration are the flying wing, variable glider and the paraglider.

2. Ground station concept

   For some customers other ground station concepts may lead to a lower cost. When a low link budget is required, and launches occur less frequently, satellite communication may be more profitable. It saves the need for a ground station and the operating cost, depending on the amount of link budget required during flight.

3. Materials and production

   Depending on the payload of a future concept, the mass of the glider can vary considerably. If there is enough interest in a low end market, perhaps less expensive materials can be used. This results in a slightly heavier frame, but also reduces the cost. Experimenting with internal layout could result in tighter packaging, which allows a thinner airfoil to be used at the fuselage.

4. Electronics

   The sensor pack will need revision for the concept to be interesting for meteorological institutes. Time could be spent on developing low mass sensors for more specialised atmospheric measurements.

5. Release and landing

   For the prototype straightforward release and landing options were considered. More development and testing will result in more reliable and lighter components for the release system. The landing range requirement of 10 m is stretched to 40 m, since more accuracy cannot be guaranteed by the current prototype. Incorporating a more accurate altitude sensor in the last part of the glide could improve the landing range, but more elaborate concepts can also be thought of. A catching net would be an appealing alternative to the current landing that would greatly increase the landing accuracy and durability.

Bibliography

[1] Remes, B. (2012). *Project Guide Design Synthesis Excercise Stratoblimp*, Delft University of Technology.

[2] WeatherBalloons.Asia. (2009). *Weather Balloon Shredding* . Available: http://www.weatherballoons.asia/weather-balloon-experts/balloon-shredding. Last accessed 19th Nov 2012.

[3] *Paparazzi autopilot* V4.2, last accesed: 22-01-2013 `http://paparazzi.enac.fr/wiki/Main_Page`

[4] *ENAC* `http://www.enac.fr/`

[5] Cook, D.R. (2000-2001). *Jet Stream Behavior* Available: `http://www.newton.dep.anl.gov/askasci/wea00/wea00067.htm`. Last accessed: 15-01-2013.

[6] American Meteorological Society, Glossary of Meteorology 2nd Edition (2012). *Jet stream - AMS Glossary* Available: `http://glossary.ametsoc.org/wiki/Jet_stream`. Last accessed: 15-01-2013.

[7] GPS.gov (2012). *GPS Accuracy* Available: `http://www.gps.gov/systems/gps/performance/accuracy/`. Last accessed: 15-01-2013.

[8] Ministerie van verkeer en waterstaat (1995) . *Regeling kabelvliegers en kleine ballons*, The Hague.

[9] Selig, Donovan, and Fraser. (1989). *Airfoils at Low Speeds*, H. A. Stokely (publisher), USA.

[10] *XFLR5*. XFLR 5 V6.09 Beta, release november 18th 2012. Last accessed 4th Dec 2012.`http://www.xflr5.com/xflr5.htm`

[11] *Fundamentals of aerodynamics* John D. Anderson Jr., Fundamentals of aerodynamics, McGraw-Hill International Edition, Singapore, 2001

[12] *Volume method* Aircraft Design: Synthesis and Analyss, Ilan Kroo . (Standford University 1999). Last accesed: 15 January 2013. `http://adg.stanford.edu/aa241/stability/taildesign.html`

[13] *Aircraft Design: A Conceptual Approach, American Institute of Aeronautics and Astronautics* D.P. Raymer, 1992

[14] *Model aircraft aerodynamics* M. Simons, Argus books,1994 , Great Brittain.

[15] Hoerner, S. F. (1965): Fluid-Dynamic Drag. Hoerner Fluid Dynamics, Brick Town, N. J., USA

[16] *Xfoil website*. Last acceses 24 december 2012. `http://web.mit.edu/drela/Public/web/xfoil/`.

[17] *Summary of low speed airfoil data volume 1* M. Selig, J. Guglielmo, Andy Broeren, P. Gigue. SolarTech Publications,1995, USA.

[18] *Low speed low turbulence wind tunnel Delft.* TU Delft. Last accesed: 22-1-2013. http://www.lr.tudelft.nl/index.php?id=25790&L=1

[19] Trips, Dennis. (2010). *Aerodynamic Design and Optimization of a Long Range Mini-UAV*

[20] *Aerospace Design and Systems Engineering Elements III*, La Rocca, G. TU Delf (2010).

[21] Engineering Toolbox team. (2012). *The Engineering Toolbox.* http://www.engineeringtoolbox.com. Last accessed 17th Jan 2012.

[22] Kroo, Ilan. (1997). *Standard Atmosphere Computations.* http://aero.stanford.edu/stdatm.html. Last accessed 17th Jan 2012.

[23] Art Hobby team. (2012). *Art Hobby.* http://www.arthobby.com. Last accessed 20th Dec 2012.

[24] Lisenby, Spencer. (2012). *DS Kinetic.* dskinetic.com. Last accessed 19th Dec 2012.

[25] Art Hobby team. (2012). *Control surface sizing.* http://www.arthobby.com. Last accessed 20th Dec 2012.

[26] *Design for air combat* Ray Whitford, Jane's Publishing Company Limited, 1987, UK.

[27] *Rocket stability* Nasa. Last accesed: 24 December 2013. http://exploration.grc.nasa.gov/education/rocket/rktstab.html

[28] emphstability figure. Free online private pilot ground school (2006). Last accesed: 24 December 2012. http://www.free-online-private-pilot-ground-school.com/Aeronautics.html

[29] *Matlab* Version R2012b. http://www.mathworks.com

[30] *Tornado* Version 135, author: Tomas Merlin, http://www.redhammer.se/tornado/support.html

[31] *Flight dynamics Lecture notes* J.A. Mulder et al. Tu Delft 2011.

[32] *Kolibri software* Lightweight structures BV. Version 2.3 . Last accesed: 10 Januari 2013. http://www.lightweight-structures.com/kolibri-composite-conceptual-design-and-analysis-tool/index.html

[33] MIT. (2006). *Area and Bending Inertia of Airfoil Sections* Available: http://ocw.mit.edu/courses/aeronautics-and-astronautics/16-01-unified-engineering-i-ii-iii-iv-fall-2005-spring-2006/systems-labs-06/spl10b.pdf. Last accessed: 18-12-2012.

[34] Tenney, C. (1998). *Servo Calculator.*

[35] Bouman, J., Castelein, D., Eikelboom, H., Groot, J. de, Hulsman, S., Knoops, R., Kuijken, L., Milis, M., Schallig, S., Wijdeveld, S. (2012) *UAVForge challenge.* TU Delft

[36] Mulder, J.A., van Staveren, W.H.J.J., van der Vaart, J.C., de Weerdt, E., in 't Veld, A.C., Mooij, E. (2011). *Flight dynamics lecture notes*, Delft University of Technology

[37] Megson, T.H.G., (2007), *Aircraft Structures for Engineering Students Fourth Edition.* Butterworth-Heinemann

[38] Totex. (2011). *Pilot Balloons* Available: http://kaymontballoons.com/Weather_Tracking.html. Last accessed: 16-12-2012.

[39] Kaymont. (2011). *Kaymont Balloons* Available: http://kaymontballoons.com/Weather_Forecasting.html. Last accessed: 02-12-2012.

[40] Hwoyee. (2009). *Hwooyee Balloons* Available: http://www.hwoyee.com/base.asp?scclassid=521. Last accessed: 14-01-2012.

[41] University Hawaii. (2002). *Lifting gases* Available: http://www.chem.hawaii.edu/uham/lift.html. Last accessed: 08-12-2012.

[42] Ger J.J. Ruijgrok. (2009). *Elements of airplande performance*, VVSD.

[43] Wikipedia. (2012). *Archimedes' Principle* Available: http://en.wikipedia.org/wiki/Archimedes'_principle. Last accessed: 14-01-2012.

[44] Paparazzi. (2013). *Paparazzi website* Available: http://paparazzi.enac.fr. Last accessed: 16-01-2012.

[45] JSBSim. (2012). *JSBSim website* Available: http://jsbsim.sourceforge.net/index.html. Last accessed: 17-01-2012.

[46] Agentschap Telecom February (2012). *Vergunningsvrije toepassingen, Agentschap Telecom* Ministerie van Economische Zaken, Landbouw en Innovatie

[47] Digi (2009). *Xbee-Pro 868 product information* . http://www.digi.com/products/wireless-wired-embedded-solutions/zigbee-rf-modules/point-multipoint-rfmodules/xbee-pro-868#overview. Last accessed 6th Dec 2012.

[48] Radiometrix (2012). *Radiometrix NTX2 NRX2 product information* . http://www.radiometrix.com/files/additional/ntx2nrx2.pdf. Last accessed 6th Dec 2012.

[49] Digi (2009). *Radiometrix NTX2 NRX2 product information* . http://www.digi.com/products/wireless/zigbee-mesh/xbee-zb-module#specs. Last accessed 6th Dec 2012.

[50] Wertz, J.R., Larson, W.J. (1999). *Space mission analysis and design*, Springer

[51] Wikipedia (2009) *ERP definition* . http://nl.wikipedia.org/wiki/Effective_radiated_power. Last accessed 6th Dec 2012.

[52] SSS Online's RF Topics *Eb/N0 Explained* . http://www.sss-mag.com/ebn0.html. Last accessed 7th Dec 2012.

[53] FruityChutes Recovery Guidelines. (2013). *FruityChutes website* Available: .http://fruitychutes.com/UAV_Recovery_Guidelines.pdf. Last accessed: 16-01-2012

[54] μBlox MAX-6 product summary. (2013). *μBlox website* Available: .http://www.u-blox.com/images/downloads/Product_Docs/MAX-6_ProductSummary_%28GPS.G6-HW-10089%29.pdf. Last accessed: 16-01-2012

[55] SpheraChutes Construction. (2013). *Spherachutes website* Available: .http://spherachutes.com/construction.asp. Last accessed: 16-01-2012

[56] Meade, D.B., Struthers, A.A., (1999), *The Parachute Problem.* Differential Equations in the New Millennium

[57] GPS Boomerang (2005). *GPS Boomerang SmartBird*. Available: http://www.gpsboomerang.com/content/view/17/41/ Last accessed 21-12-2012.

[58] KNMI (2012). *Folder buitenluchtwaarnemingen KNMI*. De Bilt: KNMI.

[59] National oceanic and atmospheric administration (2010). *It's A NOAA weather balloon*. Available: http://www.noaa.gov/features/02_monitoring/balloon.html Last accessed 22-11-2012.

[60] National oceanic and atmospheric administration (2010). *The Ozone Layer*. Available: http://www.research.noaa.gov/climate/t_ozonelayer.html Last accessed 8-01-2012.

[61] ISARRA (2013). *International Society for Atmospheric Research using Remotely-piloted Aircraft*. Available: http://www.uibcongres.org/congresos/ficha.en.html?cc=267 Last accessed: 14-01-2012.

[62] *Cansat competition* Last accesed: 15 January 2013. http://www.cansat.nl/cms/

[63] *IMAV 2013* ENAC Toulouse, France. Last accesed: 15 January 2013. http://www.imav2013.org/

Appendix A Atmospheric properties

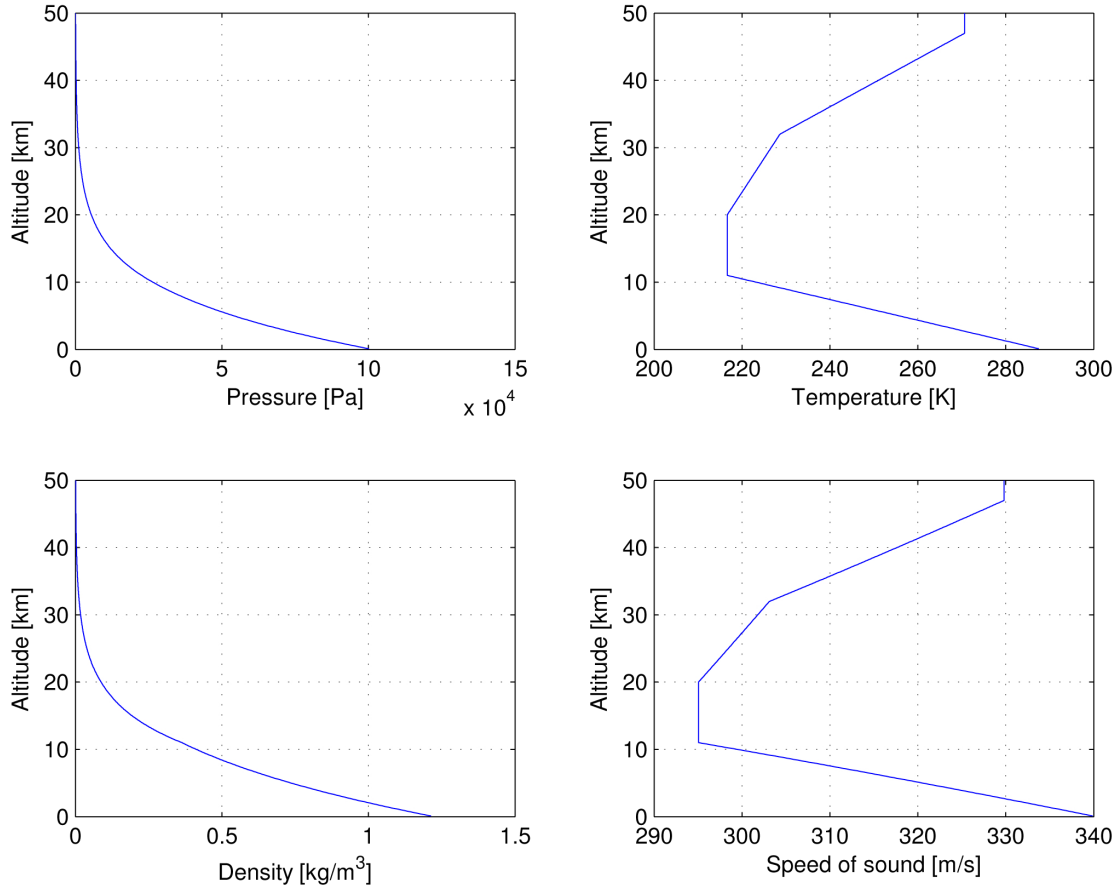

Figure A.1: Atmospheric properties as formulated by the ISA.

Appendix B Cost breakdown structure

Table B.1: Ordered parts for the ground station. The cost given is the amount paid for each part, excluding shipping cost and import tax.

Product	Brand	Type	Supplier	Cost EUR	Cost USD	Cost GBP
Satellite dish	Triax	DTS	CardWriter	26.00 €		
Tripod	Knig		Redhound	20.95 €		
GPS receiver	UBLOX	MAX-6Q	CSG Shop		$69.99	
Servo controller	Pololu	Micro Maestro 6-Channel USB Servo Controller	Pololu		$19.95	
Radio module	XbeePro	868 Dev.Kit *	Atlantik Elektronik GmbH	60.00 €		
Servo head	Endurance Robotics	PT-2 Assembled w/Hitec HS-645MG Servos	Endurance Robotics		$119.99	
				106.95 €	$209.93	£0.00

*The XbeePro is used in both the ground station and return vehicle. These are ordered as part of a development kit containing 2 XbeePro modules for the price of 120.00 €. This amount is shared over the ground station and return vehicle

Table B.2: Ordered parts for the return vehicle. The cost given is the amount paid for each part, excluding shipping cost and import tax.

Product	Brand	Type	Supplier	Cost EUR	Cost USD	Cost GBP
Airframe						
Aramid fabric		$36g/m^2$, $100cm$ x $2m$	carbonwinkel	€55.90		
Carbon rod		14 x 12 x 1000 mm	carbonwinkel	€18.64		
Foam	Rohacell	70 x 1250 x 625 mm	Emkey Plastics Ltd			£186.70
Camera window		Acrylaat buis 1000x40x2 mm	Kunststofshop.nl	€9.95		
Hinges		20x36 mm (10 pcs)	HobbyKing		$1.05	
Rockers		37.3x22.3x4 mm (10 pcs)	HobbyKing		$1.96	
Control rod (4x)		2 mm diameter, 1 m	HobbyKing		$3.92	
Clevis fastener		Nylon 2x29mm (10 pcs)	HobbyKing		$0.56	
Control horns		13.5x16mm (10 pcs)	HobbyKing		$0.97	
Electronics						
Radio module	XbeePro	868 Dev.Kit *	Atlantik Elektronik GmbH	€60.00		
Dipole antenna	Own build			€6.60		
GPS receiver	UBLOX	MAX-6Q	CSG Shop		$69.99	
Airspeed sensor	Eagle Tree	Airspeed MicroSensor V3	E-store Rotterdam	€39.75		
Autopilot control board		Lisa/M with 10 DoM Aspirin IMU	Transition Robotics, Inc.		$250.00	
Servo (4x)	Hextronik	HTX500	HobbyKing		$15.00	
Servo	HobbyKing	HKSCM9-6	HobbyKing		$2.96	
Battery charger	IMAX	B6	HobbyKing		$24.99	
Power supply	Turnigy	T-20Pro	HobbyKing		$24.99	
Battery	Turnigy	4000mAh Spektrum DX8 Intelligent	HobbyKing		$2.00	
Release mechanism			HEC Electronica	€1.50		
MicroSD	Sandisk	Sandish ultra 64GB microSD	Tweakers	€60.00		
Parachute						
Fabric	Mirai	$48g/m^2$ spinnaker nylon, $2.1m^2$	de Paddestoel	€8.66		
Ropes		18 kg tensile strength, 15m	de Paddestoel	€2.10		
Paracord		Mil-spec550 type III, 3m	paracord.nl	€1.35		
				€264.45	$398.39	£186.70

Table B.3: Ordered parts for the payload. The cost given is the amount paid for each part, excluding shipping cost and import tax.

Product	Brand	Type	Supplier	Cost EUR	Cost USD	Cost GBP
Camera	GoPro	Hero 3 Black Edition	Woodman Labs, Inc		$449.00	
Camera battery pack	GoPro	Hero 3 Battery BacPac	Woodman Labs, Inc		$59.00	
Battery for engine	Turnigy	2200mah 2S 40 80C Lipo Pack	HobbyKing		$11.22	
RC transmitter	OrangeRX	DSMX/DSM2 2.4Ghz	HobbyKing		$29.99	
RC receiver (2x)	OrangeRX	R100	HobbyKing		$22.38	
RC control unit	Turnigy	9XR	HobbyKing		$49.95	
	Turnigy	9XR Carrying Case	HobbyKing		$11.45	
	USBasp	AVR Programming Device	HobbyKing		$4.75	
				€0.00	$129.74	£0.00

Table B.4: Ordered parts for production. The cost given is the amount paid for each part, excluding shipping cost and import tax.

Product	Brand	Type	Supplier	Cost EUR	Cost USD	Cost GBP
		Resin Infusion Starter Kit	Easy Composites Ltd	€472		
Cartridge Gun Dispenser		50 ml twin tube	Easy Composites Ltd			£19.95
Epoxy Adhesive		50 ml twin tube	Easy Composites Ltd			£20.34
Chemical release agent		Easy-Lease 500ml	Easy Composites Ltd			£16.50
Glass fiber		280 g/m^2, 100cm x 2m	carbonwinkel	€9.80		
S2-Glass fiber		190 g/m^2, 100cm x 1m	carbonwinkel	€17.66		
Plug		3x Polyst. Geex. 40 37x60	Waltman's Bouwshop	€16.20		
Various			Gamma	€41.48		
Scissors		10 inch kevlar scissors	Easy composites	€45.66		
Digital scale		High capacity digital scale	Easy composites	€18.39		
Brush		Composites laminating brush 12 mm	Easy composites	€0.71		
Electrical wire cutting machine		Rent of electric wire curring machine	TU Delft	€200.00		
Crimp tool		Hex crimp tool	samenkopen.net	€26.00		
Soldering station			Various	€50.00		
Wiring and soldering products			Various	€50.00		
Various tools		Various tools needed during manufacturing	Various	€300.00		
				€1244.9	$0.00	£56.79